In-Situ Appraisal and Classification of Concrete Structures Prior Demolition:

Chemical Composition Analysis Using Handheld X-ray Fluorescence Analyzer with Cement Type-Driven Separation

TU Delft

Master Thesis
L.S.Gómez Jaramillo

In-Situ Appraisal and Classification of Concrete Structures Prior Demolition:

Chemical Composition Analysis Using Handheld X-ray Fluorescence Analyzer with Cement Type-Driven Separation

by

Laura Sofía Gómez Jaramillo

to obtain the degree of Master of Science
in Materials Science and Engineering
at the Delft University of Technology,
to be defended publicly on Tuesday November 28, 2023 at 12:30 PM.

Student number:	5567793	
Thesis committee:	Dr. Marija Nedeljković,	TU Delft, supervisor
	Prof. dr. ir. Marcel Hermans,	TU Delft, supervisor
	Prof. dr. ir. Erik Schlangen,	TU Delft
	Dr. Oguzhan Copuroglu,	TU Delft

TU Delft

Abstract

Recycled concrete aggregates (RCA) have been recognized as a sustainable solution to satisfy the demand and address the environmental impacts of the concrete industry. However, construction engineers and contractors still have reservations about RCA due to their heterogeneous origin and lower quality compared to natural aggregates. It is essential to know the properties of the parent concrete, in particular its chemical composition, before demolishing concrete structures in order to identify the source of the raw materials. Despite its importance, this has never been done before.

This thesis aims to analyze in-situ chemical composition of concrete and to identify the type of cement used in concrete structures by applying the non-destructive characterization technique of a handheld X-ray Fluorescence (hXRF) analyzer. To achieve this, laboratory experiments were performed to assess important factors in measuring cement paste and concrete surface chemical composition using the hXRF. These examined the impact of different water-to-cement (w/c) ratios, curing age, relative humidity, and carbonation on the chemical composition analysis with hXRF, and to gain valuable insights regarding the oxide concentrations of concrete and the most influential factors in hXRF measurements. The results indicated no impact on the chemical composition measurements with the hXRF despite the w/c ratios, the curing age, and carbonation. It was identified that higher relative humidity conditions than 75% affect the measurements with hXRF.

Subsequently, three case studies were considered for the in-situ assessment of chemical composition. Conducting tests with hXRF demonstrated the device's potential for analyzing concrete characteristic oxides (MgO, Al_2O_3, SiO_2, SO_3, CaO, Fe_2O_3). As a result, it facilitated cement-type recognition and provided valuable information regarding its opportunities and challenges. Drawing on insights from the literature review, laboratory experiments, and in-situ measurements, a guideline for in-situ testing of concrete composition was developed.

Acknowledgements

If someone were to ask me to define my study experience here in the Netherlands in one word, I would say 'roller-coaster.' This has been an experience full of emotions — from joy and many laughs to fear, sadness, and sometimes tears. It has been filled with challenges, but also with really good opportunities for my personal and professional development. I think I was able to overcome every obstacle during this journey thanks to many nice people I have met. Also, thanks to all of them I have memorable moments that I will remember forever.

Firstly, I want to express my gratitude to my supervisor, Marija Nedeljković, who has not only been my supervisor but also my role model. The first time I met her was via a phone call, and since that moment, her energy and passion for her profession strongly motivated me to undertake my master's thesis with her. When we met in person, she greeted me as if we had known each other all our lives, which was truly nice. When I told my friend Jacques, who did his master's thesis with her as well, he told me Marija is one of the best supervisors you can imagine, and I wholeheartedly agree. Thanks for teaching me so many interesting and relevant things in the field, things I could never have imagined learning. I am grateful for all your support, for believing in me, and for providing me with numerous great opportunities. I especially appreciate the chance I had to attend the conference and get to know your beautiful home country, Serbia. I hope we can collaborate in the near or long-term future.

Secondly, I want to thank my other supervisors on the committee Marcel Hermans, Erik Schlangen, and Oguzhan Copuroglu for their guidance and constructive and critical comments during the thesis progress meetings.

I have a long list of people that I would like to thank, and I will try not to forget anybody. I will start with my friends from the 3mE faculty: Elena, Marloes, Aditya, Paulus, Robert, Freek, Kevork, Alice, Georgiy, and Qinyi. I am incredibly grateful that life has given me the opportunity to meet all of you. I have learned so much from each of you, and you have also been a tremendous help to me. Many times, most of you supported me when I had doubts about the courses. I have enjoyed every drink, dinner, and movie with you, and for that, I am very thankful.

I also want to include my friend Natali in this list. I still remember the first time I met her at an activity organized by the Latitud Association. We have shared good meals, attended amazing Latin parties, and had nice talks. Now, I am moving to the next side of the road, the civil engineering faculty where I have met amazing people including Ameya, Farnaz, Patrick, Luis, Guilherme, Maiko, Arjan, and others who belong to the materials and environment department. I will always keep in my memories the nice chats I had in the office with Ameya and Farnaz, and also Farnaz asking "And where is the cake?" every time someone's birthday was approaching or if anyone had published an article.

My professors from my bachelor's in Colombia Giulia, Augusto, and Orlando, your personal, professional, and international experience provided me with the tools and opportunities to start dreaming of studying abroad till the point it became true, many thanks.

Last but not least, my family, including my grandma Lolis, my sister, my mom, and my dad— even though we were almost 8,000 km apart. Thank you for believing in my capabilities and for also being the ones who made it possible for me to come to the Netherlands.

Finally, what have I learned from this journey? I have learned that there is always a solution to any challenge or problem—well, except for death. There is never a perfect moment to be perfect; we are responsible for making every moment unique and special. Life sometimes has hard ways of teaching us, but everything we experience, and every challenge we face, is for a reason. It makes us stronger and wiser.

I wish you all the best in your future and thanks again for being part of my life!

Contents

List of Figures

List of Tables

Abbreviations

CDW	Construction and Demolition Waste
RCA	Recycled Concrete Aggregates
fRCA	Fine Recycled Aggregates
NA	Natural Aggregates
w/c	Water to Cement ratio
RH	Relative humidity or Rebound Hammer
GGBFS	Ground Granulated Blast-furnace Slag
EoL	End of Life
ADR	Advanced Dry Recovery
HAS	Heating Air Classification System
SCMs	Supplementary Cementitious Materials
RC	Reinforced Concrete
NDT	Non Destructive Testing
ED-XRF	Energy Dispersive X-ray Fluorescence Spectrometer
WD-XRF	Wavelength Dispersive X-ray Fluorescence Spectrometer
hXRF	Handheld X-ray Fluorescence analyzer
SDD	Silicon Drift Detector
SEM-EDS	Scanning Electron Microscopy with Energy Dispersive X-ray Spectroscopy
LIBS	Laser Induced Breakdown Spectroscopy
SIBS	Spark Induced Breakdown Spectroscopy
LA-ICP-MS	Laser Ablation Inductively Coupled Plasma Mass Spectrometry
CH	Calcium Hydroxide
CSH	Calcium Silica Hydroxide
TR	Test Region
TL	Test Locations

1

Introduction

1.1. Research background

Construction and demolition waste (CDW) is the primary global waste stream [1], with concrete rubble representing the largest fraction of CDW. To satisfy the demand and address the environmental impacts of the concrete industry, the production of recycled concrete aggregates (RCA) has been recognized as a sustainable solution [2]. However, some countries are facing oversaturation of low-grade recycled aggregates in the market [3]. Additionally, concrete producers and real state owners still have doubts about using RCA because RCA is often inconsistent in composition which may imply lower quality compared to natural aggregates (NA). Engineers, in particular, encounter uncertainties when tasked with designing structural elements using recycled concrete aggregates. This emphasizes the need for innovative solutions to improve the quality and cost-effectiveness of RCA, making them more suitable for various applications [4][5][6].

In general, assessing the quality of concrete involves a comprehensive approach, which includes examining original documents related to the concrete structure, visually inspecting it, and conducting non-destructive and destructive measurements. Visual inspections provide preliminary insights into the structure's condition, and subsequent research can delve into concrete strength, corrosion of reinforcement steel, and the presence of the alkali-silica reaction (ASR) [7][8][9]. Testing concrete structural members is crucial, covering aspects such as chemical composition, mechanical properties, load-bearing capacity, deformation capacity, and remaining service life. When a structure reaches the end of its service life or lacks sufficient load-bearing capacity, it may require demolition or repurposing [7]. In the case of demolition, thorough testing of material properties and chemical composition is essential for effective recycling. However, information about the original composition of concrete, including cement, aggregates, presence, and type of reinforcement, fibers, coatings, etc., is often limited or unavailable. Typically, only the original concrete supplier possesses this information. Otherwise, the properties of the RCA and the degree of contamination must be investigated through extensive physical and chemical laboratory analyses [4]. However, it is important to note that the concrete rubble may potentially be combined with rubble from different types of construction materials, which may contain a small number of deleterious contaminants (e.g. gypsum, bituminous materials) [6] or have experienced diverse environmental conditions. This mixing can significantly impact the quality of RCA [4].

A potential method to guarantee effective quality control of recycled concrete aggregates involves implementing selective/gradual demolition. This approach entails the gradual disassembly of structures, facilitating more precise and meticulous sorting processes [3][4][10]. Recently, a systematic approach has been introduced to evaluate concrete structures using non-destructive testing methods before their demolition. This is specifically valuable when information about the original concrete is unavailable. This classification of concrete is based on parameters like its strength and chemical composition [4].

Characterizing the concrete chemical composition is essential to improve the separation of undeteriorated concrete. This typically involves a combination of techniques like Energy Dispersive X-ray

Fluorescence Spectrometer (ED-XRF) and Scanning Electron Microscopy with Energy-Dispersive X-ray Spectroscopy (SEM-EDS), to identify specific compounds and their quantities [11]. However, utilizing these methods effectively requires expertise. Furthermore, many of these techniques involve extracting concrete samples from structures, followed by time-consuming and demanding laboratory analysis.

Handheld X-ray fluorescence analyzers (hXRF) offer a user-friendly alternative, providing an advanced non-destructive analysis method for the chemical characterization of materials. It has been applied in a wide range of areas, including art [12], geology [13], alloys [14], cementitious materials and concrete [10][15][16][17][18], and others. Some researchers aimed to investigate the chemical composition of various cement types and concrete containing them [15], as well as the influence of different factors (measurement time, moisture, surface carbonation, and matrix effect) on concrete composition measurements using hXRF [10]. However, no studies have explored the effects of curing age, different water-to-cement ratios, a wide range of relative humidity, and carbonation on the detection of concrete's characteristic oxides. Besides, no guidelines were found in the literature for the in-situ element analysis of concrete structures with hXRF.

Concrete has three skins, including the cement skin (about 0.1 mm thick), the mortar skin (about 5 mm), and the concrete skin (about 30 mm) [19][20]. Therefore, it is assumed that examining the chemical composition of the outmost layer of concrete will indicate the type of cement used, while analyzing the inner layers will reveal the type of aggregates present (as shown in Figure 1.1).

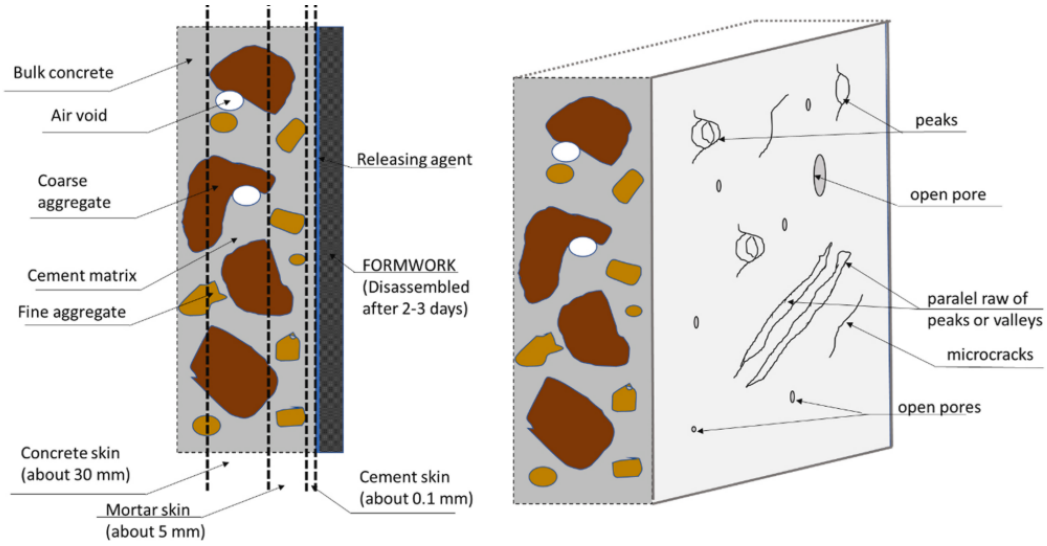

Figure 1.1: Characterization of the concrete skin [20]

Testing the chemical composition of the existing concrete structures prior to demolition can provide valuable information regarding concrete constituents, such as cement and aggregates, trace elements, and impurities. Knowing the specific type of cement used is particularly valuable for determining the potential future uses of fine recycled concrete aggregates (fRCA). For instance, it helps assess whether it can be used as an alternative raw material for clinker production [21][22] or as an admixture in new concrete [23].

1.2. Research aim and objectives

The research aim concentrates on analyzing in-situ the chemical composition of concrete and identifying the type of cement used in concrete structures by applying the non-destructive characterization technique of a handheld X-ray Fluorescence (hXRF) analyzer. To reach this aim, the following objectives are set forth:

- To investigate the impact of different water-to-cement (w/c) ratios of cement paste and concrete specimens on the measurements acquired using hXRF.

- To evaluate the impact of curing age of 1 day, 14 days, and 28 days on the chemical composition.
- To assess the impact of relative humidities of 0%, 40%, 60%, 75%, and 95% in a controlled way on the quantifications of surface chemical analysis of cement paste and concrete samples using hXRF.
- To analyze the influence of carbonation on the measurements acquired using hXRF.
- To test in situ concrete structure and identify opportunities and possible challenges.
- To propose a methodology for element composition analysis in the field of concrete structures using hXRF.

The primary significance of the current research is the evaluation of various parameters affecting hXRF measurements on pastes and concretes. Additionally, it aims to confirm the applicability of hXRF for assessing existing concrete structures. Based on the knowledge obtained during the literature review, the laboratory experiments, and the in-situ measurements, the guideline for in-situ testing of concrete composition was developed.

1.3. Research methodology

In this study, the research methodology was defined in four main parts as shown in the Figure 1.2.

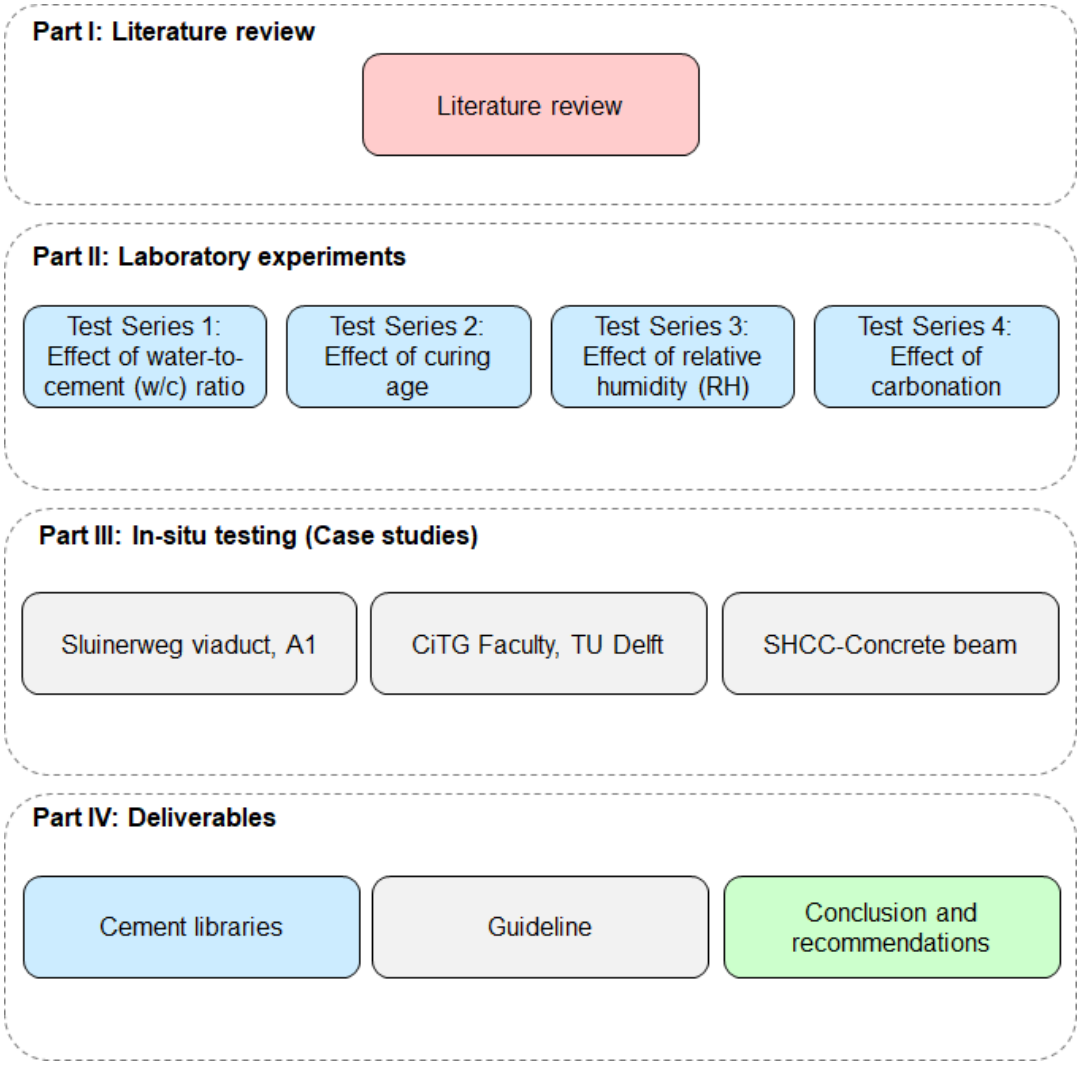

Figure 1.2: Scheme of the research methodology

In Part I, a literature review was performed to present a clear and concise overview of existing research in the field of concrete recycling processes, technologies, and quality control parameters of RCAs, and to identify the research gaps and to summarize the current knowledge concerning the element composition analysis of concrete with hXRF.

In part II, four Test Series were defined in which investigation was done in cement paste for fundamental purposes, as well as for concrete specimens. These specimens included two different cement types: CEM I 42.5 N (Portland cement) and CEM III/B 42.5 N (GGBFS cement). The effects of different water-to-cement (w/c) ratios, curing age, relative humidity levels, and accelerated carbonation were investigated. The chemical composition was tested using hXRF and results were subsequently validated by comparing the results with a Wavelength Dispersive X-ray fluorescence (WD-XRF) spectrometer, Environmental Scanning Electron Microscope, and Energy-Dispersive X-ray Spectroscopy (ESEM-EDS). The aim of these laboratory experiments was to gain valuable insights into the impact of the different effects or parameters on the characteristic oxides of both paste and concrete when measured with the hXRF.

In Part III, in-situ tests with the hXRF were conducted. Initially, the Sluinerweg viaduct on the A1 was defined as the sole case study. However, due to the challenges encountered, it was decided to include two additional case studies in this research to gain a more comprehensive understanding of the opportunities and challenges associated with in-situ testing of concrete structures and concrete structural members. It is worth noting that conducting the laboratory experiments before this part was advantageous for comprehending and critically analyzing the element analysis results obtained in the field.

In Part IV, a data analysis was conducted using data collected in Part II, facilitated by a Python code, to identify the range of characteristic oxides in concrete. Additionally, from the learnings and experience obtained from part III, a guideline for conducting in-situ testing of concrete structures with hXRF was developed. Lastly, the thesis concludes with a summary of findings and recommendations.

1.4. Thesis outline

The thesis outline is given in Figure 1.3. **Chapter 1** presents the background for this research. **Chapter 2** provides a comprehensive evaluation of existing research in the field of the concrete recycling process, technologies, and the quality control parameters of RCAs, and the current knowledge concerning the use of hXRF for the elemental composition analysis of concrete as an alternative to improve the quality of recycled concrete aggregates. In **Chapter 3**, the laboratory experiments are detailed, covering the materials used, cement paste and concrete production, methods selected for chemical composition analysis, and the specifications detailed for each Test series. **Chapter 4** presents and discusses the results obtained from the laboratory experiments. In **Chapter 5**, the different case studies considered for the in-situ chemical composition analysis with the hXRF are presented, as well as the results obtained with the respective discussion. **Chapter 6** introduces the guideline established for the in-situ appraisal of concrete chemical composition based on the learnings gained from the literature review, the experimental part, and the case studies. **Chapter 7** is the concluding chapter to reflect on the thesis by providing concluding remarks and recommendations for future research.

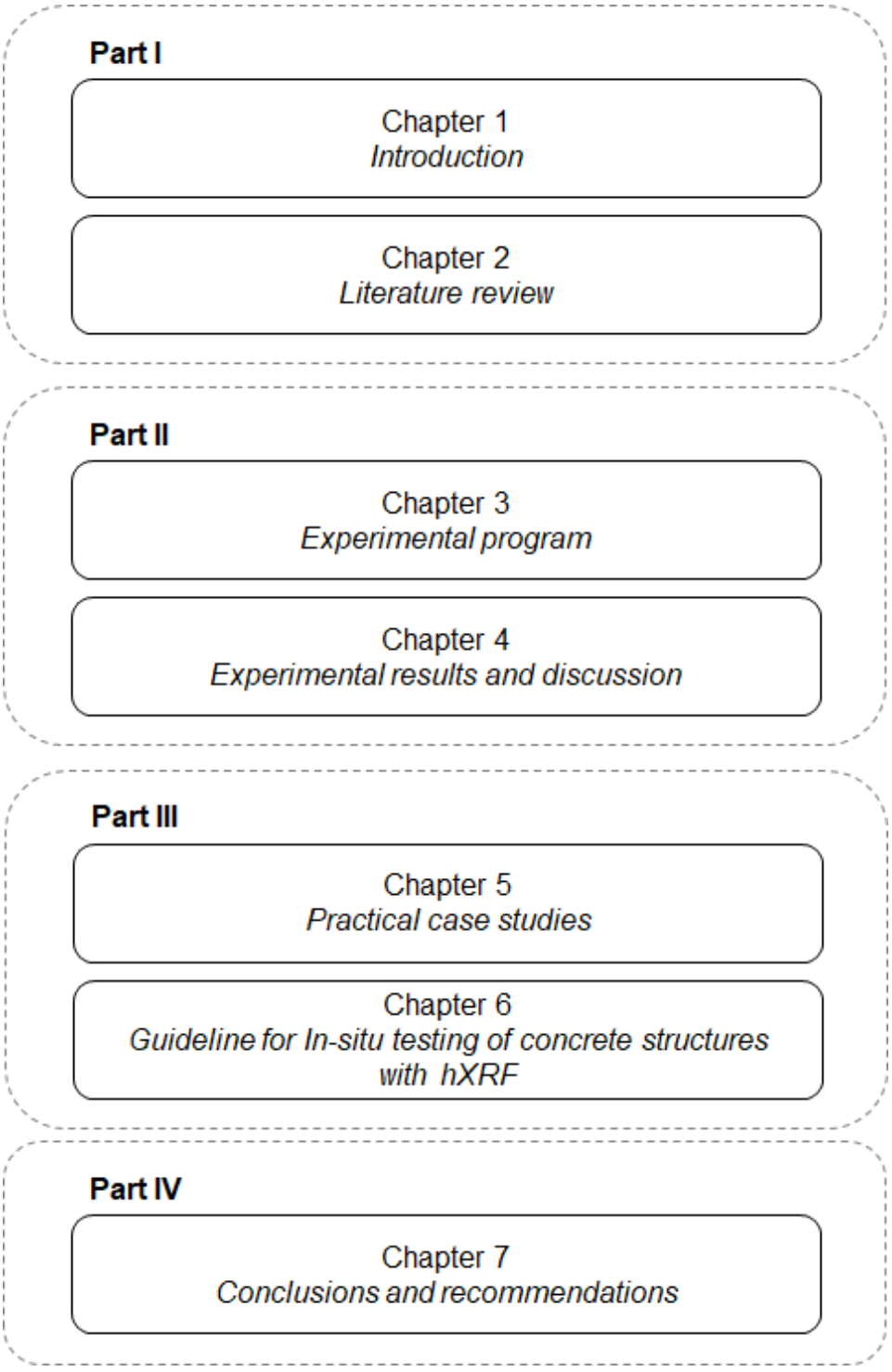

Figure 1.3: Thesis outline

2

Literature review

2.1. Concrete waste stream management: Enhancing quality of recycled coarse and fine concrete aggregates

In the past, waste management posed little concern as the population was small and there was an abundance of available space and land. However, with the evolution of the population in the last 100 years and the subsequent increase in waste production, the task of waste disposal has become more challenging. This is mainly due to the substantial quantities of waste generated and the diverse nature of its composition, which includes a large proportion of mixed waste containing chemicals, metals, and other materials [24].

In modern society, the construction industry is responsible for gross waste generation. In general, the waste generated from construction, renovation, and demolition activities from buildings, roads, bridges, and other structures is identified as construction and demolition waste (CDW) [24]. It is defined as a mixture of a wide variety of materials such as concrete, bricks, wood, metal, plastics, glass, and others [4].

China, the United States, and the European Union (EU), are the three biggest economies as well as the top three CDW generators [1]. In Europe, for instance, the construction sector produces about 450-500 million tons/year of CDW [25]. Most countries worldwide, including those in the EU, still have poor performance in terms of CDW generation, management, and recycling due to weak CDW regulations, inadequate data quality, and a limited market for secondary materials [4]. However, the European Union (EU) is working to replace the linear construction industry and waste management system with one that is circular. This transition is based on the principles of the circular economy. It is introduced as a new framework called the waste hierarchy in the EU Waste Framework Directive (2008/98/EC)) [1]. The Directive set a recycling target of 70% for non-hazardous waste to be achieved by 2020 [26]. Some European countries have already successfully met this objective of achieving 70% recycling for CDW.

The most commonly used method for recycling CDW is the crushing process to produce secondary aggregates [2]. They substitute natural aggregates (NA) in various applications, typically employed in pavement base and subbase courses, or as secondary components for creating low-strength concrete. It is mostly restricted to this kind of concrete due to challenges in quality control and lower strength [27]. This recycling process can be described as downcycling, which occurs when the recycled materials are polluted or mixed with low-quality materials [2].

Concrete constitutes a significant portion of CDW, as can be seen in Table 1. This is mainly due to the fact that the construction sector uses as much concrete and mortar compared to all other building materials combined [24]. Depending on the nature of the construction project, End-of-Life (EoL) concrete accounts from 40% to 85% of the total waste generated on-site [27].

There are five levels of treatment for EoL concrete, each serving different purposes. The first level focuses on preventing the generation of EoL concrete. The second level involves reusing concrete

elements in their original form. The third level entails recycling EoL concrete into aggregates specifically for road construction or backfilling purposes. Finally, the fifth level refers to the disposal of EoL concrete in landfills. In this context, the term “recycling of concrete” can be defined as any operation that involves reprocessing EoL concrete to obtain materials suitable for producing new concrete. On the other hand, the term “downcycling of concrete” can be defined as any operation that involves reprocessing EoL concrete to obtain materials intended for backfilling applications [2].

It is commonly recognized that in numerous EU countries, a significant portion of EoL concrete is still disposed of in landfills alongside other stone-based materials arising from structure demolitions [2]. Another major process is crushing aggregates that are used in road foundations. From an environmental perspective, a road foundation is a proper recycling route that involves relatively minimal transportation of the material from source to application. A small fraction of crushed waste concrete is used as a partial replacement for coarse aggregate in new concrete structures, but this application is not economically competitive, and its environmental benefits are comparable to the use in road foundations. However, both road foundations and partial replacement in new concrete are not sustainable solutions in the long term since the growth of road infrastructure is declining. Eventually, there will be little to no need for additional aggregates in road foundations in the future [2]. As a result, a solution will need to be found for a large amount of waste concrete that cannot be used in roads.

In the Netherlands, it is projected that the amount of concrete waste will increase from 10.5 Mt in 2003 to 22 Mt in 2025 [2]. Currently, a significant portion of concrete waste is recycled for low-grade applications such as road-based construction, indicating that only a small percentage of demolished concrete is recycled for applications with the same quality as the original material. While the demand for road-based materials will stabilize in the near future, the volume of CDW will keep on growing. The Netherlands is already experiencing saturation in the market for low-quality road-based aggregate. Moreover, industrial stakeholders in most regions are hesitant to adopt recycled concrete aggregates (RCA), and clients, concrete producers, construction engineers, and contractors still have reservations about RCA due to their typically heterogeneous nature and lower quality compared to natural aggregates [4][2][5]. This underscores the importance of exploring innovative technologies and methods to improve the quality of RCA and lower their costs compared to natural aggregates, enabling their wider application, and promoting upcycling.

The concrete recycling process involves several steps to convert waste concrete into reusable materials. Initially, the concrete rubble is collected from the demolition site or construction project and transported to the recycling plant. At the plant, the demolished concrete is crushed using crushers, with jaw and impact crushers being the most commonly used types of crushers. Magnetic separators are employed to remove ferrous metals before the crushing process. The recycling plant may also be equipped with Eddy current separators to extract non-ferrous metals. To eliminate other contaminants like wood and plastic, additional measures may be implemented [28]. These can include manual sorting or advanced procedures such as ZenRobotics. ZenRobotics (Figure 2.1) is an advanced technology that employs industrial robots equipped with various sensors, detectors, and scanners, along with artificial intelligence software, to efficiently sort different types of input materials such as metals, wood, stone, and inert materials. The system utilizes near-infrared spectroscopy, hyperspectral imaging sensors, a 3D sensor system, a high-resolution RGB camera, a metal imaging sensor, and a visual light spectrum sensor to ensure optimal sorting accuracy and efficiency [4].

To produce RCA, the final step is the size classification, which is accomplished through the process of sieving. Various equipment can be utilized for this purpose, all operating on the principle of vibrating the particles to facilitate their passage through a sieve mesh. The most commonly used equipment for sieving includes stationary screeners and trommels. After sieving, the coarse RCA and fine RCA are stored [28].

The coarse RCAs, for instance, consist of various types of particles. These include natural aggregate (NA), which separates during the crushing process and is free from old cement paste. Additionally, there are particles where natural aggregate is attached to old cement paste on one or several sides, as well as particles composed entirely of crushed old concrete [30].

The presence of attached old cement paste or mortar in these particles affects their properties, resulting in increased porosity, roughness, water absorption, greater irregularity, and lower specific mass compared to corresponding natural aggregates [30]. These factors contribute to increased permeability

Figure 2.1: ZenRobotics Technology [29]

and shrinkage, as well as the reduced compressive strength of new concrete with RCA [31]. Therefore, it is crucial to enhance the quality of RCA to align their physical, chemical, and mechanical properties with those of natural aggregates.

Researchers have explored and adopted various approaches to mitigate or partially offset the detrimental effects of RCA and improve the characteristics of new concrete. These approaches involve experimenting with different mixing methods, materials, and processes. For example, adjusting the water/cement (w/c) ratio and blending RCA with natural aggregates at various replacement ratios. Additionally, the properties of RCA can be enhanced through several quality improvement treatments. These treatment methods include removing the adhered mortar from RCA surfaces and enhancing the properties of the mortar itself [31][32].

In addition, technologically advanced processes offer the potential for improved production outcomes in terms of RCA. Traditional production methods can yield RCA with acceptable properties for concrete. However, advanced processes can enhance recovery rates, increase efficiency, and generate high-quality RCAs. Additionally, these processes have the capability to recover additional materials such as recycled fines and cement, which provide the necessary quality for various applications [4]. Examples of these advances are the Smart Crusher and Concrete to Cement and Aggregate (C2CA) technology. The Smart Crusher effectively separates concrete waste into gravel, sand, and cement without causing significant damage to each component. It achieves this by applying a crushing force that strikes a balance between the average compressive strength of the aggregates and the hardened cement paste. These crushing and grinding processes ensure the right force is exerted on the aggregates. On the other hand, C2CA technology combines Advanced Dry Recovery (ADR), see Figure 2.2 and Heating-Air Classification System (HAS), see Figure 2.3. Both mobile technologies enable on-site recycling of end-of-life concrete waste. ADR mechanically crushes and sorts concrete waste based on particle size, while HAS utilizes thermal and air classification methods to separate and activate the hydrated cement paste. The combined approach of these technologies recovers concrete waste into three product streams: coarse recycled aggregates (4-12 mm), fine recycled aggregates (0.25-4 mm), and an ultrafine fraction ($<$0.25 mm) [4][2].

Common quality control methods and advanced recycling techniques cannot assess concrete waste quality before demolition and recycling. Such information can be highly valuable for the broader utilization of RCA in structural applications [4].

RCA originates from various types of concrete waste, such as the demolition of existing concrete structures, and remaining fresh concrete from ready mix companies. Furthermore, parent concrete may have been exposed to different environmental conditions, including varying degrees of drying and wetting, chloride exposure, carbonation, chemical attacks, and alkali-aggregate reactions [4]. In a study conducted by Tam *et al.* [32], it was found that the origin of the concrete waste strongly influences the properties of the RCA. Consequently, an alternative approach to ensure proper quality management of RCA can be through selective or gradual demolition of concrete structures [4][30].

Selective demolition, also known as ”construction in reverse” or ”deconstruction,” involves a series of demolition activities aimed at separating and sorting building structural members and valuable ma-

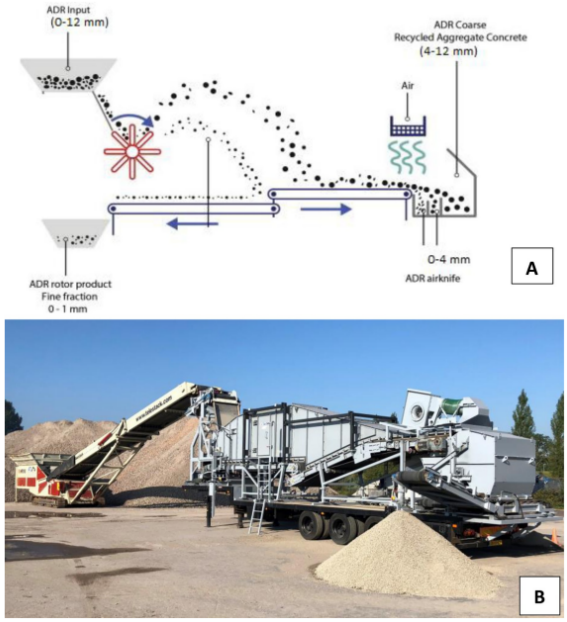

Figure 2.2: (A) A sketch of ADR working principles; (B) ADR installation on-site [33]

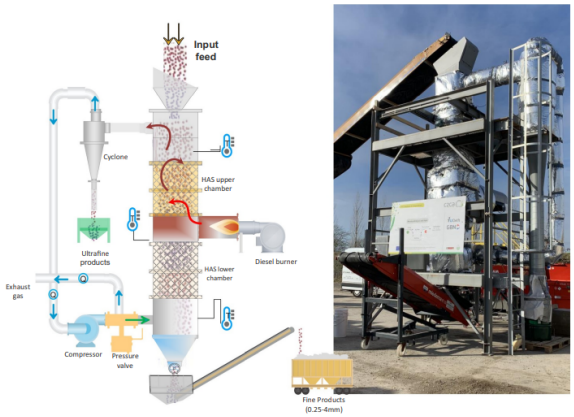

Figure 2.3: A sketch of heating air classification system (HAS) for recycling concrete fines [33]

terials [34]. In a broader sense, selective demolition offers several advantages compared to traditional demolition methods. These advantages include land preservation, secondary raw material utilization, environmental protection, and cost reduction in demolition expenses. Moreover, adaptive planning of deconstruction works and optimizing cost-effective processes can lead to significant reductions in both the duration and costs of deconstruction. By emphasizing the environmental aspects of construction in design codes and providing designers with more opportunities for material sourcing, the chances of reuse through smart demolition and selective dismantling can be further enhanced. Nonetheless, despite its numerous advantages, selective demolition still faces significant challenges that may not be easily overcome. For example, there is a lack of specific workflows or visualization tools established for selective demolition. Additionally, selective demolition requires additional time, space, and skilled labor, which can be seen as constraining factors in some cases, leading many owners and contractors to choose traditional demolition methods [4][34].

The selective demolition of concrete structures necessitates a thorough plan and workflow. Nedeljković *et al.* [4] proposed a selective demolition workflow, using a concrete bridge as a case study (Figure 2.4). The workflow comprises three main parts. Firstly, the bridge parts are sorted based on characteristic quality indicators such as cement type, aggregate type, concrete strength, and contamination levels

(with concrete elements being characterized prior to demolition). This enables recyclers to select concrete that aligns with their crushing technology and business model. Secondly, concrete is recycled. Finally, it can be further classified into separate stockpiles based on its origin and quality, including high-strength concrete without contamination, normal-strength concrete without contamination, lightweight aggregate concrete without contamination, and contaminated concrete. This advanced classification benefits concrete producers by providing information on the origin and quality of materials upon delivery. The following sections provide an overview of the quality indicators and the non-destructive techniques that can be essential for efficient concrete sorting before demolition.

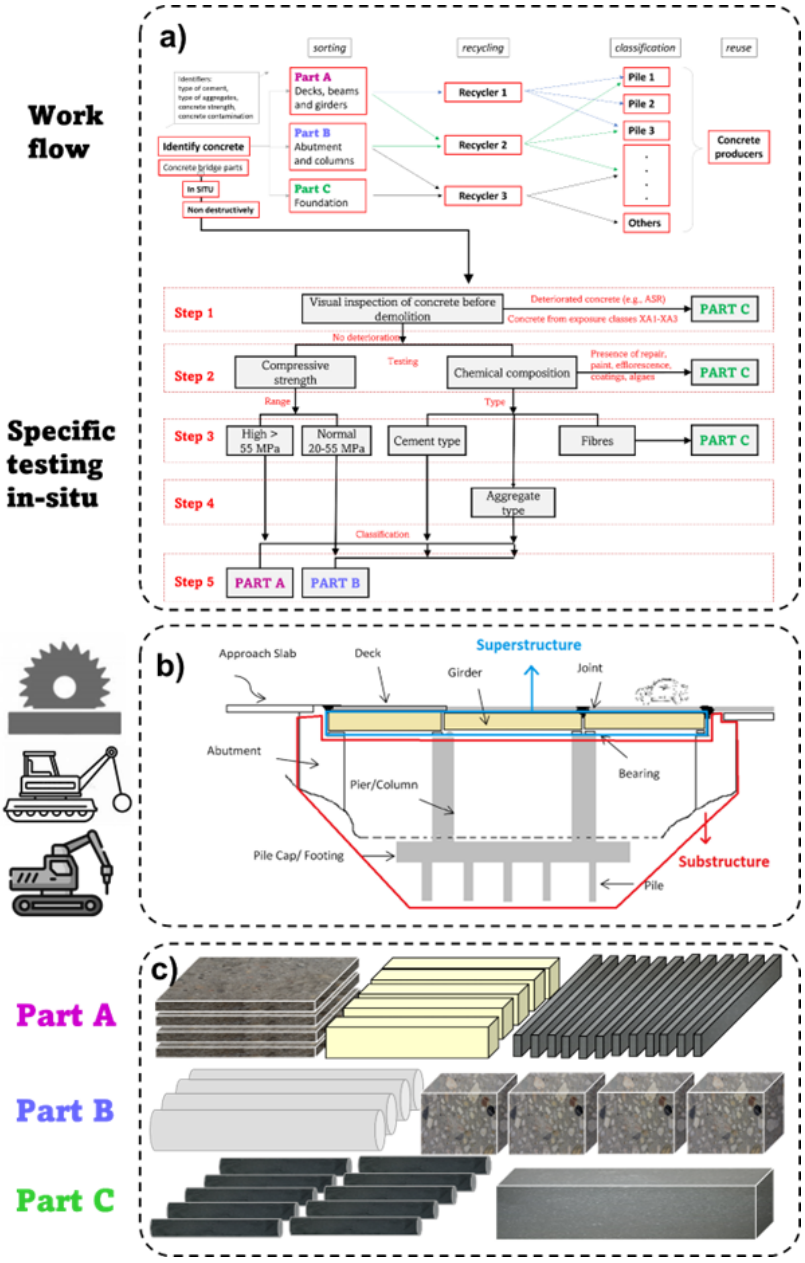

Figure 2.4: a) Workflow to implement in demolition projects, including specific in-situ testing and classification of concrete members based on strength and composition, b) an example of concrete bridge parts, c) their sorting prior to recycling and classification of concrete members based on a) [4]

Improving the quality assessment of the RCA not only increases their applications and improves their properties but it also decreases materials going into landfills and reduces the consumption of natural aggregates.

2.2. Concrete sorting prior demolition: Characteristic quality indicators for parent concrete

Research studies have demonstrated that Recycled Concrete Aggregate (RCA) holds the potential for use in new concrete. Much like Natural Aggregates (NA), RCA requires evaluation of aspects including particle-size distribution, absorption, abrasion, and more, to ensure conformity with national standards. The properties of RCA can vary due to factors such as the source of the aggregate or quality of the original demolished concrete (parent concrete), the recycling plant's concrete waste crushing method, and the limited availability of comprehensive quality data for CDW. Consequently, the establishment of quality control parameters becomes paramount. These parameters should enable the effective classification of distinct types of generated RCA based on their physical, mechanical, and chemical properties [35]. As shown in Figure 2.5 certain parameters are considered quality criteria for each property.

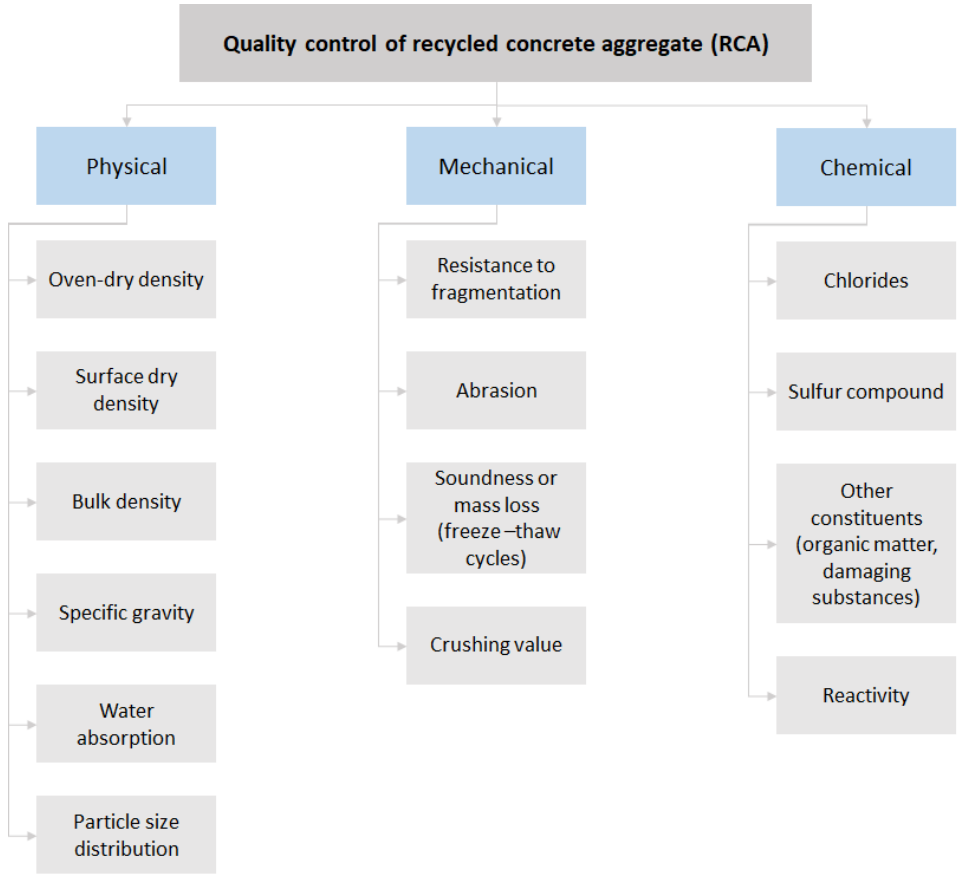

Figure 2.5: Quality control parameters of RCA

The physical characteristics of RCA, as outlined in national standards and guidelines (e.g., EN 12620, RILEM, CSIRO, etc.), can be categorized into five parameters. Among these, oven-dry density and water absorption are the most commonly utilized. Parameters such as bulk density and specific gravity appear less frequently [35]. Recycled aggregates possess lower density compared to NA, and RCA has reduced specific gravity and high water absorption due to the presence of residual mortar content (RMC) adhered to the original NA particles. This results in higher creep, shrinkage, lowered strength, and reduced durability of concrete once it reaches its hardened state. Moreover, the use of RCA in new concrete may exhibit a reduction in modulus of elasticity and workability, along with an increased demand for water in its fresh state [35][36][37].

The mechanical properties of the original materials exert a significant influence on the mechanical performance of concrete produced using RCA. This performance is primarily characterized by key parameters, including the Los Angeles abrasion coefficient, which gauges the aggregate's resistance to fragmentation during handling, while soundness evaluates the mass loss of the aggregate due to its

resistance against disintegration caused by various factors, notably weathering and freeze-thaw cycles [35]. Additionally, it has been observed that the mechanical properties (compressive strength, splitting tensile strength, bond strength, and modulus of elasticity) decreased when NA is replaced with RCA in concrete [36].

Chemicals like chloride and sulfate can cause corrosion and deterioration of hardened concrete. As a result, these parameters are frequently considered when analyzing aggregate quality. The presence of chlorides in RCA is not linked to the aggregate type; instead, it is influenced by factors such as the use of specific additives and exposure to marine conditions or freezing in the presence of deicing salts [35].

As mentioned in the previous chapter, RCA is obtained from various sources and undergoes crushing stages, resulting in the deterioration of its physical and mechanical properties. To enhance RCA productivity and utility, Kumar et al. conducted a study [37] aimed at estimating the approximate material properties of RCAs. They established four quality categories (high quality, medium quality, low quality, and poor quality) based on RCA quality parameters. To validate the classification of each quality category for RCA, performance parameters were taken into consideration (refer to Figure 2.6). Even though some of the parameters appear to be interesting for RCA's quality classification, these are considered once the structures have been demolished and the waste streams have been mixed.

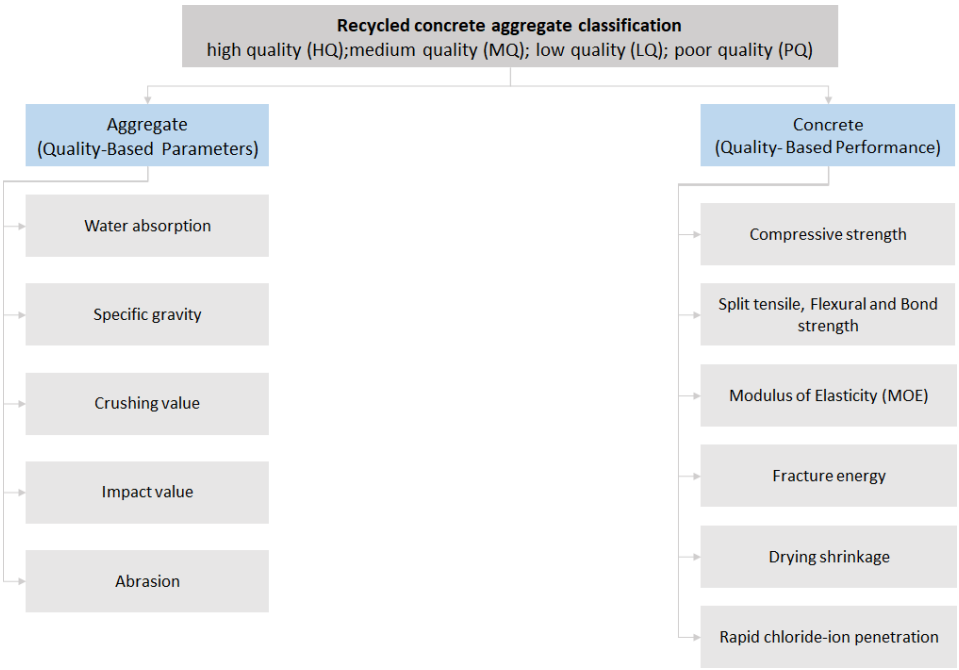

Figure 2.6: Quality parameters for RCA classification [37]

Nedeljković *et al.* [38] discussed the utilization of fine recycled aggregates (fRCA) and the challenges associated with its widespread adoption in their study. In this study, they provide several recommendations and observations regarding the quality control and practical application of fRCA. These recommendations include the promotion and enforcement of selective demolition in concrete structures to obtain material with a minimum level of contamination. Furthermore, it is crucial to consider the influence of fRCA quality in relation to various factors, such as the type of parent concrete, recycling techniques employed, and the storage methods utilized (see Figure 2.7).

In a comprehensive technical state-of-the-art paper addressing challenges and opportunities, as well as facilitation strategies needed to advance the complete re-utilization of waste concrete as a valuable resource, Villagrán-Zaccardi *et al.* [23] discussed the potential use of waste concrete in new concrete and mortar, specifically focusing on fine recycled concrete aggregates and recycled powder (produced by grinding fRCA in ball mills). This includes their role as cement replacement (either as supplementary cementitious materials (SCMs) or as an inert material, filler), alternative raw materials for clinker production, and their application in asphalt mixtures. The study also highlights the importance

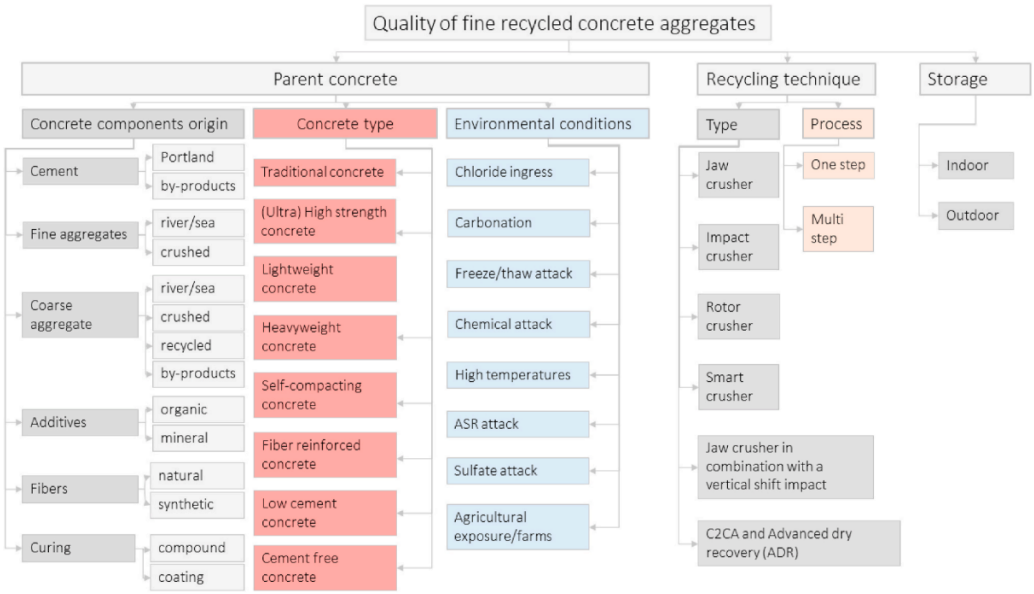

Figure 2.7: An overview of factors which may influence the quality of fRCA [39]

of selective demolition to enhance the quality of recycled products.

In the context of concrete reuse, several factors need to be considered when assigning it a new purpose. These factors include production methods (prefabricated or cast in place), application area (environmental class), and, consequently, exposure to various environmental conditions (such as varying conditions of drying and moistening, chloride exposure, carbonation, chemical attack, alkali-aggregate reactions, etc.) [7]. Figure 2.8 illustrates the parameters for reuse assessment of concrete products.

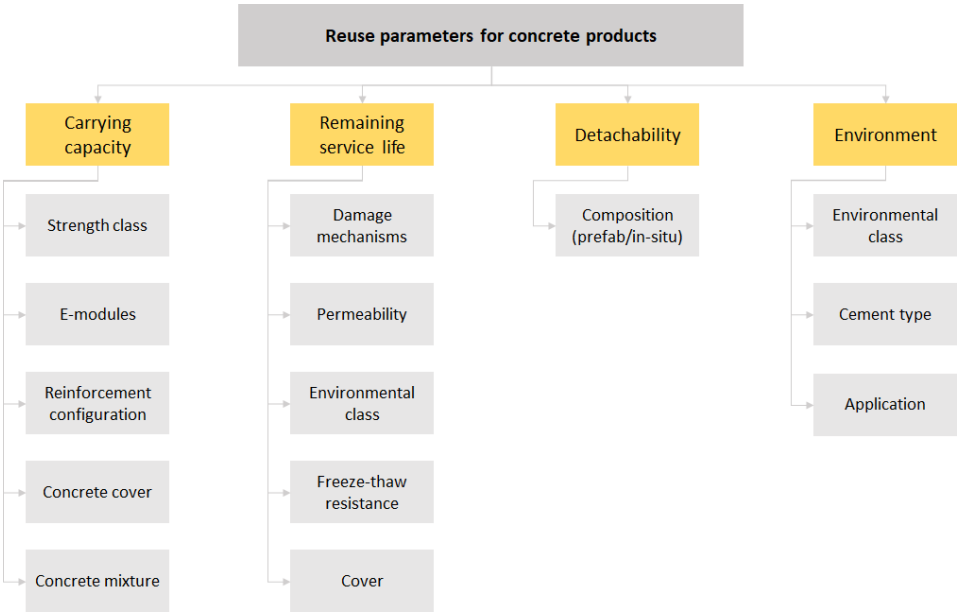

Figure 2.8: Reuse parameters for concrete products adopted from [7]

To maximize the value of RCA and its application, there is an urgent need for the implementation of selective demolition. This should involve characteristic quality indicators for the classification of various types of concrete before the demolition of concrete structures. These quality indicators can encompass visual inspections to assess deterioration (such as cracking, efflorescence, spalling, algae, steel corrosion, and others), as well as measurements of parent concrete's chemical composition. These three

quality indicators can be correlated with the properties of RCA and their production methods. This correlation may include factors like energy consumption during crushing, strength, and the types of cement and aggregates used in the parent concrete. Determining which parts of the parent concrete structure can be recycled together and which parts should be kept separate is essential for obtaining concrete batches of known and consistent quality [4]. This approach can complement recycling practices and aggregate treatment that occur after the demolition of concrete structures.

Furthermore, it is worth considering the collection of original documents related to the existing structure, where possible. These documents may contain valuable information, such as drawings, specifications, details about prefabricated elements, and construction methods used on-site.

2.3. Standard practices for appraising strength of concrete structures in-situ

Reinforced concrete (RC) structures (e.g., buildings, bridges, tunnels, and dams) deteriorate due to various factors such as aging, material defects, construction deficiencies, exposure to harsh environmental conditions, and unforeseen excessive loads. Typically, deterioration involves a combination of three main mechanisms: physical, chemical, and mechanical. For instance, physical deterioration can arise from freeze-thaw cycles, nonuniform volume changes, temperature gradients, and abrasion. Chemical deterioration can occur due to carbonation, chloride ingress, sulfates, acid attack, or alkali-aggregate reactions. Meanwhile, mechanical deterioration results from static and/or dynamic loads, as well as construction faults like premature loading during construction. These deterioration processes can have severe consequences, including structural issues like sudden collapse, loss of lives, material damage, and significant disruption to infrastructure networks [8][9]. To prevent disasters and identify flaws and defects in concrete elements, periodic monitoring and surveillance of these structures are necessary to ensure their structural integrity [40]. Engineers typically conduct visual inspections to detect defects and potential causes in concrete structures. Samples are collected from specific locations of a structure and tested in the laboratory. Based on the test results, engineers can determine the appropriate interventions for the structure, such as maintenance, repair, or demolition if necessary. Assessing the compressive strength is crucial in evaluating the structural capacity of both new and existing concrete structures [8][9]. Additionally, chemical testing helps evaluate the durability of reinforced concrete [41] and identifies causes of deterioration [11].

When it comes to estimating the compressive strength of concrete, the standard method involves extracting cores from the structure to evaluate their quality and estimate the compressive strength. However, this process of extracting samples is often labor-intensive, expensive, and time-consuming. Additionally, the samples are typically taken from specific locations, which may not fully represent the overall condition of the structure. Moreover, this method is considered destructive and can potentially impact structural integrity, necessitating subsequent repairs. To overcome these limitations, non-destructive testing (NDT) methods are employed to assess the concrete quality and identify sampling locations without causing damage. Common NDT methods include the rebound hammer (RH) and ultrasonic pulse velocity (UPV) tests, which are convenient for assessing concrete strength in situ at construction sites. However, NDT methods can be unreliable if not correlated with destructive test results. Measurement uncertainties, model uncertainties, statistical uncertainties of sampling, and uncontrolled factors like saturation and carbonation of the concrete can also affect the reliability of the results. To enhance accuracy, combining NDT methods, particularly the RH and UPV tests known as the SonReb method, has been extensively researched. Furthermore, standards such as EN 12504-2:2021 and EN 12504-4:2021 provide guidelines for determining the rebound index and ultrasonic pulse velocity, respectively, while EN 13791:2019 offers guidance for assessing in situ concrete compressive strength in structures. RILEM TC249-ISC also provides recommendations for non-destructive assessment of concrete strength in situ [4][9][42].

On the other hand, the European Standard is devoted to strength evaluation in concrete buildings and components, with a main focus on characteristic strength assessment and concrete strength class determination [42]. In the standard, it is described what aspects need to be determined and documented before conducting testing in situ. It explains how the test regions, test locations, and number of measurements can be specified. The standard also outlines the requirements for core testing and

determining the in situ compressive strength. It provides guidance on evaluating the results obtained from both in situ and laboratory testing. Additionally, the standard addresses which actions can be taken in case of uncertainty regarding the assessment of concrete strength [42]. Table 2.1 summarizes some of the general specifications expressed in the standard.

Table 2.1: Summary of general specifications in standard EN 13791 for assessment of in-situ compressive strength

Investigation objective and test parameters: - The objective of the investigation - Standards, test methods, and assessment techniques to be applied - Test region(s) and test locations - Number of measurements per test location - If cores are taken (specification of diameter and length, technique to be used to prepare the ends of the cores)
Test regions, test locations, and number of tests: - Test regions (TR): may compromise a series of similar elements and in case the objective is to determine the characteristic in situ compressive strength, test locations should be selected to take into account the typical variations in strength within elements - Test locations (TL): number of tests dependent on the volume of concrete involved - Number of tests: Minimum nine (9) readings with RH, and minimum one (1) reading with UPV
Core testing and the determination of the in situ compressive strength: - Cores: Determination of their densities, they should be free from reinforcement, min three (3) cores should be taken for a particular test area, ideally the core diameter should be in the range 75 mm to 100 mm

Alternatively, the RILEM TC249-ISC recommendation for non-destructive in situ strength assessment of concrete not only emphasizes strength evaluation but also underscores the importance of assessing the quality of this evaluation. This recommendation is particularly applicable in cases where the assessment of compressive strength in existing concrete structures has been performed using core samples and combined with non-destructive measurements.

In the RILEM TC249-ISC, the concrete strength assessment is divided into three main steps: (a) data collection, which includes NDT measurements and core strength measurements; (b) model identification consists of processing information at locations where both core strength and NDT test results are available; and (c) strength assessment, as illustrated in Figure 2.9 [42] [43].

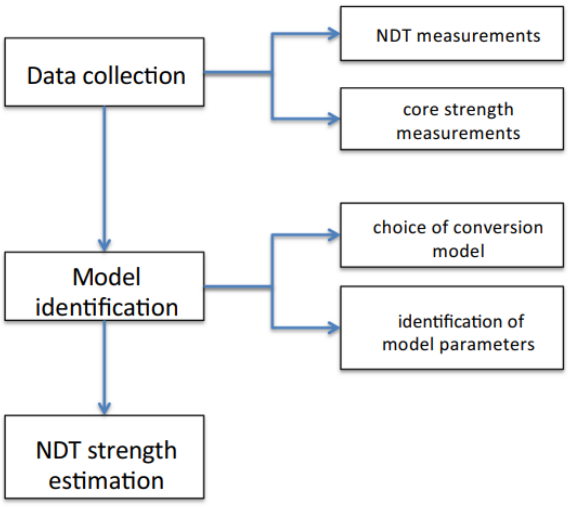

Figure 2.9: Three main steps of the standard concrete strength assessment process [43]

Before testing the compressive strength in situ, it is important to consider certain points as described in Table 2.2. Additionally, planning the testing should precede the actual tests. This planning phase

should involve methods such as core testing, ultrasonic pulse velocity (UPV), rebound hammer (RH), pull-out test (Capo-test), and micro-core testing (cores with a diameter smaller than 50 mm) for assessing the compressive strength of concrete [43].

Table 2.2: Key questions to be answered before in-situ investigation [43]

Context and objective of the investigation: - What is the objective of the investigation? - What questions have been asked by the engineers or by the structure managers?
Details of the structure to investigate: - What type of structure is it? - What is the age of the structure? - What is the exposure situation of the different structural concrete members? - Are there any durability problems?
Constraints of the investigation: - Which faces will be investigated (lateral, bottom, or top faces)? - What are the constraints in terms of accessibility to the structure? - Is coring allowed? - What is the surface condition of the components and how can it affect the use of NDT?

Furthermore, conducting a preliminary visual inspection is crucial to gain an overview of the structure's condition. This inspection should include identifying the position of the reinforcement, high-stress areas, and damaged sections, and assessing factors like carbonation and exposure effects (e.g., sunlight, rain, wind). Lastly, it ensures that the surface to be investigated is properly prepared [43].

When collecting data, it is recommended to initiate the process with Non-Destructive Testing (NDT) measurements as the first step. By using the NDT test readings obtained from different TL, it becomes possible to limit the TR for assessment, define the number of cores (see Figure 2.10), and accurately identify the conversion model. Conditional coring is recommended, which means that the core sampling locations should be decided after analyzing the NDT test results. This approach results in a more dependable conversion model.

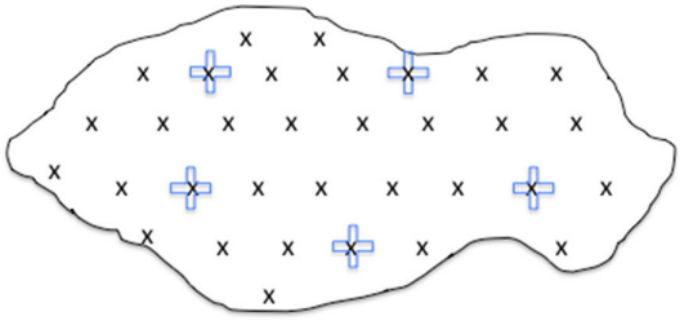

Figure 2.10: Illustration of available test results (continuous black line= test region, black "x"= NDT test locations, blue crosses=core strength test locations, here Nc=5) [43]

Furthermore, before extracting cores from the concrete structure, it is important to decide which structural members will undergo testing. Whenever feasible, the test locations chosen for NDTs and core tests should be situated in the compression zone of the concrete member. This is because the tension zone often exhibits more microcracks and lower in situ strength. The selection of core testing locations depends on whether the structural element is lightly loaded or a major load-bearing component. For columns and walls, both core sampling and NDTs should be performed near the top of the column and wall. In particular, it is preferable to conduct NDTs on the underside of slabs and beams in areas with negative bending moments. The number of core tests should be limited to the bare minimum because of cost, speed, and damages caused [44].

According to the standard NEN-EN 12504-1, a test report should include information such as the description and identification of the test specimen, the date of coring, visual inspection findings, length

and diameter of the core as received, storage conditions of the specimen, and other relevant details [45].

The model identification stage involves processing information from locations where both NDT strength results and core strength results are available, forming a series of pairs. Model identification helps to find the values of model parameters that minimize discrepancies between estimated strength and measured strength at the same locations. Finally, local strength (strength of an individual specimen), mean strength and strength standard deviation are estimated, and the uncertainty or statistical error of the data is quantified [42].

The root mean square error (RMSE) and the coefficient of determination (r^2) can be used as statistical indicators for the evaluation of the accuracy of the non-destructive concrete strength assessment. The model provides a better data fit when the value of r^2 is approaching 1 and the RMSE indicator is approaching 0 [43][9].

2.4. Techniques for appraising chemical composition of concrete

Determining the element composition of cement or concrete can be important for various purposes, including quality control, and research. Specialized techniques are available for conducting chemical composition analysis of cement and concrete, including Energy Dispersive X-ray Fluorescence Spectrometer (ED-XRF), Handheld X-ray Fluorescence (hXRF) analyzer, Micro X-ray Fluorescence (μXRF), Scanning Electron Microscopy with Energy-Dispersive X-ray Spectroscopy (SEM-EDS), Laser-Induced Breakdown Spectroscopy (LIBS), Handheld Laser-Induced Breakdown Spectroscopy (hLIBS), Spark-Induced Breakdown Spectroscopy (SIBS), Laser Ablation Inductively Coupled Plasma Mass Spectrometry (LA-ICP-MS), and others. However, some of these techniques involve stationary and expensive equipment and extensive expertise [11]. Furthermore, most of these techniques are destructive since they involve extracting a concrete sample from the structure and subjecting it to analysis in a laboratory. The extraction process can be arduous and time-consuming.

The working principle and features of the techniques mentioned before are explained in Table 2.3 and Table 2.4.

Table 2.3: Methods for chemical composition analysis

Method	Working Principle
XRF	• It uses high-energy X-rays (photons) to interact with a sample • Atoms in the sample emit secondary X-rays when hit by the high-energy X-rays • It identifies and quantifies the elements in the sample by measuring the energy and intensity of the emitted secondary X-rays
SEM-EDS	• Sample bombarded with high-energy electrons • High-energy electrons displace inner-shell electrons and vacancies are created • Atoms quickly fill the vacancies with higher-energy electrons resulting in this transition in X-ray emission • It identifies and quantifies element concentrations
LIBS	• High-energy laser pulse is generated and focused onto the sample's surface • Laser pulse rapidly heats and vaporizes a small portion of the sample, creating a high-temperature plasma • The plasma emits light as it cools down, producing characteristic emission spectra of the elements present in the sample
SIBS	• Generation of an electrical spark discharge or discharge between two electrodes • The spark creates a hot plasma that emits light • The emitted light is collected and analyzed for element composition
LA-ICP-MS	• High-energy laser vaporizes material from the sample (laser ablation) in the form of a fine aerosol • The aerosol is transported into an inductively coupled plasma (ICP), which ionized the aerosol • The ions are introduced into a mass spectrometer, which detects the ions and records their mass-to-charge ratios, providing information about the element composition of individual nanoparticles

While the working principles are similar among the three types of XRF (desktop, micro, and handheld), their main differences are related to their size, portability, and application areas.

Table 2.4: Features of the techniques for analyzing chemical composition

Method	Destructive (D)/ Non-destructive (ND)	Range of detectable elements	Portability
ED-XRF	D	Nearly all elements	Not portable
hXRF	ND	Mg-U	Portable
μXRF	D	Nearly all elements	Portable and Not portable
SEM-EDS	D	Nearly all elements	Not portable
LIBS	D	Nearly all elements	Not portable
hLIBS	D	Nearly all elements	Portable
SIBS	D	Nearly all elements	Not portable
LA-ICP-MS	D	Nearly all elements	Not portable

XRF is a widely applied method for quantitative and qualitative elemental analyses of cement powders, as outlined in the European standard EN 196-2:2014 [4].

SEM-EDS is a well-known method for imaging and elemental analysis of materials, offering high spatial resolution. It provides detailed information about small features, including the size, shape, and composition of tiny structures or particles within a sample. However, it has certain disadvantages, such as extended measurement times and specific requirements for sample preparation.

In the study conducted by Taefi *et al.* [46], the SIBS method was introduced for the analysis of cement powders. The potential and drawbacks of the SIBS technique, in comparison with XRF for the analysis of powdered products, were discussed. The main advantages of SIBS include fast analysis, absence of sample preparation, and cost-effectiveness. Meanwhile, XRF is the key technique for characterizing the element composition of materials in cement factories; however, it requires sample preparation and extensive apparatus. Some of the disadvantages of SIBS compared to XRF include its lower sensitivity to heavy elements and higher measurement error. Additionally, for the quantitative determination of each element, the preparation of calibration curves and several standard samples containing the major, minor, and trace elements are needed [46].

Some research has been conducted using LA-ICP-MS for the analysis of the chemical composition of cement clinker phases [47], multi-element analysis of concretes, particularly during chloride or sulfate attacks [48], and for monitoring the ingress of biogenic sulfuric acid into hardened cement paste [49]. This technique provides low detection limits, enabling the analysis of trace element concentrations. However, it lacks a simple calibration system for different types of materials, and it is a destructive technique as it involves vaporizing the sample [47].

For the case of μXRF, its equipment constraints restrict its ability to analyze large vertical and horizontal concrete surfaces in real time on-site [15].

Cutting-edge non-destructive techniques employed in laboratories for assessing the composition of concrete include, hLIBS and hXRF, see Figure 2.11. LIBS has been used mainly for the determination of deleterious elements such as chloride or sulfur in building materials such as concrete, mortar, and cement. It can detect elements from the entire periodic table, but it is particularly well-suited for identifying light elements such as hydrogen (H), lithium (Li), beryllium (Be), boron (B), carbon (C), nitrogen (N), and oxygen (O). This is an analysis that hXRF is unable to perform, as hXRF can detect elements ranging from magnesium (Mg) to uranium (U) [50]. In spite of that, hXRF is non-destructive, while LIBS is micro-destructive due to laser-induced material removal, making repeated analyses at the same spot impossible. This limitation poses challenges when analyzing valuable items like cultural heritage artifacts or very small samples that cannot yield meaningful LIBS spectra without complete destruction [51].

The handheld XRF (hXRF) is a qualitative and semi-quantitative technique that utilizes the fluorescence properties of materials to analyze their composition, both in laboratory and in situ. The literature has identified several factors that can affect measurements using this technique, leading to underestimated element concentrations and reduced result reliability. These factors include the presence of air

Figure 2.11: Portable non-destructive techniques for analyzing material's composition (a) hLIBS [52]; (b) hLIBS parts and working principle [53]; (c) hXRF [54]; (d) hXRF parts and working principle [55]

between the device's tip and the specimen, moisture content, and sample heterogeneity [56][10]. Both moisture content and air can interfere with the X-ray beam, causing X-ray absorption. However, the impact of moisture can be mitigated by drying the sample test surface, while sample heterogeneity can be addressed by predicting the sample's structure using calibration models integrated into the hXRF software. Calibration involves converting signals detected by the device and establishing a relationship between element weight percentages and X-ray intensities [10].

On the other hand, hXRF offers several advantages, including ease of use, non-destructive testing, portability for fieldwork, rapid results, minimal sample preparation, and the ability to analyze numerous spots [4][57]. hXRF has been applied in various domains, such as geology [13], medicine [58], art [12], mineral exploration [59], archeology [60][61], environmental investigations [62][63], cultural heritage [64][65][66], and cementitious materials and concrete [10][15][16][17][18], demonstrating its promise for chemical characterization. Despite its broad range of applications and numerous advantages, this device has not yet been thoroughly studied or applied to quantify the chemical element composition of in-situ concrete structures.

To address this gap, a methodology can be developed to estimate the composition of in-situ concrete. This methodology can draw upon existing practices and standards used for in-situ compressive strength analysis. It aims to identify the type of cement and aggregates in concrete and determine the extent

of concrete contamination. Such an approach would offer several advantages, including ensuring the accurate identification of concrete at its source prior to the demolition of a concrete structure, enhancing demolition efficiency, guiding the quality assessment of RCAs, and reducing the reliance on standard chemical tests in the laboratory.

2.5. Use of Handheld X-ray Fluorescence spectrometer (hXRF) in concrete

2.5.1. Assessment of Concrete Mixture Proportions

The durability and performance of concrete pavements depend on factors like concrete mix proportioning and uniformity control. Monitoring these proportions can be done through batch tickets and quality control testing. Batch tickets provide information about materials and proportions used in each concrete batch, while quality control testing involves analyzing concrete samples in a laboratory, often using XRF analysis. However, batch tickets may be unreliable due to errors in material loading, calibration, and water addition after dispatch. Moreover, laboratory XRF analysis can be costly and time-consuming [16]. Taylor *et al.* [16] looked into the use of handheld XRF equipment to check and gauge the proportion of concrete mixtures before construction work begins.

The utilization of the XRF technique in the chemical composition analysis of concrete mixtures offers benefits in terms of speed, accuracy, and precision. However, it brings some challenges in specimen preparation, which involves creating a uniformly flat surface [16]. Besides, the device poses problems in the detection of elements lighter than magnesium. Thus, a preliminary investigation was conducted to describe the potential use of a portable XRF technique to determine the proportions of fresh concrete [67].

In the research study done by Taylor *et al.* [16], tests were conducted on powders, paste, and mortar samples using a handheld Niton XL3t900 GOLDD+ analyzer. To examine the chemical composition of the powder materials, tests were performed on 5 distinct types of cementitious materials, including Type I Portland cement, Class C fly ash, Class F fly ash, silica fume, and slag cement. To minimize contamination, the powder samples were placed in an open-topped containers and the surfaces were covered with 6-micron polypropylene sheets to minimize contamination. Fine aggregates were oven-dried in order to reduce the moisture content. For the preparation of paste (cementitious materials + water) and mortar (cementitious materials + sand + water) samples, ASTM C109 and ASTM C305 standards were followed. The samples were molded into 3 cubes per mixture. In total 15 paste mixes and 15 mortar mixes were prepared, all with a water-to-binder (w/b) ratio of 0.45. The supplementary cementitious materials (SCM) used were fixed at 0.20, and 40% by mass for both the paste and mortar mixes. Additionally, for the mortar mixes, the cementitious-to-sand ratio was fixed at 1:3 by mass. The measurement time using the portable XRF was 15 minutes per sample in order to provide sufficient time for a reasonable repeatable analysis. Once the results were obtained, they were expressed as an average of the three samples per mixture.

Regarding the results obtained in the investigation for the cementitious materials, the results were reported by the handheld XRF as element percent by mass. They were converted into oxides considering the atomic weights of the data. Once the data was obtained, they were compared with the standard ASTM C150 for Type I Portland cement Table 2.5. It was observed that most of the oxide's percentages were within the expected range but the SO_3 content was considerably above the expected level.

Desktop XRF and portable XRF were used to test the composition of fine aggregates. The percentage of undetected elements differed significantly between the two devices when comparing the two data sets. This difference may be attributed to sampling error but also calibration method.

After the paste mixtures were tested, it was observed that the percentage of detected elements in SCMs decreased compared to the cementitious materials. In addition, the proportions of SCM estimated using an Excel program's solver function showed a strong correlation with the measurements obtained from the handheld XRF, as demonstrated in Figure 2.12a. When water was included in the calculations, the prediction error of mix proportions increased (see Figure 2.12b).

For the case of the mortar, it was observed that the percentage of detected elements decreased compared to the cementitious materials and the paste mixtures. The SCM content was predicted includ-

Table 2.5: The comparison of the test results obtained from the portable XRF and the ASTM C150 recommended chemical composition range [16]

Chemical composition,%	ASTM C150 min-max	XRF Portable Device
SiO_2	18.7-22.0	18.21
Al_2O_3	4.7-6.3	3.67
Fe_2O_3	1.6-4.4	4.63
CaO	60.6-66.3	62.95
MgO	0.7-4.2	3.12
SO_3	1.8-4.6	8.55

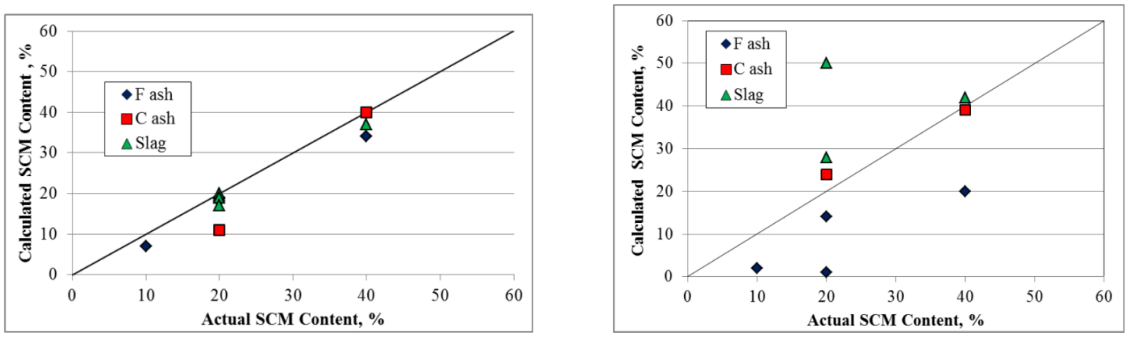

(a) (b)

Figure 2.12: (a) The relationship between tested and designed SCM content (b) The relationship between tested and actual SCM content when the water presence is included [16]

ing the sand content by using the solver function, similar to the analysis that was done for paste mixes. The calculations revealed that the sand content constituted 30% of the mass. However, discrepancies were observed between the tested and actual SCM content when considering the sand content in the relationship (Figure 2.13a). To address this, the calculations were repeated with a fixed sand content of 15% because the original analysis, which relied on the depth of penetration into the sample, did not accurately represent the mixture without a fixed sand content. Despite this adjustment, Figure 2.13b demonstrates that errors persisted in the relationship between the tested and designed SCM content, albeit slightly reduced compared to the previous errors.

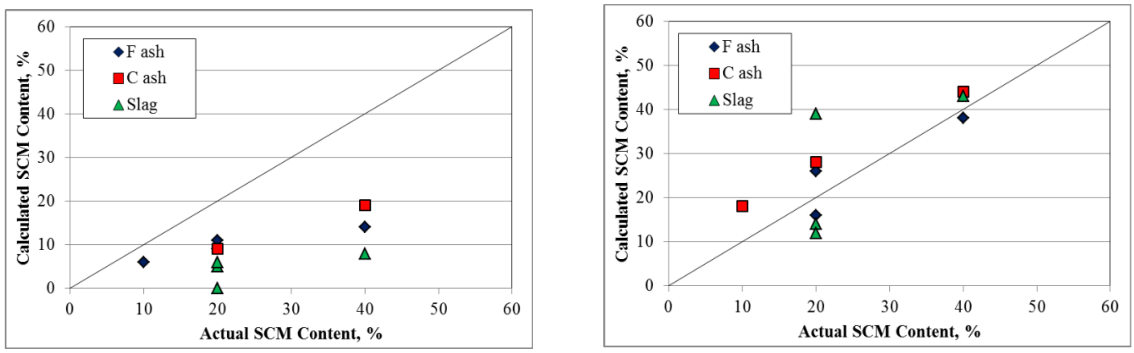

(a) (b)

Figure 2.13: (a) The relationship between tested and designed SCM content with sand (b) The relationship between tested and designed SCM content [16]

In this study was concluded that the handheld XRF seems a promising device for analyzing the chemical composition of powder materials, cement paste, and mortar. However, the heterogeneity of the mortar samples reduces the accuracy of the analysis.

2.5.2. Determination of cement and aggregate type in hardened concrete

Recently, two studies have been attempted for the assessment of chemical composition in cementitious materials and in hardened concrete using a handheld X-ray Fluorescence analyzer (hXRF). In addition, the factors that influence the results obtained with the portable device have been analyzed.

In the first place, in the research conducted by Nedeljković *et al.* [15], tests were performed on five different types of cement powders (CEM I 42.5N, CEM I 52.5R, CEM II/B-V, CEM III/A 52.5, CEM III/B 42.5), two supplementary cementitious materials (fly ash and ground granulated blast furnace slag), limestone filler, crushed aggregate, round river sands, and three concrete samples. The concrete samples consisted of CEM I 42.5N (Portland cement)-SC1, CEM II/B-V 42.5N (Portland–fly ash cement)-SC2, and CEM III/B 42.5N (GGBFS cement)-SC3. The tests were conducted using a Bruker S1 TITAN 800 handheld Energy Dispersive X-ray Fluorescence (hXRF) analyzer with a measurement time of 30 seconds, and the accelerating voltage was set at 15 keV. The results were validated using a desktop XRF and Energy-dispersive X-ray Spectroscopy (EDS). The aim of this study was to assess the applicability of hXRF for characterizing the chemical composition of powders and hardened concrete for the purpose of concrete sorting based on cement type. Additionally, the effect of concrete surface conditions, (water-saturated, air-dried, and oven-dried), measurement duration (30, 60, 90, 120 s), and repeatability on the concrete surface and concrete´s surface layer scanning on handheld XRF measurements were studied.

Table 2.6 shows the element concentrations of the selected powders that were tested using hXRF, with the BRUKER calibration method for cement, desktop XRF, and EDS. For two of the main element oxides of the powders, a strong correlation was observed between hXRF-desktop XRF results (coefficient of determination r^2 of 0.995) and hXRF-EDS results(coefficient of determination r^2 of 0.991).

Table 2.6: Bulk chemistry comparison between hXRF, desktop XRF, and EDS for powders [15]

	Method	River sand		GGBFS		Fly ash		CEM I 42.5 N		CEM II B-V 42.5 N		CEM III/B 42.5 N	
		wt.%	StdErr	wt.%	StdErr	wt.%	StdErr	wt.%	StdErr	wt.%	StdErr	wt.%	StdErr
CaO	hXRF	0.81	±0.02	41.46	±0.10	2.66	±0.05	63.55	±0.12	41.99	±0.10	50.13	±0.12
	desktop XRF	0.73	±0.02	39.03	±0.14	4.65	±0.06	63.86	±0.13	44.21	±0.14	47.11	±0.14
	EDS	0.92	±0.09	38.48	±0.32	3.98	±0.07	64.81	±0.29	43.78	±0.35	45.05	±0.40
SiO_2	hXRF	95.44	±0.99	34.92	±0.74	51.15	±1.37	23.83	±0.55	43.35	±0.10	28.75	±0.67
	desktop XRF	93.07	±0.21	34.19	±0.38	55.39	±0.40	20.23	±0.33	32.28	±0.38	29.11	±0.37
	EDS	95.85	±0.04	33.49	±0.18	59.66	±0.18	20.16	±0.09	31.71	±0.17	27.34	±0.13
Al_2O_3	hXRF	0.84	±0.16	10.06	±0.42	20.52	±0.64	3.59	±0.30	3.91	±0.30	6.46	±0.38
	desktop XRF	3.27	±0.10	13.97	±0.14	23.84	±0.25	4.84	±0.13	10.90	±0.18	10.02	±0.18
	EDS	1.7	±0.19	14.13	±0.10	22.2	±0.18	4.65	±0.04	11.00	±0.09	9.27	±0.10
MgO	hXRF	1.71	±0.01	7.39	±1.03	4.00	±1.10	2.09	±0.97	2.63	±0.89	6.17	±1.08
	desktop XRF	0.18	±0.01	8.55	±0.38	1.56	±0.07	1.65	±0.07	1.21	±0.06	5.89	±0.14
	EDS	0.13	±0.03	8.69	±0.12	1.64	±0.05	1.51	±0.04	1.34	±0.08	5.34	±0.09
Fe_2O_3	hXRF	0.48	±0.01	1.83	±0.02	15.73	±0.056	3.87	±0.04	5.48	±0.04	2.51	±0.03
	desktop XRF	0.59	±0.02	0.30	±0.14	6.40	±0.07	3.28	±0.05	3.81	±0.06	1.19	±0.03
	ESEM-EDS	0.45	±0.12	0.13	±0.15	6.00	±0.34	3.01	±0.29	3.05	±0.26	1.87	±0.29
SO_3	hXRF	0.10	0.03	1.95	±0.06	1.27	±0.06	1.71	±0.05	1.44	±0.053	4.24	±0.08
	desktop XRF	-	-	1.20	±0.38	0.76	±0.03	2.83	±0.07	2.48	±0.07	2.82	
	EDS	0.17	0.03	2.22	±0.04	0.55	±0.04	2.35	±0.04	6.35	±0.13	9.00	±0.16

In the case of chemical composition analysis of water-saturated concrete samples, a significant increase in CaO concentrations was observed, while concentrations of SiO_2, Al_2O_3, MgO, and SO_3 decreased, with the latter being unidentifiable. This phenomenon could be attributed to the increased photoelectric absorption effect and X-ray scattering. Furthermore, the CaO content in concrete SC1 with CEM I was overestimated due to calcium leaching from the concrete surface followed by carbonation. This issue is less pronounced in concrete specimens SC2 and SC3, as they possess lower CaO content compared to SC1. Consequently, it was concluded that the drying process enhances the accuracy of the results, reducing the impact of water saturation on the measurements.

Regarding the results obtained on the effect of different measurement durations on the element concentration on dried concrete surfaces (see Figure 2.14), it was concluded that 30 s was sufficient for the identification of the main elements on the concrete surfaces (MgO, Al_2O_3, SiO_2, CaO, Fe_2O_3) with hXRF, and no significant change was observed with longer measurement durations.

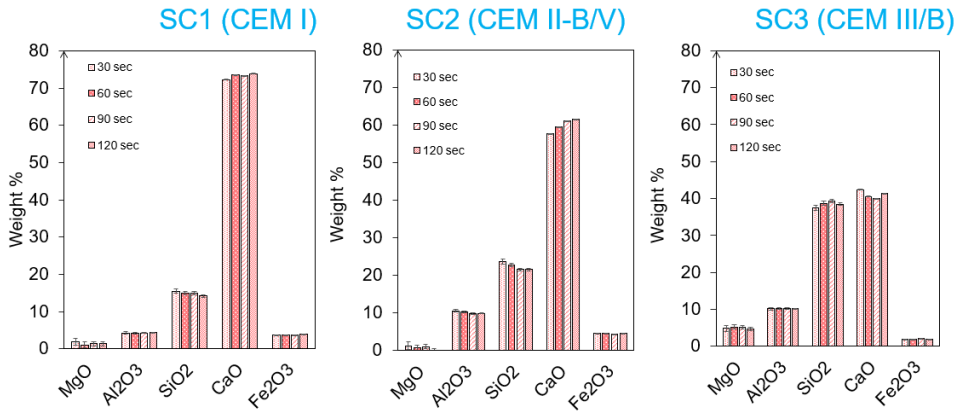

Figure 2.14: Effect of measurement duration on the chemical composition of dried concrete surfaces [15]

Finally, the study also concluded that it is possible to effectively differentiate between the composition of concrete on its surface, primarily consisting of cement paste, and its inner layers, which are composed of cement mortar and aggregates. SiO_2 and CaO serve as characteristic elements for making this distinction. It is noteworthy that the inner layers exhibit a considerably higher SiO_2 content compared to the surface, providing strong evidence for the siliceous nature of the aggregates used in concrete production.

On the other hand, Aoustin's research [10] investigated 14 different concrete mixes, incorporating various sizes of river gravel and three types of cementitious materials (CEM I 42.5N, fly ash, and ground granulated blast furnace slag). The analysis was performed using a Bruker S1 TITAN 800 handheld Energy Dispersive X-ray Fluorescence (hXRF) analyzer. The study aimed to show how hXRF can effectively distinguish concrete mixes based on their chemical composition. In this study, the impact of several factors influencing hXRF results, including measurement time, measurement pattern, moisture, surface carbonation, and the presence of aggregates on the surface (matrix effect), was assessed.

A 30-second analysis time was determined to be appropriate, as a longer measurement time did not yield more accurate results. It was concluded that the measurement pattern does not significantly impact the accuracy of the results. Therefore, measurements should be taken in a random pattern to save time. Regarding the other factors (moisture, surface carbonation, and matrix effect), it was found that they have the most significant impact. Lighter elements may be more affected by moisture due to the absorption of secondary X-rays by capillary water. In the case of surface carbonation, experiments showed an increase in the weight percentages of CaO, Fe_2O_3, and K_2O. The formation of calcium carbonate crystals at the surface justifies the increase in CaO. Ultimately, it was identified that the impact of the matrix is attributed to the composition of the concrete's outer layer, the presence of aggregates at the surface, and the pore system.

2.5.3. Quantification of Chloride Ion in Cement-based Materials

Several factors can contribute to the shortened service life of concrete structures. These factors include chemical attack, insufficient maintenance, alkali-silica reaction (ASR), freeze-thaw damage, steel reinforcement corrosion, and others. Steel reinforcement corrosion, for instance, is predominantly induced by the presence of chloride ions. The extent of chloride penetration depends on its ease of diffusion. When chlorides are present in sufficient concentration, known as chloride threshold or critical chloride content (C_{crit}), the passive layer on the surface of steel bars is destroyed [68]. As a result, it is important to identify the areas where the structure is affected by chloride ingress in order to repair it and avoid concrete and steel deterioration. Structural codes in Europe and North America aim to control the 'maximum' chloride concentration allowed in concrete infrastructure. Table 2.7 shows the maximum allowable chloride concentrations for fresh concrete.

Table 2.7: Chloride limits for fresh concrete, wt.% of cement [68]

Standard	wt.% cement	Conditions
ACI 222	0.2	reinforced concrete in dry conditions
	0.1	reinforced concrete in wet conditions
	0.08	prestressed concrete
BS8110	0.35	reinforced concrete
Eurocode	0.2-0.4	reinforced concrete
	0.1-0.2	prestressed concrete

Chinchón-Payá *et al.* [18] investigated the calibration of a handheld XRF analyzer to measure the concentration of chloride ions in cement-based materials. The study also aimed to explore its usage for in-situ assessment of chloride concentration on concrete structures surfaces.

The first step in the study involved laboratory calibration, which entailed comparing the readings of chloride concentration in mortar and concrete samples obtained using a handheld Olympus Innov-X Delta XRF analyzer with the results obtained from potentiometric titration of chloride ions. One potentiometric test was conducted and three hXRF measurements were taken per sample. In total, 91 samples were tested. Some of them were prepared with ordinary Portland cement (OPC) with known and unknown chloride content, while others were taken from cores that had been removed from the existing structure. Once the results were validated, it was found that using the end-point potentiometric value as an accurate measure, the correlation between the two analytical techniques was R^2=0.92 at a 90.0% confidence interval (Figure 2.15). Additionally, a calibration factor for hXRF of 1.16 was determined, meaning that the chloride concentration in the structure is equal to the reading of the portable device multiplied by 1.16 [18].

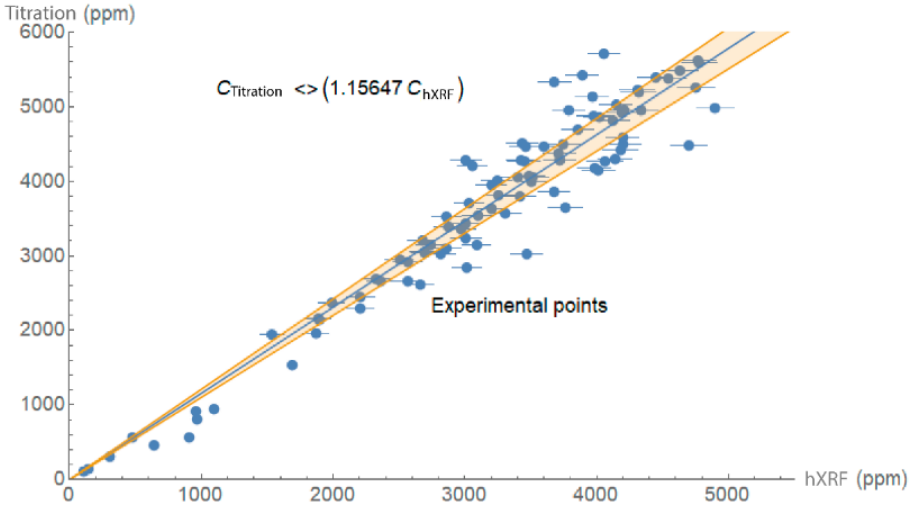

Figure 2.15: Chloride ions found by titration vs. chloride ions quantified by hXRF [18]

Substantial deterioration was observed in a concrete beam of the structure under study (see Figure 2.16a). The potential areas affected by corrosion were tested. For this purpose, electrochemical readings were taken using a GECOR device, which is corrosion analysis equipment. These readings included concrete resistivity, corrosion potential, and corrosion current density, allowing the assessment of the corrosion risk for the element. To identify areas with a high probability of corrosion, 19 points or measurements were taken (refer to Figure 2.16b). Subsequently, hXRF was utilized to identify and mark the concrete areas requiring repair based on an objective criterion. The applied criterion was the 0.4% chloride content threshold (by weight of cement) specified in the Spanish structural concrete code and the Eurocode 2.

(a) (b)

Figure 2.16: Concrete structure studied (a) Condition concrete structure analyzed (b) Points measured on the surface of the beam [18]

In the existing legislation, chloride concentration is expressed as a percentage of cement weight, whereas measurements obtained with the handheld analyzer were based on total sample weight. For the calculations, the cement content in reinforced concrete for structural members was assumed to be 275 kg/m^3. Therefore, by applying the chloride concentration threshold specified in the legislation and considering the critical chloride concentration value based on the sample weight, it was determined to be 990 ppm.

Finally, Figure 2.17 presents a corrosion probability diagram that was generated based on potential corrosion and resistivity mapping. The diagram illustrates different regions on the analyzed girder, indicating the likelihood of corrosion with low probability denoted in green, intermediate in yellow, and high probability in red. Additionally, Figure 2.17 displays the chloride concentration values and highlights the specific areas that were identified for rehabilitation. The diagram also showcases the initial target for rehabilitation as well as the actual area that underwent repairs based on the findings of this study [18].

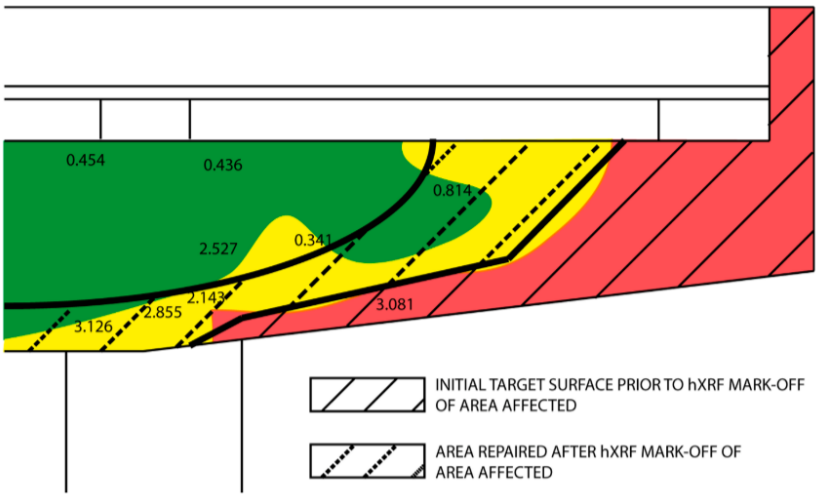

Figure 2.17: Electrochemical mapping and chloride concentration in wt% cement [18]

According to this study, it appears that handheld XRF can be effectively employed for quantifying chloride concentrations on the surfaces of concrete structural members. It is worth noting that the specific type of hXRF used in this study may be employed in either an Ag, Au, or Ta anode X-ray tube. The X-ray tube anode material matters. Using a rhodium (Rh) anode X-ray tube can make chloride quantification difficult due to the overlap between Cl K-shell and Rh L-shell X-ray emissions unless a filter [69] or mathematical algorithm is used. However, the study does not mention such measures.

2.6. Research needs

The major component of any selective demolition project should be concerned with the evaluation of the concrete quality, chemical composition, and mechanical properties, in the structure. Since no previous experience is available with in situ concrete chemical composition testing methods, handheld XRF has been proposed for this purpose based on previous research on rocks [70]. Concrete can be seen as an artificial rock. To develop an appropriate non-destructive testing strategy for the chemical composition of concrete, an assessment of concrete surfaces should be first conducted in the laboratory to identify and determine the key parameters of influence for concrete surface non-destructive testing and to evaluate the feasibility of using the handheld XRF method.

Several aspects must be given careful consideration in order to obtain accurate hXRF measurements of the elements present in the samples and be able to identify cement type, aggregate type used, and level of contamination of the concrete. Therefore, the following matters should be investigated:

- The effect of various environmental conditions, such as a wide range of relative humidities (RH), and carbonation, on hXRF measurements in cement paste, mortar, and/or concrete level.
- The effect of varying water-to-cement ratios on hXRF analysis of the chemical composition of cement paste, mortar, and/or concrete surface.
- Analysis of the impact of concrete aging on chemical composition analysis with hXRF.
- The influence of the presence of coatings or paint on the concrete surface on hXRF measurements.
- Investigation on the detection level of chlorides with hXRF.
- Identification and specification of the range of concrete's characteristic oxides to be able to classify concrete by cement type.
- Procedure that can be followed to perform elemental composition analysis in-situ of concrete structures with hXRF.

3

Experimental program

This chapter describes the materials used in this research work and provides a detailed description of the mix design and sample preparation for cement paste and concrete samples, the methods employed for chemical composition analysis (hXRF, WD-XRF, ESEM-EDS), and the details of the defined Test Series.

The experimental program consisted of Four Test Series: (1) testing the chemical composition of cement paste and concrete mixtures with different water-to-cement (w/c) ratios ranging from 0.35 to 0.76; (2) testing the chemical composition of paste and concrete after curing for 1 day, 14 days, and 28 days; (3) testing paste and concrete chemical composition under varying surface relative humidities (RH) of 0%, 40%, 60%, 75%, and 95%; (4) testing the chemical composition of paste and concrete, which were subjected to accelerated carbonation.

3.1. Materials

The following materials were used for the production of the cement paste specimens: CEM I 42.5 (Portland cement), CEM III/B 42.5 (GGBFS), and water.

The concrete specimens were produced using the following materials: CEM I 42.5 N (Portland cement), CEM III/B 42.5 (GGBFS cement), river sand (0-4 mm), gravel (4-16 mm), and water.

The selection of the cement types was motivated by the following reason:

- According to a report from CE Delft [71], which details the distribution of cement types in total concrete production in the Netherlands, the most commonly used types in 2017 were CEM III/B, CEM I, and CEM III/A.

To achieve relative humidity (RH) conditions of 60% and 75%, the following salts were used: sodium bromide (NaBr) and sodium chloride (NaCl).

3.2. Cement Paste Production

3.2.1. Mix design

For Test Series 1, the mixtures had different water-to-cement (w/c) ratios of 0.35, 0.38, 0.42, 0.48, 0.54, 0.63, and 0.76. In Test Series 2, Test Series 3, and Test Series 4 cement paste was cast with a w/c ratio of 0.54 (M3).

Table 3.1: Proportions of paste mixtures (g)

	Cement paste mixtures						
	M1	M2	M3	M4	M5	M6	M7
w/c	0.76	0.63	0.54	0.48	0.42	0.38	0.35
Water	100	100	100	100	100	100	100
CEM I 42.5N (CEM III/B 42.5N)	132	159	185	208	238	263	286

3.2.2. Sample preparation

The cement and water were mixed until the paste appeared homogeneous. Subsequently, the paste was cast into molds with a 50 mm diameter (Figure 3.1) and thickness of about 10 to 15 mm. For each mixture, three disks were cast. To prevent the paste from adhering, the molds were greased with a release agent. Then, the molds were gently shaken to eliminate any trapped air.

Figure 3.1: Casting cement paste disks

The samples were demolded seven days after casting. To prepare for the subsequent experiments, using Struers LaboPoL-60 grinding and polishing machine samples were ground to remove any remnants of the release agent and to flatten the surfaces. The grinding process for each grain size (P-grade 220 and P-grade 320) involved approximately one minute of grinding for each face of the paste disk, followed by cleaning with an ultrasonic cleaner after each step. After grinding, the samples were submerged in ethanol in order to dry them.

(a) Disk before grinding **(b)** Disk after grinding

Figure 3.2: Cement paste disk appearance before and after grinding

Ultimately, the paste disks were labeled as shown in Table 3.2, Table 3.3, Table 3.4, and Table 3.5 depending on their Test Series. In Test Series 1, the paste disks were produced using CEM III/B 42.5

N. In Test Series 2, the sample M3-1 from Test Series 1 was used for the hXRF measurements. For Test Series 3 and 4, the paste disks were cast using both CEM I 42.5 N and CEM III/B 42.5 N.

Table 3.2: Labeling paste specimens for Test Series 1

CEM III/B 42.5 N	M1-1	M2-1	M3-1	M4-1	M5-1	M6-1	M7-1
	M1-2	M2-2	M3-2	M4-2	M5-2	M6-2	M7-2
	M1-3	M2-3	M3-3	M4-3	M5-3	M6-3	M7-3

Table 3.3: Labeling paste specimens for Test Series 2

CEM III/B 42.5 N	M3-1

Table 3.4: Labeling paste specimens for Test Series 3

	0%	40%	60%	75%	95%
CEM I 42.5 N	M3-1	M3-1	M3-1	M3-1	M3-1
	M3-2	M3-2	M3-2	M3-2	M3-2
	M3-3	M3-3	M3-3	M3-3	M3-3
CEM III/B 42.5 N	M3-1	M3-1	M3-1	M3-1	M3-1
	M3-2	M3-2	M3-2	M3-2	M3-2
	M3-3	M3-3	M3-3	M3-3	M3-3

Table 3.5: Labeling paste specimens for Test Series 4

CEM I 42.5 N	M3-1
	M3-2
	M3-3
CEM III/B 42.5 N	M3-1
	M3-2
	M3-3

3.3. Concrete Production

3.3.1. Mix design

The consistency class was selected with a slump of 100 mm to 150 mm according to NEN-EN 206+NEN 8005:2017. Therefore, the water content was equal to 190 kg/m^3. The volume of air was considered to occupy 2% of the total concrete volume. Table 3.6 shows seven different concrete mix designs (M1-M7) used in this study.

For Test Series 1, the mixtures had different water-to-cement (w/c) ratios of 0.35, 0.38, 0.42, 0.48, 0.54, 0.63, and 0.76. In Test Series 2, Test Series 3, and Test Series 4 concrete cubes were cast with a w/c ratio of 0.54 (M3).

Table 3.6: Proportions of concrete mixtures (kg/m^3)

	Concrete mixtures						
	M1	M2	M3	M4	M5	M6	M7
w/c	0.76	0.63	0.54	0.48	0.42	0.38	0.35
Water	190	190	190	190	190	190	190
CEM I 42.5N (CEM III/B 42.5N)	250	300	350	400	450	500	550
Sand 0-4 mm	841	821	801	780	760	740	720
Gravel 4-16 mm	1028	1003	978	954	929	904	880

3.3.2. Sample preparation

The raw materials were placed in a 40 L mixer in the specified sequence: coarse aggregates, fine aggregates, cement, and water. The sand and gravel were mixed for 1 minute. Then, the cement was added, and the mixture was further mixed for 1 minute. Finally, the water was added, and all components were mixed for an additional 3 to 5 minutes, depending on the desired consistency of the mixture.

The concrete cubes were cast into moulds 150 × 150 ×150 mm³. For each mixture three cubes were cast, Cube 1 (C1), Cube 2 (C2), and Cube 3 (C3). The molds were oiled before casting in order to prevent the paste from adhering. Next, the molds were placed on a compaction table, and the concrete was poured into two layers. After filling the molds halfway, they were compacted for 10 seconds to eliminate trapped air. Following this step, the smooth surface of the fresh concrete was leveled using a straight edge.

The samples were demolded 24 hours after casting. In order to proceed with the first set of experiments (Test Series 1), seven concrete cubes (one cube from each mix) were used. The rest of the samples were wrapped in a plastic film, and placed inside large plastic bags. Then, cubes were stored in a room maintained at a temperature of 20 °C and relative humidity of 50% (see Figure 3.3), until they were needed for the tests. The decision to wrap the concrete specimens in plastic film and store them in large plastic bags was made to prevent surface efflorescence.

(a) (b) (c)

Figure 3.3: Demolding and wrapping of concrete cubes (a) After casting, (b) Wrapping of the specimens with the plastic film, (c) Placing samples in plastic bags

In order to conduct measurements for Test Series 1 using handheld X-ray fluorescence (hXRF), Wavelength-Dispersive X-ray Fluorescence (WD-XRF) and Environmental Scanning Electron Microscope and Energy-Dispersive X-ray Spectroscopy (ESEM-EDS), it was necessary to reduce the size of the concrete cubes. As a result, lines were drawn on two surfaces of each concrete cube using a carbon pencil to indicate where to make cuts in order to obtain smaller concrete specimens (Figure 3.4). For Test Series 1, the specimens M1-SI-1, M2-SI-1, M3-SI-1, M4-SI-1, M5-SI-1, M6-SI-1, and M7-SI-1 (see Table 3.7), and the specimens of Test Series 2 had dimensions of 30 mm × 30 mm × 20 mm. For the rest of the specimens of Test Series 1, and Test Series 3 and 4 specimens of 50 mm × 50 mm × 20 mm were used.

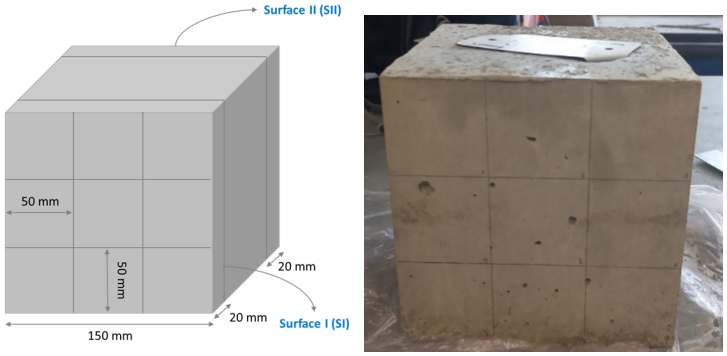

(a) (b)

Figure 3.4: Guidelines for cutting concrete cube (a) Schematic concrete cube, (b) Real cube

The specimens were cut using two different saws. The first saw, depicted in Figure 3.5a, with a blade thickness of 3 mm, was used to cut the two surfaces (SI and SII) from each cube. The second saw, shown Figure 3.5b, with a blade thickness of 1 mm, was used to cut the smaller cubes. Both cutting sessions were conducted under wet conditions for safety reasons. Dry cutting results in the release of a significant amount of dust into the air.

After cutting, the samples were first submerged in ethanol for approximately 10 seconds and then dried with compressed air (about 20 seconds per sample), see Figure 3.6a. However, it was observed that some parts of the samples remained wet. Consequently, the decision was to place the specimens in an oven at 105 °C for only 15 minutes to prevent any potential cracking on the surfaces but to ensure that the sample surfaces were thoroughly dried (Figure 3.6b).

Finally, the samples were labeled as shown in Table 3.7, Table 3.8, Table 3.9, and Table 3.10 depending on their test series.

In Test Series 1, the concrete cubes were produced using CEM III/B 42.5N, and three size-reduced concrete samples (1, 2, and 3) were taken from C1 for each mixture, specifically for the hXRF measurements. For the measurements using WD-XRF and ESEM-EDS only sample 1 from each mixture

(a) (b)

Figure 3.5: Saws used for preparing hXRF, WD-XRF, and ESEM-EDS concrete samples (a) Saw used to cut the cube surfaces, (b) Saw used to cut the concrete cubes 50 mm x 20 mm x 50 mm and 30 mm x 20 mm x 30 mm

(a) (b)

Figure 3.6: Drying set up (a) Ethanol, (b) Oven

was tested.

In Test Series 2, the sample M3-SI-1 from Test 1 was used for the hXRF measurements.

In Test Series 3, the concrete cubes were cast using both CEM I 42.5N and CEM III/B 42.5N. Three size-reduced concrete samples (1, 2, and 3) were taken from either C1 or C2 and used for hXRF measurements.

In Test Series 4, the concrete cubes were cast using both CEM I 42.5N and CEM III/B 42.5N. Three size-reduced concrete samples (1, 2, and 3) were taken from C2 and used for hXRF measurements.

Table 3.7: Labeling concrete specimens for Test Series 1

CEM III/B 42.5 N	M1-SI-1	M2-SI-1	M3-SI-1	M4-SI-1	M5-SI-1	M6-SI-1	M7-SI-1
	M1-SI-2	M2-SI-2	M3-SI-2	M4-SI-2	M5-SI-2	M6-SI-2	M7-SI-2
	M1-SI-3	M2-SI-3	M3-SI-3	M4-SI-3	M5-SI-3	M6-SI-3	M7-SI-3

Table 3.8: Labeling concrete specimens for Test Series 2

CEM III/B 42.5 N	M3-SI-1

Table 3.9: Labeling concrete specimens for Test Series 3

	0%	40%	60%	75%	95%
CEM I 42.5 N	M3-C2-SII-1 M3-C2-SII-2 M3-C2-SII-3	M3-C2-SII-1 M3-C2-SII-2 M3-C2-SII-3	M3-C1-SI-1 M3-C1-SI-2 M3-C1-SI-3	M3-C2-SII-1 M3-C2-SII-2 M3-C2-SII-3	M3-C2-SII-1 M3-C2-SII-2 M3-C2-SII-3
CEM III/B 42.5 N	M3-C2-SII-1 M3-C2-SII-2 M3-C2-SII-3	M3-C2-SII-1 M3-C2-SII-2 M3-C2-SII-3	M3-C1-SII-1 M3-C1-SII-2 M3-C1-SII-3	M3-C1-SII-1 M3-C1-SII-2 M3-C1-SII-3	M3-C1-SII-1 M3-C1-SII-2 M3-C1-SII-3

Table 3.10: Labeling concrete specimens for Test Series 4

CEM I 42.5 N	M3-C2-SII-1 M3-C2-SII-2 M3-C2-SII-3
CEM III/B 42.5 N	M3-C2-SI-1 M3-C2-SI-2 M3-C2-SI-3

3.4. Methods

3.4.1. Bruker S1 Titan 800 hXRF

For this thesis, a Bruker S1 Titan 800 handheld X-ray Fluorescence (hXRF) analyzer was utilized. It is a portable device, designed and used for non-destructive element analysis of various materials. It features a Rhodium (Rh) target X-ray tube with a power rating of 4W, a high-performance graphene Silicon Drift Detector (SDD) with a resolution of 145 eV, a five-position automatic filter changer, a digital pulse processor, and a color touchscreen LCD as shown in Figure 3.7a and Figure 3.10b. It weighs 1.5 kg including the Li-Ion rechargeable battery [72].

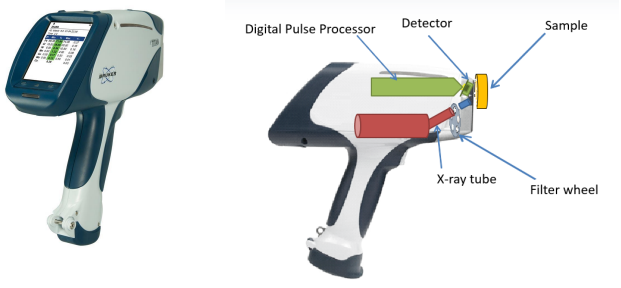

(a) (b)

Figure 3.7: (a) Bruker S1 Titan 800 hXRF, (b) Parts of hXRF

The X-ray tube consists of five components: a cathode, an anode, an envelope, a housing, and a window. These components work together to generate X-rays with specific energy while also controlling the heat and excess radiation produced by the anode [10]. The X-ray tube emits an X-ray beam at a 45-degree angle from the center of the analyzer's tip, with an adjustable power range from 6 to 50 kV [15]. This X-ray tube can produce a standard spot size of 8 mm, with optional sizes of 5 mm or 3 mm. The equipment used includes a 5 mm X-ray beam spot size and is capable of measurements ranging from 10 to 300 seconds [72] [10]. The SDD is composed of six different parts: a collimator assembly, an electron trap, a window, a sensor, a Field Effect Transistor (FET), and a detector cooling system. The detector converts the energy of the X-rays emitted by the sample into a voltage signal of proportional size. Subsequently, the electronics associate the elements with the received signals [10]. Despite the option to use filters for enhanced element detection, this study chose not to do so. Previous findings have reported more precise measurements without filters, especially when analyzing historical mortars resembling concrete [66].

A wide range of calibration options is available for the S1 TITAN to address various common applications (alloy identification and quality control, scrap metal recycling, precious metals, wear metals in oil, mining, environmental consumer safety, and others). Calibrations can be customized to precisely meet specific requirements, with the available calibrations depending on the instrument model. Some typical calibration examples include alloy analysis, precious metals, food quality, and limestone (to analyze raw and prepared limestone, cement, and gypsum) [73].

Calibration is a process that converts the count rate of elements into weight percentages of associated oxides. Each material needs a specific calibration due to its chemical composition and matrix differences. To create the calibration model, chemical composition measurements are taken from certified reference materials with known compositions. The count rate of each element is linked to the weight percentage of the corresponding oxide. Only the oxides present in the standard calibration sample will be detected and quantified in the associated mode. The $Bruker^{TM}$ calibration for cement mode is based on samples with a similar chemical composition to the one being analyzed. The cement calibration method includes elements and their analysis ranges that are characteristic of cementitious materials (MgO, Al_2O_3, SiO_2, P_2O_5, SO_3, K_2O, CaO, TiO_2, MnO, Fe_2O_3) [10][15], which is available in the hXRF device used in this study.

The composition analysis of the cement paste and concrete samples was carried out considering an accelerating voltage set at 15 keV. For measurement time, it was decided to set it at 30 seconds, following recommendations from previous studies that found this duration to be suitable for concrete analysis [10][15][16].

The hXRF device was attached to its portable test stand. To ensure that the samples were consistently placed in the same position for each test, guiding lines were drawn, as depicted in Figure 3.8. In Figure 3.9, an example of the hXRF setup is shown. Once each sample was positioned, 10 consecutive measurements were taken without moving or lifting the sample between measurements.

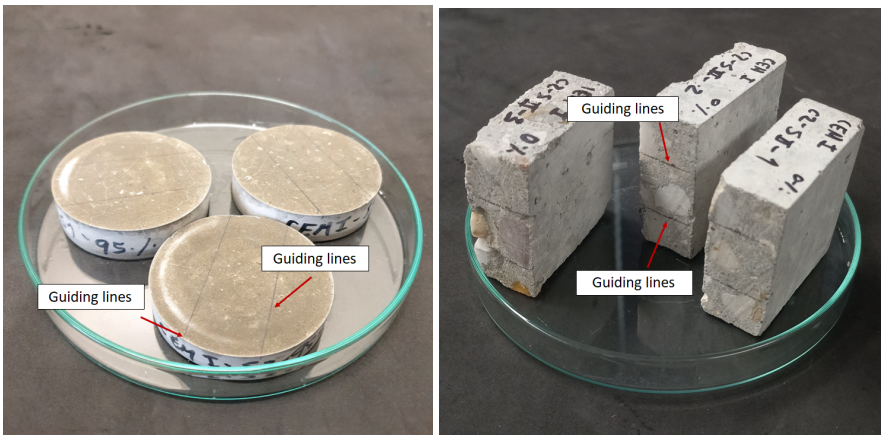

(a) Paste **(b)** Concrete

Figure 3.8: Guiding lines for placement of paste and concrete samples on the hXRF test stand

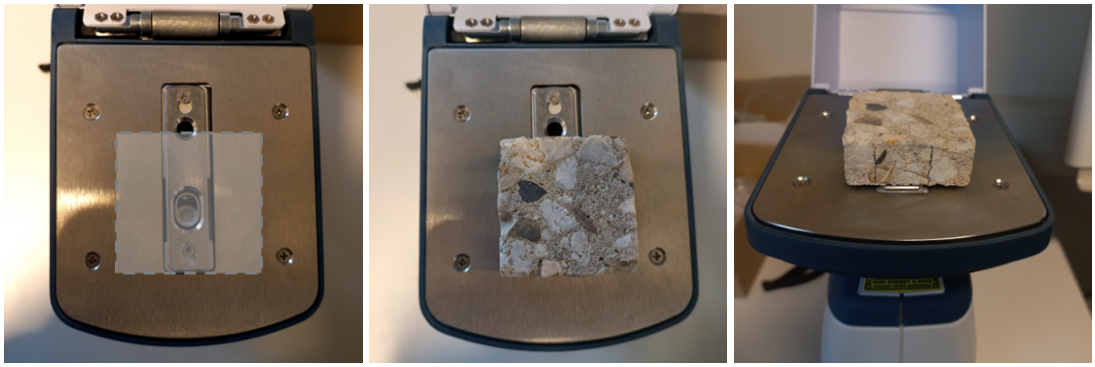

Figure 3.9: hXRF setup and placement of concrete sample

3.4.2. WD-XRF

Samples were also analyzed using a Panalytical Axios Max Wavelength Dispersive X-ray Fluorescence (WD-XRF) spectrometer with an X-ray tube power of 4 kW (Figure 3.10). This instrument features an X-ray tube that serves as the source to irradiate the sample. The resulting fluorescence emitted by the sample is detected using a wavelength-dispersive system. Analyzing crystals are components used to separate X-rays based on their wavelengths or energies, enabling the identification of each element's characteristic radiation. This analysis can be conducted either sequentially, measuring X-ray intensities at various wavelengths one by one, or simultaneously, where X-ray intensities at different wavelengths are measured all at once [74].

(a) WDXRF **(b)** Sample in the WD-XRF

Figure 3.10: WD-XRF

3.4.3. ESEM-EDS

The ESEM-EDS analysis was performed with a Thermo Fisher™ Ultradry EDS detector (Figure 3.11). It operates with an energy beam ranging from 6 to 50 kV and has a beam size of 125 µm, which can be reduced to analyze a smaller area. Unlike hXRF, the ESEM-EDS can work in a vacuum and uses a windowless Silicon Drift Detector (SDD) that provides high-resolution detection for lighter elements like Beryllium (Be), with a resolution of 129 eV. The analysis was performed at an accelerating voltage of 15 keV. To analyze the chemical composition of concrete, elements associated with expected concrete oxides (MgO, Al_2O_3, SiO_2, P_2O_5, SO_3, K_2O, CaO, TiO_2, MnO and Fe_2O_3) were selected in the ESEM-EDS software.

To ensure that the area analyzed with hXRF was the same for the ESEM-EDS analysis, lines were drawn to delineate the analysis area (see Figure 3.12).

The area analyzed in each paste and concrete sample by hXRF, WD-XRF, and ESEM-EDS is shown in Figure 3.13a and Figure 3.13b. On one hand, the size of the area analyzed with hXRF was a disc with

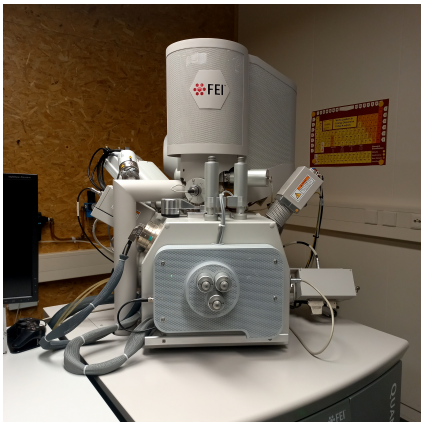

Figure 3.11: ESEM-EDS

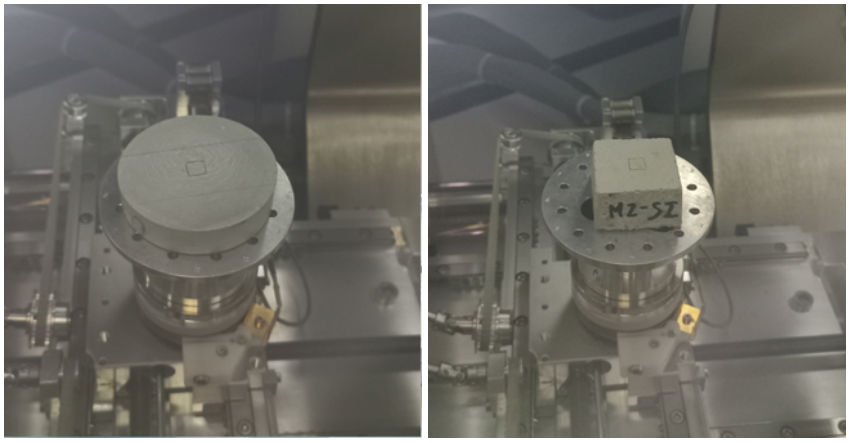

(a) Paste **(b)** Concrete

Figure 3.12: Placement of paste and concrete sample in the ESEM-EDS and analysis area contour

a diameter of 5 mm, corresponding to the size of the X-ray beam emitted by the device. On the other hand, the area examined with WD-XRF corresponded to a diameter of 27 mm. Finally, the area under analysis with ESEM-EDS was a rectangle measuring 3.3 mm × 2.2 mm, observed at a magnification of 125×.

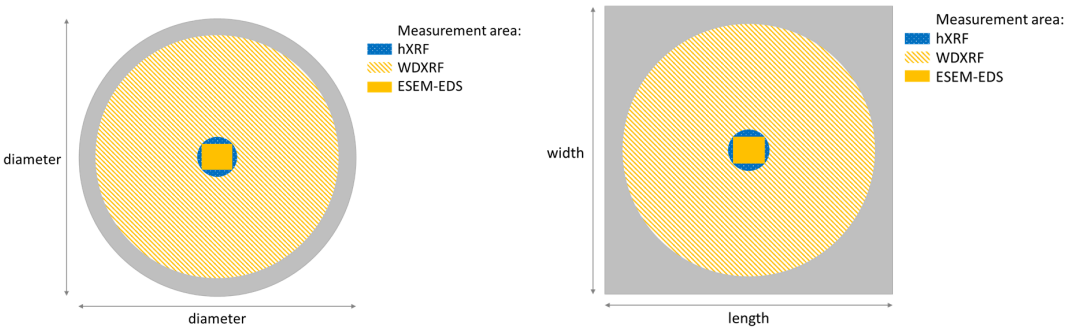

(a) Paste **(b)** Concrete

Figure 3.13: Measurement areas with hXRF, WD-XRF, and ESEM-EDS

3.5. Specifications Test Series to determine the impact of different parameters on hXRF measurements

Concrete structures have been exposed to various environmental conditions in the field for many years. Therefore, before conducting in-situ measurements, it is important to investigate whether factors such as carbonation and surface moisture affect the chemical composition or oxide concentrations of the concrete. It should be noted that some of these factors may potentially influence the element analysis measurements. Additionally, concrete chemistry was analyzed by producing mixes with different water-to-cement (w/c) ratios and cement types (CEM I and CEM III/B). As mentioned before, the tests were carried out using hXRF, and some of the experiments were supported through comparison with WD-XRF and ESEM-EDS. By conducting laboratory experiments valuable insights could be gained regarding the oxide concentrations of concrete, the most influential factors in hXRF measurements, and other necessary parameters. The next sections provide a detailed explanation of the Test Series specifications.

3.5.1. Test Series 1: Effect of different water-to-cement ratio

Once the specimens were dried, those intended for this Test Series were taken for the analysis of their surface chemical composition using hXRF.

Subsequently, the paste specimens M1-1, M2-1, M3-1, M4-1, M5-1, M6-1, M7-1, and the concrete specimens M1-SI-1, M2-SI-1, M3-SI-1, M4-SI-1, M5-SI-1, M6-SI-1, and M7-SI-1, were selected for the element analysis using WD-XRF, performed seven days after the initial hXRF measurements. Testing with ESEM-EDS was carried out a day after tests with WD-XRF. Between testing periods, the samples were stored in zipper bags as shown in Figure 3.14 within a vacuum chamber to minimize efflorescence at the concrete surface.

(a) Paste **(b)** Concrete

Figure 3.14: Samples Test Series 1

3.5.2. Test Series 2: Effect of curing age

For this Test Series, the paste sample M3-1 and concrete sample M3-S-1 from Test Series 1 were used. The measurements conducted with hXRF during Test Series 1 provided results for day 1, and then measurements were performed at 14 days and 28 days. The samples were stored in the vacuum chamber during periods when testing was not being conducted.

3.5.3. Test Series 3: Effect of relative humidity

For this Test Series, various setups (Figure 3.15) were defined to create the necessary environmental conditions for conducting this experiment. Table 3.11 displays the equipment or materials used, along

with the temperatures and relative humidities considered in this Test Series.

(a) Oven

(b) Climate chamber

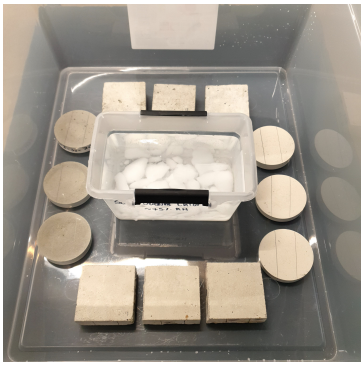

(c) Salt-saturated solution

(d) Curing room

Figure 3.15: Setups Test Series 3

Table 3.11: Specifications Test Series 3

RH	0%	40%	60%	75%	95%
Equipment/ materials used	Oven	Climate chamber	Salt-saturated solution sodium bromide (NaBr)	Salt-saturated solution sodium chloride (NaCl)	Curing room
Temp.	40 °C	20 °C	20 °C	20 °C	20 °C

Once the samples were dried, it is worth noting that hXRF measurements were conducted for all the samples before their exposure to different environmental conditions, serving as the reference values.

As found in the literature [75], to achieve a relative humidity (RH) of 60% and 75%, the salts sodium bromide (NaBr) and sodium chloride (NaCl) can be respectively used. Therefore, salt-saturated solutions were prepared with these salts and placed in plastic containers. To ensure and monitor the desired RH levels, an EL-USB-2 Humidity-Temperature Datalogger was placed in the containers for 24 hours. The graphs obtained from the sensor for 60% and 75% RH can be seen in Figure 3.16 and Figure 3.17. It was considered that the samples were in equilibrium with their environment or had reached the respective relative humidity when their weight remained almost the same for two consecutive days. The samples were estimated to have reached the desired relative humidity after approximately 10-13 days. After this period, the hXRF measurements were performed again.

ESEM-EDS measurements were taken from the samples (CEM I M3-1, CEM III/B M3-1, CEM I M3-C2-SII-1, CEM I M3-C1-S1-1, CEM III/B M3-C2-SII-1, and CEM III/B M3-C1-SII-1) that were exposed in the 0%, 60%, and 95% RH. These measurements were performed 15 days after the last hXRF measurements.

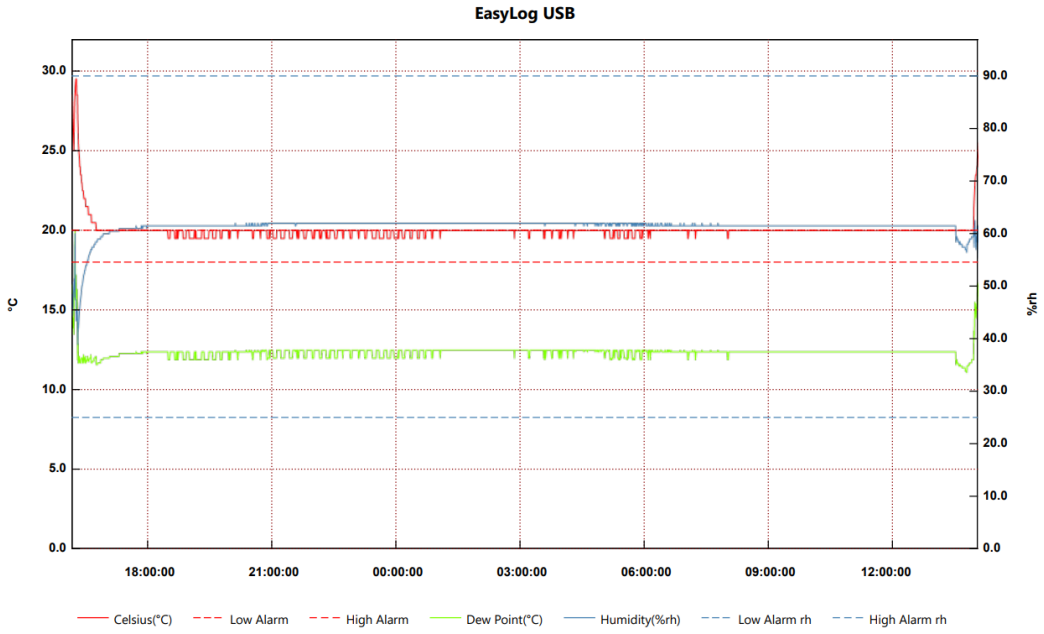

Figure 3.16: Monitoring relative humidity 60%

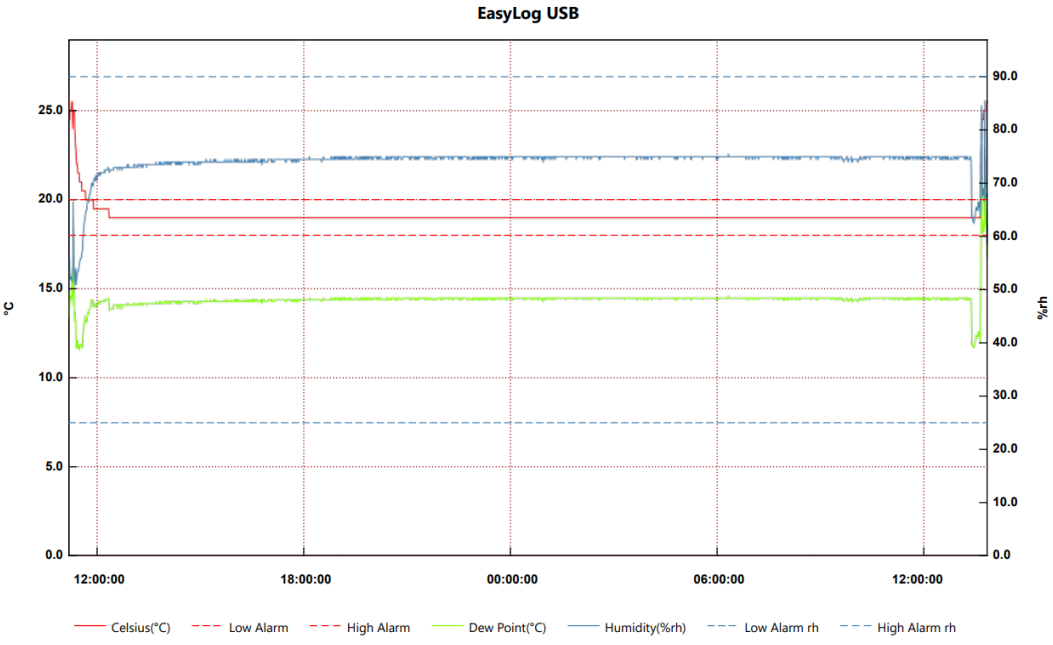

Figure 3.17: Monitoring relative humidity 75%

3.5.4. Test Series 4: Effect of carbonation

Once the samples intended for this Test Series were dried, they were initially tested with the hXRF. Then, they were placed in plastic containers, as shown in Figure 3.18a, and transferred into a carbonation chamber (Figure 3.18b). The chamber maintained a relative humidity (RH) of 60%, a carbon dioxide (CO_2) concentration of 1% volume/volume (v/v), and a temperature of 20°C.

(a) **(b)**

Figure 3.18: (a) Samples for carbonation Test and (b) Carbonation chamber

Initially, all the samples were exposed to accelerated carbonation for seven days. On the seventh day, two paste disks and two concrete samples (CEM I M3-1, CEM III/B M3-1, CEM I M3-C2-SII-1, and CEM III/B M3-C2-SI-1) were collected, broken into pieces, and sprayed with the phenolphthalein indicator—a pH indicator that changes color within a specific pH range. This step aimed to verify the carbonation depth; phenolphthalein is colorless in acidic solutions and turns pink or red in basic solutions.

Observations revealed partial carbonation of the concrete surface or only a few millimeters of carbonation depth, particularly in CEM I-cast samples. Consequently, it was decided to leave the rest of the samples for an additional 15 days to ensure that all the samples were fully carbonated or nearly fully carbonated. On the 15th day, the phenolphthalein method was employed once more to assess the depth of carbonation in the samples.

In Figure 3.19a, for instance, it can be seen that the cement paste disk cast with CEM I was almost carbonated (pink color indicates noncarbonated zone; if there are no signs of pink color, it means that the sample is carbonated, as seen in the case of CEM III/B Paste in Figure 3.19c). With this verification, the remaining carbonated samples (CEM I M3-3, CEM III/B M3-3, CEM I M3-C2-SII-3, and CEM III/B M3-C2-SI-3) were used for the final hXRF measurements.

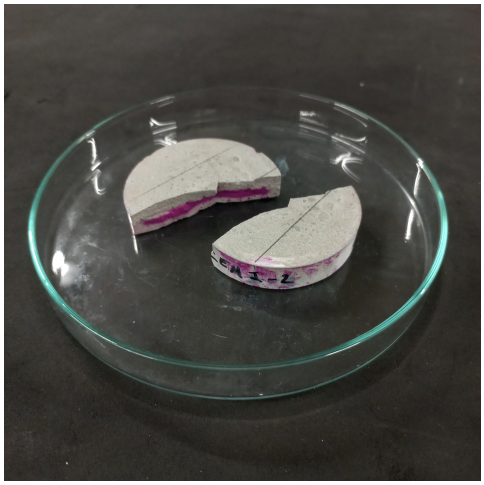

(a) CEM I Paste

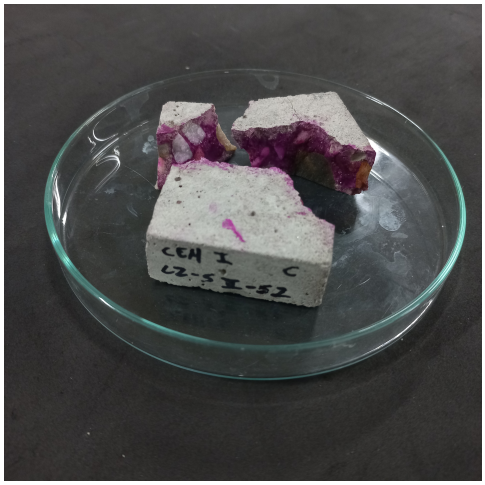

(b) CEM I Concrete

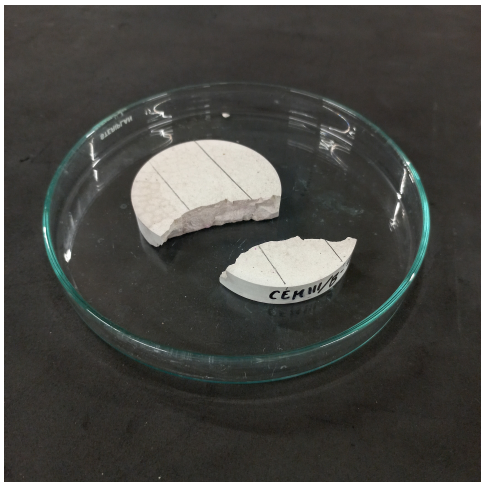

(c) CEM III/B Paste

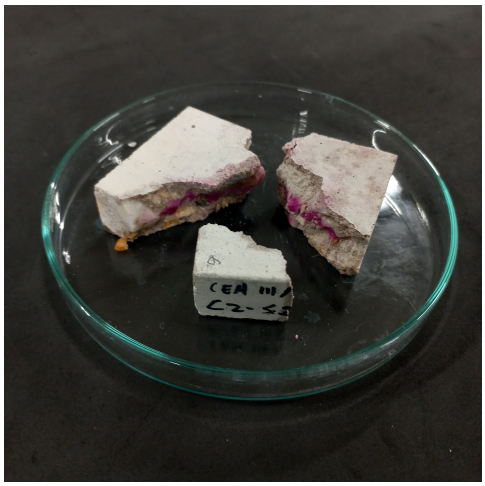

(d) CEM III/B Concrete

Figure 3.19: Paste and concrete samples after 15 days of accelerated carbonation

4

Experimental results and discussion

As mentioned in chapter 2, previous studies have explored the potential use of handheld XRF analyzers to assess the chemical composition of powder materials, such as river sand, cement, fly ash, cement paste, mortar, and hardened concrete. These studies have also investigated the quantification of chloride concentration in concrete, as well as the factors that can influence the results obtained with handheld XRF, including measurement time, acquisition pattern, moisture, surface carbonation, and matrix effect [10][15][16][17].

No previous studies have assessed the impact of varying water-to-cement (w/c) ratios, curing ages, exposure to diverse relative humidities, and carbonation on paste and concrete mixes. It is hypothesized that the concentrations of characteristic oxides (MgO, Al_2O_3, SiO_2, SO_3, CaO, Fe_2O_3) in both paste and concrete surfaces, as determined by chemical analysis using handheld XRF, will remain consistent regardless of changes in w/c ratios, curing time, relative humidity, and carbonation. This chapter presents the results obtained from the analysis of these factors in the four-Test Series.

4.1. Effect of different water-to-cement ratio

Portland cement is prepared by grinding Portland cement clinker with one or more forms of calcium sulfate, usually gypsum. The chemical composition of Portland cement involves both major and minor oxides. The main relevant oxides are CaO, SiO_2, Al_2O_3 and Fe_2O_3, whereas the minor oxides include MgO, SO_3, and some alkali oxides (K_2O and Na_2O) and sometimes the inclusion of other compounds, P_2O_5, TiO_2, MnO, and so forth [76].

In the case, of blast furnace cements CEM III, in addition to Portland cement clinker, it contains between 36 and 95% mass of Ground granulated blast furnace slag (GGBFS). The slag contains the same oxides (SiO_2,Al_2O_3, CaO) that make up Portland cement but in different proportions [77].

The main relevant oxides form different mineral phases or compounds, including tricalcium silicate (C_3S, or alite), dicalcium silicate (C_2S, or belite), tricalcium aluminate (C_3A, or celite), and tetracalcium aluminoferrite (C_4AF), or brownmillerite). When cement is mixed with water, it undergoes a chemical reaction known as hydration. During this process, hydration products are formed, including calcium silicate hydrate (C-S-H) gel, calcium hydroxide (CH), and ettringite. These products play a crucial role in determining the strength and durability of concrete. Therefore, different water-to-cement ratios in cement paste or concrete mix design affect properties such as workability and strength. It influences the amount of water available for the hydration reactions, the porosity, and the density of the material [78]. It is hypothesized that there is no change in the chemical composition of cement paste or concrete when different water-to-cement ratios are used. The chemical reactions during hydration involve cement compounds and water, without altering the original chemical composition of the cement. The fundamental composition of the cement paste and concrete surface primarily depends on the composition of the clinker used to produce the cement.

Figure 4.1, Figure 4.2, Figure 4.3, Figure 4.4, Figure 4.5, and Figure 4.6 provide information about the weight percentage (y-axis) on the different major chemical elements of the paste and concrete samples which were cast with different w/c ratios (x-axis). The bar plots representing the minor oxides can be found in the Appendix A.

It is noteworthy that in the paste samples, the element concentrations remained consistent regardless of the w/c and the sample tested. This observation supports the hypothesis and confirms the reproducibility of the handheld XRF measurements.

In the case of concrete, slight fluctuations were observed among the samples, which can be attributed to the impact of matrix heterogeneity, as discussed in [10], rather than being a result of variations in the mix design. Concrete surfaces can be categorized into three distinct types: surfaces occupied only by paste, surfaces where aggregates are present, and surfaces with the presence of voids. The presence of aggregates in the paste leads to higher concentrations of SiO_2 when compared to the silica content of pure paste. By comparing Figure 4.3a with Figure 4.3b, it becomes evident that there is an increase in silica content on the concrete surface compared to the paste. This increase appears to directly impact the weight percentage of CaO oxide and some of the lighter elements. This effect is due to the normalization of the oxides to achieve a total weight percentage of oxides equal to 100%.

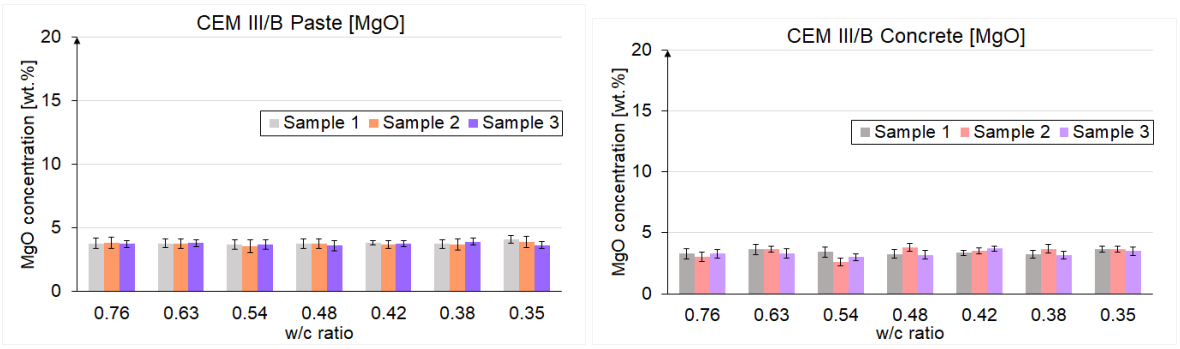

(a) CEM III/B Paste

(b) CEM III/B Concrete

Figure 4.1: Chemical composition analysis [MgO] with hXRF on paste and concrete surfaces with different w/c ratios

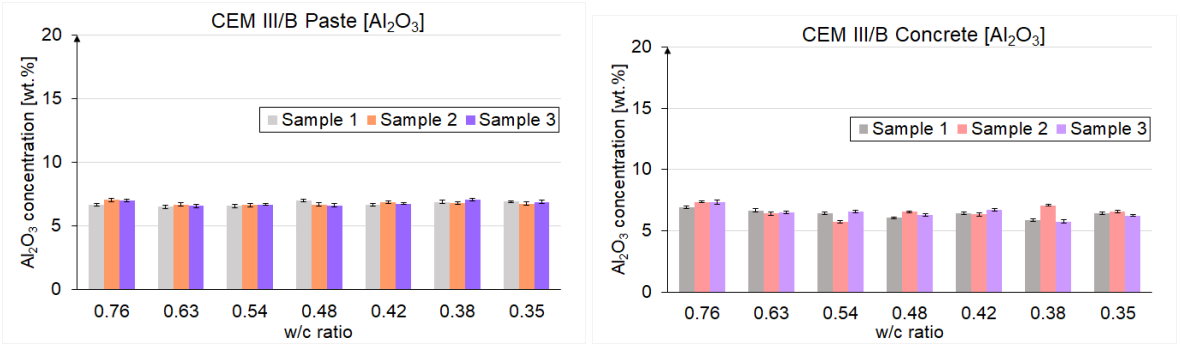

(a) CEM III/B Paste

(b) CEM III/B Concrete

Figure 4.2: Chemical composition analysis [Al_2O_3] with hXRF on paste and concrete surfaces with different w/c ratios

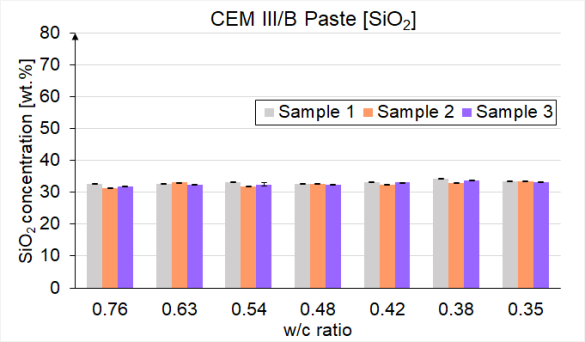

(a) CEM III/B Paste

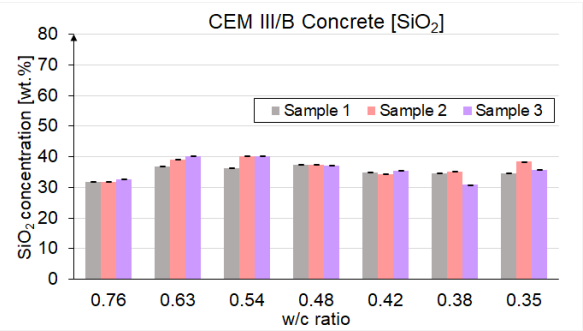

(b) CEM III/B Concrete

Figure 4.3: Chemical composition analysis [SiO_2] with hXRF on paste and concrete surfaces with different w/c ratios

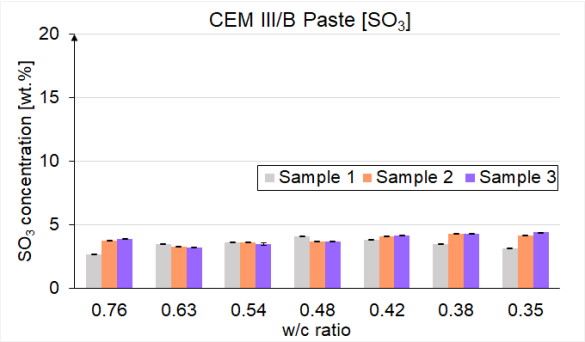

(a) CEM III/B Paste

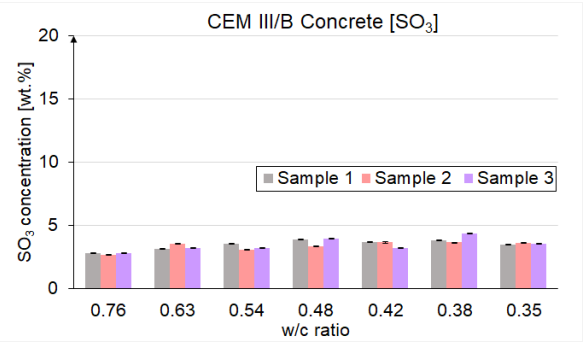

(b) CEM III/B Concrete

Figure 4.4: Chemical composition analysis [SO_3] with hXRF on paste and concrete surfaces with different w/c ratios

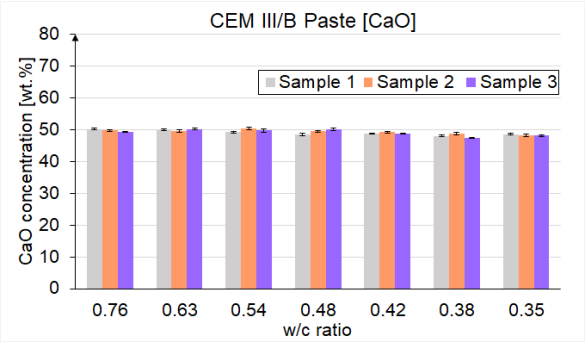

(a) CEM III/B Paste

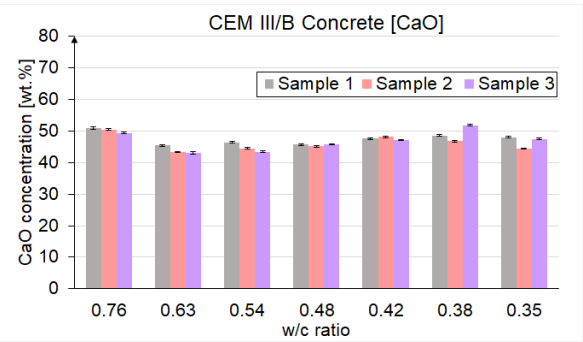

(b) CEM III/B Concrete

Figure 4.5: Chemical composition analysis [CaO] with hXRF on paste and concrete surfaces with different w/c ratios

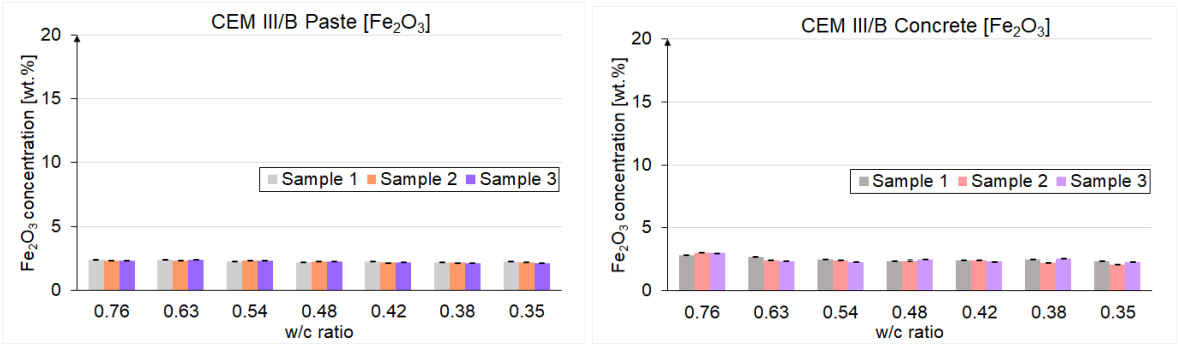

(a) Paste **(b)** Concrete

Figure 4.6: Chemical composition analysis [Fe_2O_3] with hXRF on paste and concrete surfaces with different w/c ratios

Moreover, based on the results obtained at both the paste and concrete levels, it is evident that analyzing the chemical composition at the sample surfaces provides insight into the type of cement used in the mix. When comparing the oxide results at the paste and concrete levels with the chemical composition of CEM III/B found in the literature (see Table 4.1), they fall within the reported values. For instance, considering the results for MgO, the concentrations are consistently below 5 wt%, aligning with the literature's reported range of approximately 3 to 5 wt%.

Table 4.1: CEM III/B (cement powder) chemical composition based on literature

	Oxide (wt.%)					
Reference	MgO	Al_2O_3	SiO_2	SO_3	CaO	Fe_2O_3
[79]	3.12	10.60	26.40	2.72	45.95	2.47
[15]	5.89	10.02	29.11	2.82	47.11	1.19
[80]	5.55	9.09	30.67	4.93	46.21	1.17
[77]	5.37	6.58	34.71	3.09	46.44	2.29
	4.97	6.46	33.26	3.00	48.33	2.56
	5.09	6.40	33.41	3.08	46.67	2.41
	5.14	6.39	33.51	3.05	46.63	2.32
	4.65	6.19	32.00	3.01	48.41	2.53
	4.85	6.31	32.91	3.04	47.71	2.48
	5.20	6.35	33.50	3.04	46.03	2.17
	4.76	6.23	32.05	3.01	47.67	2.37
	4.97	6.21	32.80	3.16	46.66	2.25

Table 4.2 and Table 4.3 give an overview of hXRF, WD-XRF, and ESEM-EDS results for the surface chemical composition of the paste samples M1-1, M2-1, M3-1, M4-1, M5-1, M6-1 and M7-1, and the concrete samples M1-SI-1, M2-SI-1, M3-SI-1, M4-SI-1, M5-SI-1, M6-SI-1, and M7-SI-1. It can be seen that there are variations in the results for some oxide concentrations among the different methods. For instance, when examining SiO_2, the element concentrations obtained with hXRG differ by nearly 8 wt% compared to the other two methods. Similarly, for CaO, the difference is approximately 8 to 10 wt%. However, there seems to be a high level of agreement among the methods when analyzing MgO, Al_2O_3, and Fe_2O_3. These variations in the chemical composition values can be attributed to several factors, including sample preparation, sample heterogeneity, and the presence of calcium carbonate ($CaCO_3$) polymorphs. These polymorphs may have formed due to the surface efflorescence of the samples during the transportation of samples from one location to another for testing and during the testing process with WD-XRF and ESEM-EDS methods.

Although there is no consensus on all oxide concentrations among the methods, the evaluation of hXRF results involves comparing them with oxide values reported in the literature as well. These values from the literature are considered as the true or ideal references, as the analysis of cement composition was conducted on the bulk of dry cement powder, which was prepared and analyzed in

a homogeneous material. As a result, it can be seen that the measured values (hXRF data) shown in Table 4.2 and Table 4.3 are within or close to the true values.

Table 4.2: Surface chemistry comparison between hXRF, WD-XRF, and EDS for cement paste

Sample	w/c	Method	MgO	Al_2O_3	SiO_2	P_2O_5	SO_3	K_2O	CaO	TiO_2	MnO	Fe_2O_3
M1-1	0.76	hXRF	3.79	6.67	32.68	0.27	2.70	0.69	50.21	0.46	0.14	2.38
		WDXRF	3.60	6.46	24.73	0.25	1.84	0.67	58.38	0.58	0.14	2.39
		EDS	3.56	6.42	27.56	0.21	1.71	1.28	56.80	0.46	0.02	1.98
M2-1	0.63	hXRF	3.80	6.51	32.58	0.29	3.47	0.55	49.87	0.44	0.14	2.35
		WDXRF	3.55	6.37	24.53	0.24	1.95	0.56	58.81	0.46	0.15	2.52
		EDS	3.12	6.22	26.93	0.20	1.88	1.03	57.90	0.67	0.09	1.96
M3-1	0.54	hXRF	3.70	6.58	33.21	0.27	3.61	0.56	49.24	0.44	0.14	2.26
		WDXRF	3.60	6.51	24.80	0.25	2.12	0.59	58.03	0.64	0.16	2.31
		EDS	3.17	6.64	27.58	0.21	2.30	1.15	55.77	0.72	0.12	2.34
M4-1	0.48	hXRF	3.78	6.68	32.71	0.25	3.70	0.58	49.44	0.46	0.15	2.25
		WDXRF	3.72	6.65	25.01	0.22	2.56	0.66	57.16	0.48	0.14	2.31
		EDS	3.15	6.55	25.73	0.17	3.20	1.45	57.00	0.77	0.26	1.72
M5-1	0.42	hXRF	3.82	6.65	33.29	0.25	3.83	0.63	48.74	0.43	0.14	2.23
		WDXRF	3.65	6.55	24.73	0.24	2.49	0.66	57.56	0.62	0.16	2.29
		EDS	3.15	6.84	27.52	0.19	3.99	1.45	54.17	0.61	0.04	2.05
M6-1	0.38	hXRF	3.76	6.89	34.25	0.26	3.49	0.59	48.06	0.42	0.13	2.17
		WDXRF	3.77	6.63	25.40	0.25	2.08	0.55	57.41	0.55	0.15	2.34
		EDS	3.60	6.92	28.27	0.20	2.49	1.14	54.98	0.49	0.13	1.77
M7-1	0.35	hXRF	4.10	6.91	33.36	0.26	3.15	0.83	48.56	0.44	0.14	2.25
		WDXRF	3.83	6.54	24.97	0.26	2.05	0.93	57.14	0.53	0.16	2.32
		EDS	3.36	6.84	26.93	0.13	2.20	2.03	55.88	0.68	0.15	1.80

Table 4.3: Surface chemistry comparison between hXRF, WD-XRF, and EDS for concrete

Sample	w/c	Method	MgO	Al_2O_3	SiO_2	P_2O_5	SO_3	K_2O	CaO	TiO_2	MnO	Fe_2O_3
M1-SI-1	0.76	hXRF	3.28	6.92	31.85	0.18	2.80	0.58	50.96	0.49	0.15	2.83
		WDXRF	2.81	7.20	24.50	0.20	2.05	0.75	57.89	0.52	0.16	2.83
		EDS	2.42	6.35	23.77	0.08	1.66	1.09	60.72	0.60	0.00	2.69
M2-SI-1	0.63	hXRF	3.64	6.68	36.71	0.23	3.15	0.75	45.50	0.49	0.15	2.72
		WDXRF	3.58	6.65	29.73	0.25	2.11	0.79	52.76	0.49	0.16	2.56
		EDS	3.63	6.32	29.41	0.15	2.64	0.92	53.88	0.68	0.00	2.36
M3-SI-1	0.54	hXRF	3.42	6.43	36.25	0.21	3.56	0.61	46.46	0.46	0.14	2.49
		WDXRF	3.31	6.41	28.69	0.24	2.33	0.64	54.29	0.53	0.15	2.50
		EDS	3.11	5.99	27.28	0.14	2.82	1.10	56.66	0.61	0.00	2.31
M4-SI-1	0.48	hXRF	3.25	6.06	37.43	0.21	3.86	0.57	45.72	0.45	0.14	2.37
		WDXRF	3.27	6.32	26.76	0.22	2.80	0.55	55.91	0.69	0.15	2.59
		EDS	2.63	5.24	25.58	0.16	3.87	0.86	59.91	0.07	0.22	1.46
M5-SI-1	0.42	hXRF	3.35	6.46	34.98	0.23	3.71	0.69	47.56	0.46	0.15	2.44
		WDXRF	3.31	6.24	25.78	0.21	2.37	0.65	57.40	0.50	0.17	2.48
		EDS	2.85	5.24	24.88	0.23	2.93	1.08	60.20	0.81	0.00	1.78
M6-SI-1	0.38	hXRF	3.24	5.89	34.61	0.23	3.81	0.56	48.61	0.46	0.15	2.48
		WDXRF	3.31	6.21	24.57	0.23	2.85	0.53	58.10	0.58	0.16	2.70
		EDS	3.53	5.56	23.47	0.13	4.50	0.86	59.45	0.57	0.00	1.93
M7-SI-1	0.35	hXRF	3.66	6.43	34.64	0.25	3.50	0.55	48.00	0.47	0.15	2.37
		WDXRF	3.45	6.38	25.51	0.24	2.42	0.48	57.62	0.47	0.17	2.45
		EDS	3.12	6.66	25.05	0.07	3.40	0.98	57.30	0.81	0.18	2.43

Finally, statistical analysis was conducted, and the minimum and maximum values for each oxide obtained are presented in the summary tables in Appendix A.

4.2. Effect of curing age

Figure 4.7 shows the major element oxide concentrations measured (y-axis) on the paste and concrete surfaces after 1 day, 14 days, and 28 days of curing. It can be seen that the oxides remain similar regardless of the age of the paste and concrete specimens.

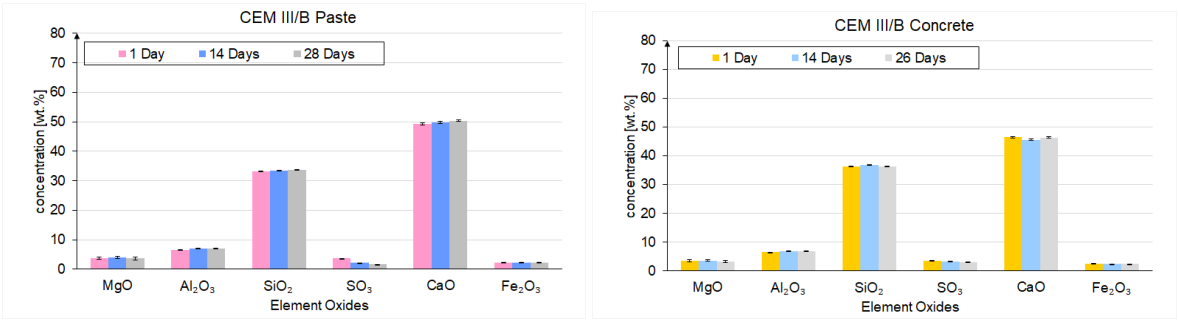

(a) Paste **(b)** Concrete

Figure 4.7: Chemical composition analysis with hXRF on paste and concrete surfaces after different curing ages

In addition, descriptive statistics, including the average, standard deviation, and coefficient of variation, for the data obtained from the hXRF analysis of samples M3-1 and M3-SI-1 are summarized in Table 4.4 and Table 4.5.

The standard deviation provides information about the amount of dispersion in a set of values, indicating how much individual data points differ from the mean (absolute variability). In contrast, the coefficient of variation (CoV) offers a relative measure of data point dispersion in relation to the mean. In other words, it expresses the standard deviation's deviation in percentage terms relative to the mean. A higher coefficient of variation suggests greater relative variability or dispersion, indicating that data points are more spread out relative to the mean.

Examining Table 4.4, it can be observed that, for the specific case of MgO and P_2O_5, the standard deviations reported are 0.35%, 0.35%, 0.49% and 0.03%, 0.02%, 0.02%, respectively. Similarly, from Table 4.5, the standard deviations are 0.44%, 0.29%, 0.39%, and 0.04%, 0.06%, 0.06%. These values represent low variation of the data points with respect to the average. However, when looking at the CoV, MgO and P_2O_5 show the highest values, indicating the highest relative variability among the oxides.

In contrast, for elements like SiO_2 and CaO, the CoV is smaller compared to the other oxides, suggesting lower relative variability. This insight highlights that light elements present in low concentrations have a higher relative variability than those present in light and heavy elements with higher concentrations. Consequently, hXRF seems to be more reliable in the assessment of oxides present in the material in higher concentrations. This was also observed in the statistical analysis that was performed in the other Test Series or analyzed effects.

Table 4.4: Composition of M3-1 paste surface obtained with hXRF

Sample	w/c	No. Days		MgO	Al_2O_3	SiO_2	P_2O_5	SO_3	K_2O	CaO	TiO_2	MnO	Fe_2O_3
			Average (wt.%)	3.70	6.58	33.21	0.27	3.61	0.56	49.24	0.44	0.14	2.26
			Std. Dev (wt.%)	0.35	0.12	0.14	0.03	0.02	0.02	0.30	0.01	0.00	0.03
M3-1	0.54	1 Day	CoV (%)	9.51	1.89	0.43	10.68	0.62	3.81	0.62	1.52	2.60	1.20
			Minimum (wt.%)	3.25	6.39	32.97	0.23	3.56	0.52	48.54	0.42	0.13	2.20
			Maximum (wt%)	4.34	6.78	33.39	0.31	3.63	0.58	49.66	0.45	0.14	2.29
			Average (wt.%)	3.92	6.99	33.33	0.26	2.17	0.83	49.71	0.44	0.13	2.24
			Std. Dev (wt.%)	0.35	0.11	0.09	0.02	0.02	0.01	0.33	0.01	0.00	0.02
M3-1	0.54	14 Days	CoV (%)	9.02	1.54	0.26	8.77	0.95	0.87	0.66	1.96	2.63	1.06
			Minimum (wt.%)	3.39	6.82	33.19	0.22	2.15	0.81	49.13	0.42	0.13	2.20
			Maximum (wt%)	4.57	7.14	33.43	0.30	2.22	0.83	50.14	0.46	0.14	2.27
			Average (wt.%)	3.69	6.91	33.60	0.25	1.59	0.71	50.38	0.45	0.14	2.29
			Std. Dev (wt.%)	0.49	0.08	0.12	0.04	0.02	0.01	0.30	0.01	0.00	0.02
M3-1	0.54	28 Days	CoV (%)	13.24	1.19	0.37	16.49	1.55	1.28	0.60	1.52	2.39	0.85
			Minimum (wt.%)	3.06	6.76	33.47	0.15	1.53	0.69	49.98	0.44	0.13	2.25
			Maximum (wt%)	4.40	7.05	33.87	0.29	1.62	0.73	50.84	0.46	0.14	2.31

Table 4.5: Composition of M3-SI-1 concrete surface obtained with hXRF

Sample	w/c	No. Days		MgO	Al_2O_3	SiO_2	P_2O_5	SO_3	K_2O	CaO	TiO_2	MnO	Fe_2O_3
			Average (wt.%)	3.42	6.43	36.25	0.21	3.56	0.61	46.46	0.46	0.14	2.49
			Std. Dev (wt.%)	0.44	0.08	0.15	0.04	0.03	0.01	0.30	0.01	0.00	0.03
M3-SI-1	0.54	1 Day	CoV (%)	12.75	1.27	0.41	17.81	0.89	1.01	0.64	1.32	2.92	1.06
			Minimum (wt.%)	2.79	6.28	36.05	0.15	3.49	0.60	46.00	0.45	0.14	2.45
			Maximum (wt%)	4.28	6.54	36.53	0.26	3.60	0.62	46.93	0.47	0.15	2.52
			Average (wt.%)	3.53	6.83	36.78	0.24	3.20	0.96	45.55	0.45	0.13	2.33
			Std. Dev (wt.%)	0.29	0.08	0.11	0.06	0.04	0.01	0.26	0.01	0.00	0.02
M3-SI-1	0.54	14 Days	CoV (%)	8.20	1.21	0.31	23.64	1.38	0.70	0.58	1.40	3.52	1.02
			Minimum (wt.%)	3.04	6.66	36.59	0.11	3.12	0.95	45.00	0.44	0.13	2.29
			Maximum (wt%)	4.19	6.94	36.90	0.32	3.28	0.97	45.90	0.46	0.14	2.37
			Average (wt.%)	3.33	6.84	36.21	0.24	2.98	1.06	46.32	0.47	0.14	2.41
			Std. Dev (wt.%)	0.37	0.15	0.11	0.06	0.04	0.01	0.28	0.00	0.00	0.02
M3-SI-1	0.54	28 Days	CoV (%)	11.18	2.24	0.31	23.08	1.25	0.88	0.61	1.00	3.36	0.87
			Minimum (wt.%)	2.81	6.61	35.95	0.15	2.93	1.04	45.84	0.46	0.13	2.37
			Maximum (wt%)	3.94	7.05	36.33	0.33	3.04	1.07	46.70	0.47	0.15	2.44

4.3. Effect of relative humidity

Figure 4.8 and Figure 4.9 shows the weight percentage of CaO and SiO_2 (y-axis) of the paste and concrete samples that were exposed to dried conditions (0%), 40%, 60%, 75% and 95% RH.

According to the information collected from the literature about the chemical composition of CEM I (see Table 4.6), the typical values for CaO and SiO_2 are up to about 68 wt%, and 26 wt%, respectively. Regarding the chemical composition of CEM III/B (see Table 4.1), the typical values for CaO and SiO_2 are up to about 48 wt%, and 10 wt%, respectively. Bearing this in mind, it can be seen in Figure 4.8 that there is a significant increase in the calcium oxide concentration at 95% RH, which is a concentration value not characteristic of either CEM I or CEM III/B. This increase can be attributed to efflorescence, which is a deposit of salts, usually whitish in color, formed on the surface of porous materials (concrete, bricks, mortar, and others) [81]. Efflorescence usually consists of carbonates of calcium, sodium, and potassium originating from the cement. However, efflorescence ($CaCO_3$), specifically calcium carbonates, notably calcite, often occurs on the surfaces of concrete elements [81][82]. Carbonates of calcium are the product of chemical reactions between atmospheric carbon dioxide (CO_2) and calcium hydroxide, and the presence of H_2O in the environment. The reaction that produces calcium carbonate is the same as the reaction known as carbonation, which involves the diffusion of CO_2 within the material, the dissolution of CO_2 in water as carbonic acid (H_2CO_3) in the pore solution, subsequent dissociation into HCO_3 and CO_3^{2-} ions, the dissolution of solid $Ca(OH)_2$ (calcium hydroxide) with the release of calcium (Ca^{2+})and hydroxyl OH^- ions, and the precipitation of (Ca^{2+}) with CO_3^{2-} to form $CaCO_3$ (calcium carbonate) [83], where the precipitation or leaching of the calcite polymorphs are driven by concentration gradients. These reactions can be synthesized in the following overall chemical reaction:

$$Ca(OH)_2 + CO_2 \longrightarrow CaCO_3 + H_2O$$

According to López-Arce et al. [83] relative humidity higher than 75% leads to the formation of amorphous calcium carbonate, monohydrocalcite, calcite, aragonite, and vaterite with larger particle sizes and higher crystallinity than at the lower RH. These findings can explain the observed increase in calcium oxide at the sample surfaces exposed to 95% RH, as a consequence of calcium carbonate formation which is further investigated with ESEM-EDS.

Table 4.6: CEM I (cement powder) chemical composition based on literature

	Oxide (wt.%)					
Reference	MgO	Al_2O_3	SiO_2	SO_3	CaO	Fe_2O_3
[76]	1.67	5.04	21.02	2.58	64.18	2.85
[80]	1.92	4.60	20.32	3.20	63.12	3.30
[79]	2.28	4.49	20.18	3.45	63.83	2.64
[15]	1.65	4.84	20.23	2.83	63.86	3.28
[84]	1.0-4.0	4.0-8.0	16.0-26.0	0.1-2.5	58.0-68.0	2.0-5.0

On the other hand, as observed in Figure 4.8b, the CaO concentration at 0% is 67 wt.% and 69 wt.%. These elevated values are attributed to inappropriate drying of the concrete samples from the beginning, which caused efflorescence in the early stages of the assessment or experiment.

Regarding the CaO weight percentage reported at 40% RH in Figure 4.8b, it is lower than the CaO content typically found in CEM I. This reduction can be explained by the segregation of aggregates at the concrete surface, as shown in Figure 4.9b. The amount of silica detected was 37 wt.% and 35 wt.%, which notably influences the detection of lower calcium oxide concentrations.

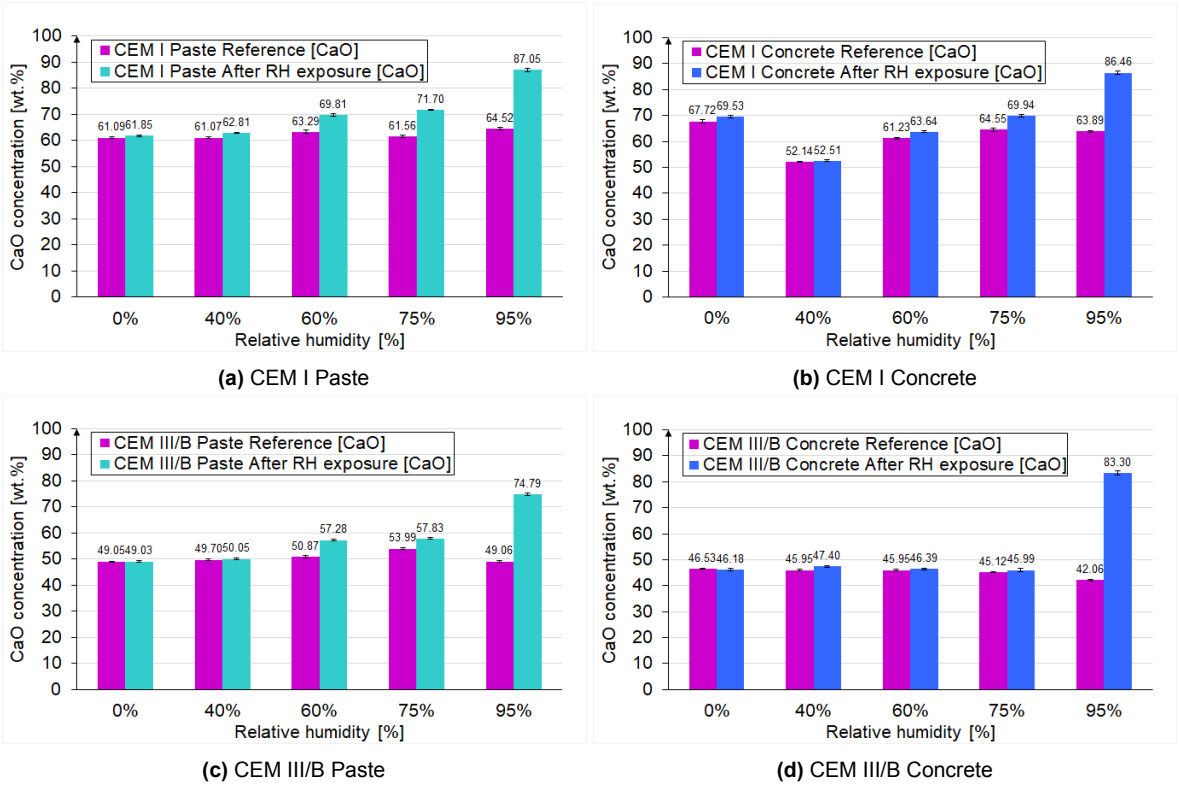

(a) CEM I Paste **(b)** CEM I Concrete

(c) CEM III/B Paste **(d)** CEM III/B Concrete

Figure 4.8: Chemical composition analysis [CaO] with hXRF on paste and concrete surfaces exposed at different relative humidities

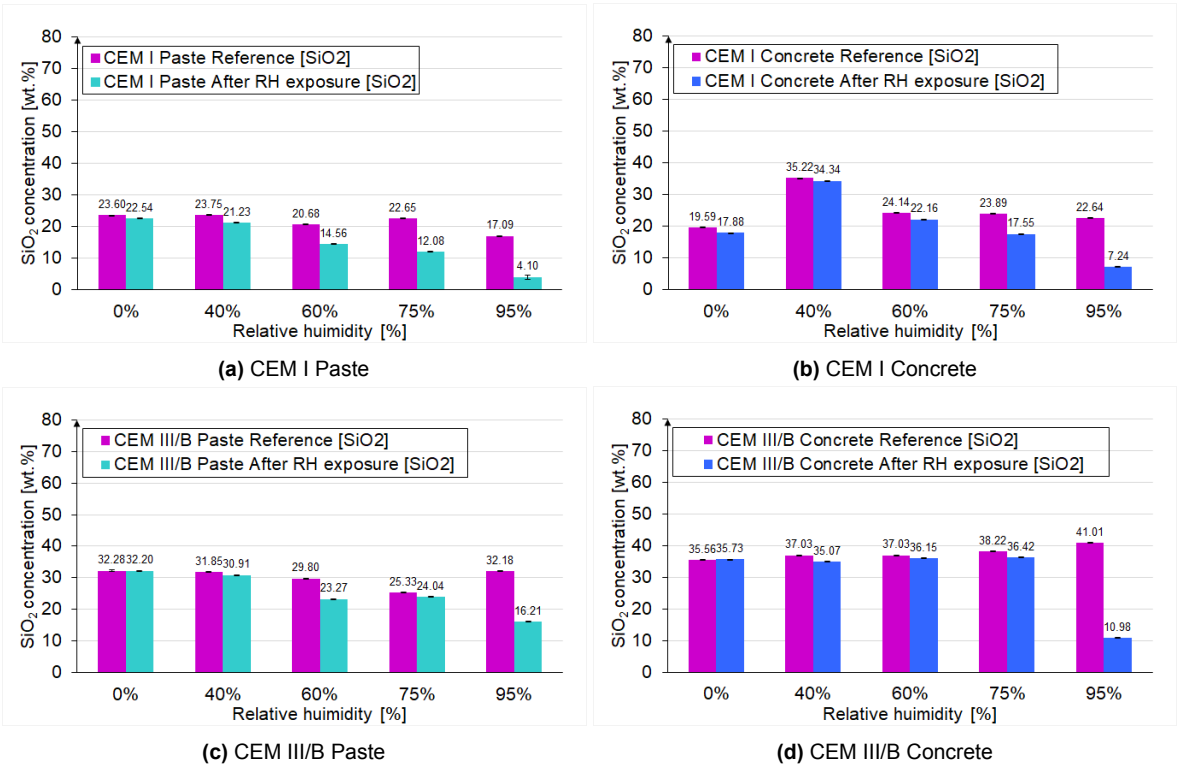

(a) CEM I Paste **(b)** CEM I Concrete

(c) CEM III/B Paste **(d)** CEM III/B Concrete

Figure 4.9: Chemical composition analysis [SiO_2] with hXRF on pastes and concrete surfaces exposed at different relative humidities

Besides the hXRF measurements, pictures were taken with the ESEM-EDS, these calcium carbonate crystals present at the surface are clearly visible (see Figure 4.10).

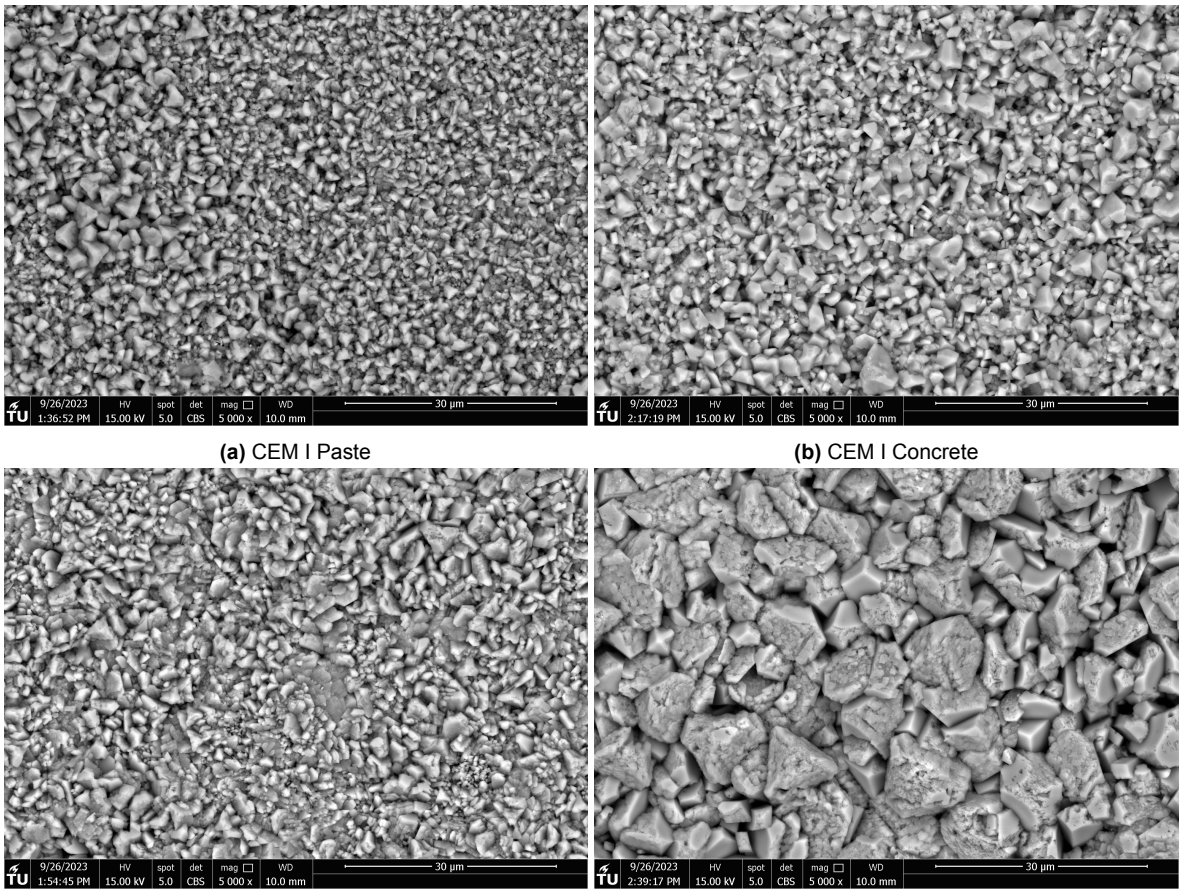

(a) CEM I Paste **(b)** CEM I Concrete

(c) CEM III/B Paste **(d)** CEM III/B Concrete

Figure 4.10: ESEM Photos $CaCO_3$ in paste and concrete surfaces

Chemical composition analysis was also performed with ESEM-EDS for the samples that were exposed to 0%, 40%, and 95% RH. It is important to highlight that these measurements were carried out almost one month later compared to the last round of hXRF measurements conducted for this Test Series. As a result, CaO concentrations of up to 98 wt% can be seen in Table 4.7 and Table 4.8, particularly in the case of 95% RH.

Table 4.7: Chemical composition analysis with ESEM-EDS on paste and concrete surfaces exposed at different relative humidities (CEM I)

	0%		40%		95%	
	CEM I Paste	CEM I Concrete	CEM I Paste	CEM I Concrete	CEM I Paste	CEM I Concrete
MgO	0.95	1.34	1.09	1.3	0.87	0.46
Al_2O_3	5.47	2.53	4.91	3.67	0.66	0.3
SiO_2	20.95	15.94	21.44	23.3	2.77	1.49
P_2O_5	0.4	0.16	0.37	0.17	—	—
SO_3	3.26	0.93	3.21	1.64	0.09	0.06
K_2O	2.72	2.01	2.84	1.16	0.46	0.11
CaO	62.94	73.36	62.63	65.23	94.45	96.7
TiO_2	0.58	0.66	0.65	0.56	—	0.58
MnO	0.06	0.03	0.11	0.14	—	—
Fe_2O_3	2.67	3.04	2.76	2.82	0.71	0.3

Table 4.8: Chemical composition analysis with ESEM-EDS on paste and concrete surfaces exposed at different relative humidities (CEM III/B)

	0%		40%		95%	
	CEM III/B Paste	CEM III/B Concrete	CEM III/B Paste	CEM III/B Concrete	CEM III/B Paste	CEM III/B Concrete
MgO	3.21	3.14	2.89	2.6	0.72	0.48
Al_2O_3	7.23	6.56	6.91	5.96	0.37	0.58
SiO_2	26.64	27.68	27.21	24.27	1.18	5.18
P_2O_5	0.19	0.14	0.19	0.09	-	-
SO_3	4.14	2.71	4.02	0.79	0.12	-
K_2O	2.25	1.19	2.06	1.78	0.17	0.16
CaO	53.88	55.38	53.97	61.95	96.95	93.26
TiO_2	0.65	0.92	0.67	0.46	0.1	0.02
MnO	0.01	0.29	0	0.13	0.06	-
Fe_2O_3	1.81	1.98	2.09	1.97	0.34	0.32

The increase in the calcium weight percentage should decrease the concentration of other elements. However, for the particular case of the data obtained from hXRF, the decrease seems to occur only in a few elements such as Al_2O_3, SiO_2, and SO_3. In the case of K_2O, the weight percentage increases in different proportions. Finally, no impact is observed on P_2O_5, TiO_2, MnO, and Fe_2O_3. The bar plots of these oxides can be found in Appendix B.

In summary, the surface chemical composition of the paste and concrete samples does not change regardless of their exposure to different relative humidities. What happens is that at high relative humidity, surface efflorescence occurs, and as a result, the measurements obtained with hXRF are affected.

4.4. Effect of carbonation

Aggressive environments result in the chemical degradation of concrete, of which carbonation is a slow degradation process that is, however, very important for long-term durability assessment. The carbonation process results in a decrease in pH, leading to the corrosion of reinforcing bars in concrete [80]. The corrosion products are more voluminous than the parent steel, causing tensile stresses in the concrete cover and subsequently, its cracking and spalling over a relatively short period ($<$ 10 years after corrosion initiation). In the period of 10 to 20 years, steel cross-section loss may cause insufficient tensile capacity and thus may threaten structural integrity and safety. Therefore, carbonation is one of the most important deterioration mechanisms in predicting the long-term behavior of concrete [85].

In order to assess this process, as mentioned in chapter 3, the samples were exposed to accelerated carbonation with a CO_2 concentration of 1% and a relative humidity maintained at 60% during a carbonation period of 15 days. Previous studies have indicated that carbonation reaches its maximum level at relative humidities (RH) between 50% and 70%. At RH $<$ 50%, there is inadequate moisture for carbonation to occur, and at RH $>$ 70%, pore blockage by water presence tends to inhibit CO_2 ingress, as concrete becomes more saturated [86]. Considering the fact that efflorescence mostly occurs at RH higher than about 75%, as analyzed in the previous section, and that the optimum RH value for carbonation to happen is between 50% and 70%, it is expected to have carbonated samples, as shown in chapter 3, but not leaching of calcium carbonate polymorphs.

Figure 4.11 shows the chemical composition (MgO, Al_2O_3, SiO_2, SO_3, CaO, Fe_2O_3) of paste and concrete surfaces before being exposed to accelerated carbonation, and after the samples were carbonated. The plotted data reveals a remarkable degree of stability, with no significant fluctuations, which implies that carbonation does not affect the elemental analysis with hXRF, and consequently, if a concrete structure is carbonated this probably can not be identified when performing chemical composition analysis at the concrete surface with hXRF.

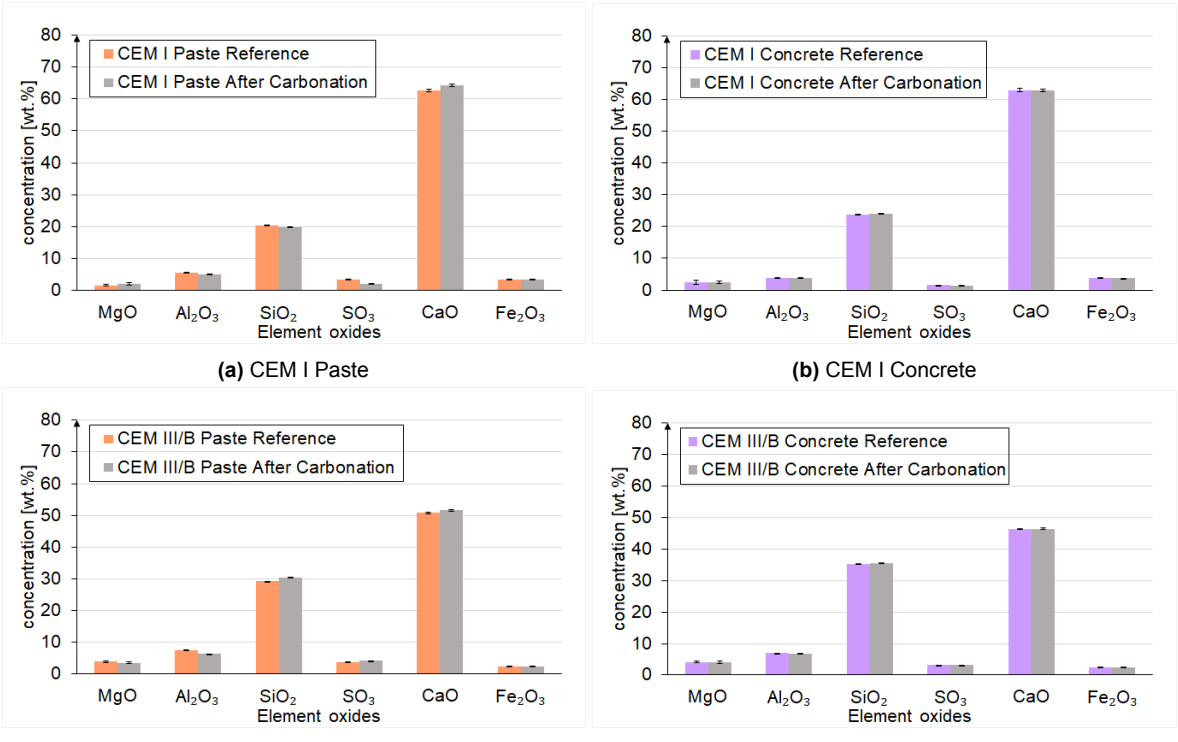

(a) CEM I Paste

(b) CEM I Concrete

(c) CEM III/B Paste

(d) CEM III/B Concrete

Figure 4.11: Effect of carbonation on the chemical composition of paste and concrete surfaces

5

Practical case studies

This chapter presents various case studies that were considered to assess in-situ the chemical composition of concrete surfaces using handheld XRF. It includes an explanation of how the assessments were carried out in each case, the challenges encountered, and the opportunities associated with in-situ testing of concrete structures.

5.1. Case study 1: Sluinerweg viaduct (KW03), A1

The Sluinerweg viaduct, built in 1970 near Apeldoorn, the Netherlands (see Figure 5.1), is a reinforced concrete structure. It features 4 spans, a width of 14.95 m, and a length of 76 m. According to the records of the viaduct, the concrete mix design for the viaduct included Portland cement, coarse aggregates (5.6-32 mm), and fine aggregates (0-5.6 mm).

Figure 5.1: Sluinerweg viaduct (KW03), A1

The inspection of the Sluinerweg viaduct began with a visual examination of its various concrete structural members, including foundations, columns, beams, support beams and walls. This initial inspection helped to determine the locations for core sample extraction and handheld XRF analysis. It was decided to extract core samples for additional analysis of their surface chemical composition in the laboratory, with validation against the in-situ hXRF measurements.

In the context of core extraction, the decision was made to extract cores from the columns and the foundation due to safety and accessibility considerations. Before the core extraction process, a cover

meter (Figure 5.2a) was employed to pinpoint the location of the steel reinforcement. Subsequently, a grid, marked with crayon lines as indicated in Figure 5.2b and Figure 5.2c, was drawn to correspond with the information obtained from the cover meter. Once these guiding lines were established, the person responsible for core extraction proceeded with the work.

(a) Cover meter **(b)** Grid column **(c)** Grid foundation

Figure 5.2: Identification of reinforcement position

Three cores were extracted per column (Figure 5.3a) and three from the foundation (Figure 5.3b). In the case of the foundation cores, it was necessary to remove the soil in order to facilitate their extraction. Subsequently, the cores were labeled and stored in a plastic box to transport them. Images of the cores with their respective information of length and diameter are presented in Appendix D.

(a) Column **(b)** Foundation

Figure 5.3: Cores extraction from columns (a) and foundation (b)

During the visual inspection, it was noted that the surfaces of the columns and walls were covered with a layer known as 'Kristal Cement Graniet (KCG).' The presence of granite in this layer led to the detection of high concentrations of SiO_2 (see Table 5.1) during hXRF analysis. However, there were areas where the concrete surfaces were not covered by this layer. As shown in Figure 5.4 the lower section of the column, the sides and bottom of wall surfaces, and the beam surfaces were suitable for in-situ element analysis.

Table 5.1: Chemical composition analysis KCG layer

No.Measurements	MgO	Al_2O_3	SiO_2	P_2O_5	SO_3	K_2O	CaO	TiO_2	MnO	Fe_2O_3
1	1.22	4.70	**79.06**	0.29	1.85	1.48	9.29	0.23	0.02	1.85
2	<LOD	1.69	**68.36**	<LOD	2.97	0.47	26.03	0.06	0.03	0.38
3	1.01	2.29	**59.98**	<LOD	4.27	0.49	31.48	0.10	0.01	0.30

(a) Column **(b)** Wall

(c) Wall **(d)** Beams

Figure 5.4: Identification of concrete surfaces without KCG layer for testing with hXRF

Over the nine columns and the twenty-three beams present in the viaduct, without any surface treatment, more than 10 measurement points were taken with handheld X-ray fluorescence (hXRF) from one column, specified as Column 2, the side of the wall, the bottom of beams 2, 9, 10, 12, 13, 14, 15, 16, 22, and 23. The bottom and sides of beams 11 and 17 were also analyzed (see Figure 5.5). It was observed that the bottom of the column had both dry and wet surfaces. Consequently, the measurements were conducted on a dry surface, as shown in Figure 5.6a, because performing the analysis on wet surfaces leads to the attenuation of the fluorescence X-ray signal, with lightweight elements being the most affected [87]. To be able to test the beams in a safe work environment and reach them, safety equipment was needed, a cherry picker (Figure 5.7a) and scaffolding (Figure 5.7b). After performing the first set of measurements, it was noted that marking or delineating the measurement points, together with photography records, might be helpful for later stages of the appraisal in case some data points need verification or double-checking. Consequently, for the rest of the concrete structural members, the measurement areas were marked. The marked points can be observed in Figure 5.6b and Figure 5.6c.

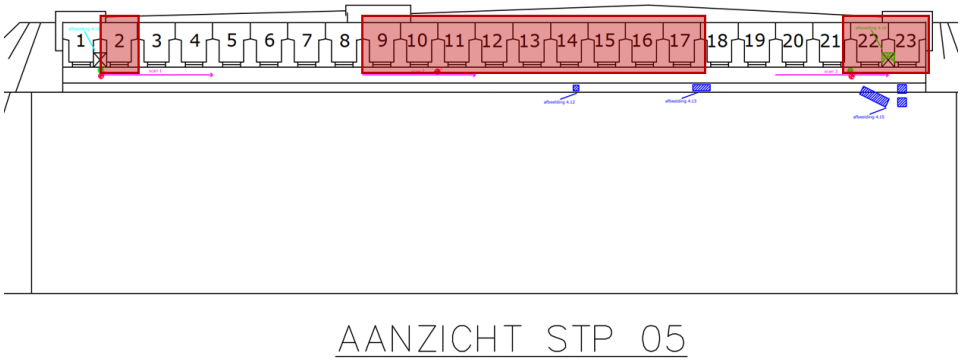

Figure 5.5: Drawing Sluinerweg tested beams with hXRF

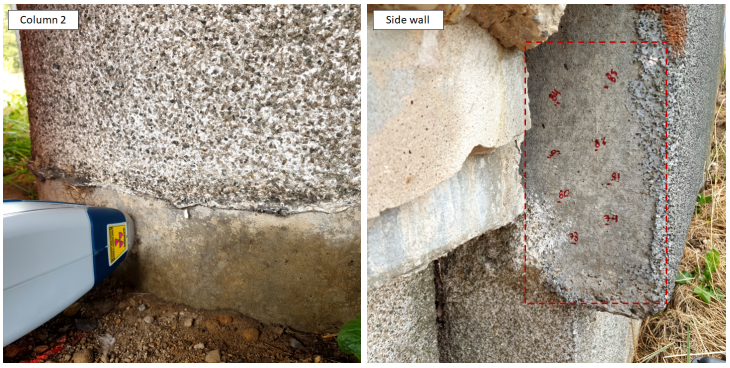

(a) Column 2 **(b)** Side wall

(c) Beam 17

Figure 5.6: Measured concrete structural members and measurement points

(a) Cherry picker **(b)** Scaffolding

Figure 5.7: Safety measures

The averages of the hXRF measurements from Column 2 and Side wall are summarized in Table 5.2. It is evident from this table that most of the oxide concentrations fall within the typical ranges reported in the literature Table 4.6 and the experimental section of this thesis (chapter 4), characteristics of CEM I. However, there are exceptions, one notable example being the SiO_2 weight percentage from the wall, which was reported as 31.43 wt.%, higher than the typical 20% found in CEM I. This increase can be attributed to the greater presence of fine aggregates in the cement skin or concrete surface.

Table 5.2: Chemical composition analysis of Sluinerweg concrete elements with hXRF

Category		MgO	Al_2O_3	SiO_2	P_2O_5	SO_3	K_2O	CaO	TiO_2	MnO	Fe_2O_3
Column 2	Average (wt.%)	1.47	5.01	21.16	0.80	1.10	0.74	66.84	0.31	0.07	2.90
	Std. Dev (wt.%)	0.18	0.25	0.48	0.06	0.05	0.02	0.95	0.01	0.01	0.06
	CoV (%)	12.31	4.97	2.27	7.91	4.26	2.57	1.42	2.74	7.71	2.10
Side wall	Average (wt.%)	1.69	4.81	**31.43**	0.49	0.73	0.67	56.19	0.37	0.07	3.65
	Std. Dev (wt.%)	0.21	0.30	2.78	0.12	0.34	0.04	3.07	0.02	0.01	0.21
	CoV (%)	12.55	6.26	8.86	25.65	45.80	5.59	5.47	6.05	9.80	5.87

In Figure 5.8, the bottom of beam 11 is shown. In Table 5.3, the raw data of all the spots analyzed with hXRF in beam 11 are presented. Notably high concentrations of SO_3 were reported, exceeding typical CEM I levels, which should not exceed approximately 3 wt.%. A hypothesis is put that the elevated sulfur concentrations can be attributed to the formation of black crusts on the concrete surfaces.

One of the most common effects of pollution on building surfaces is the formation of a black crust. It appears as a dark coating, and the color is attributed to the accumulation of carbonaceous particles from diesel exhaust and domestic boilers [88] on the material surface. Sulphanation between the carbonate and sulfur compounds occurs and induces the transformation of carbonates, such as calcite ($CaCO_3$) and dolomite ($CaMg(CO_3)_2$), into calcium sulfate or gypsum ($CaSO_4 \cdot 2H_2O$) [89]. In addition, a study conducted by Wang *et al.* [89] utilized the Thermo Scientific Niton XL3t 950 portable XRF device (pXRF) to characterize the main chemical element contents of a host rock. The sulfur content was notably higher, ranging from 10 wt.% to 30 wt.% (due to the presence of black crust). This can explain the elevated weight percentages reported in all the beams analyzed in this study. The black color from the black crust can be clearly visualized in Figure 5.9a, where the beams are located above the traffic line, compare to the beams located above the bike path Figure 5.9b.

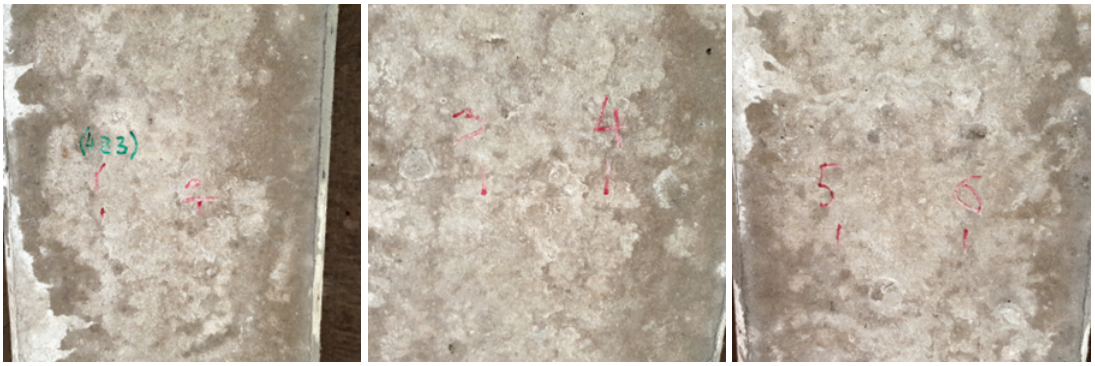

(a) **(b)** **(c)**

Figure 5.8: Beam 11 bottom

Table 5.3: Chemical composition analysis of Sluinerweg Beam 11 with hXRF

	Beam 11										Bottom of the beam
Spot	MgO	Al_2O_3	SiO_2	P_2O_5	SO_3	K_2O	CaO	TiO_2	MnO	Fe_2O_3	Classification
1	<LOD	5.07	**25.75**	0.38	4.84	2.49	54.44	0.52	0.13	5.96	Sand on the surface
2	<LOD	0.63	2.22	0.51	**41.37**	0.79	49.48	0.11	0.17	4.00	Black crust
3	2.00	4.33	27.85	0.36	**10.88**	2.21	46.48	0.43	0.12	5.34	Black crust
4	1.85	1.79	7.12	0.51	**28.72**	1.40	53.37	0.21	0.18	4.85	Black crust
5	<LOD	3.74	23.61	0.40	**13.85**	2.07	49.97	0.39	0.12	5.40	Black crust
6	<LOD	0.53	4.19	0.39	**42.61**	0.68	47.33	0.09	0.15	3.46	Black crust
7	<LOD	<LOD	<LOD	0.19	**43.11**	0.60	51.59	<LOD	0.14	2.78	Black crust
8	<LOD	1.60	9.62	0.44	**34.17**	1.29	48.51	0.13	0.14	3.55	Black crust
9	<LOD	1.71	10.27	0.32	**25.81**	1.41	55.44	0.22	0.13	4.28	Black crust
10	<LOD	3.27	16.84	0.40	**18.20**	1.84	54.19	0.29	0.14	4.57	Black crust
11	<LOD	0.57	2.66	0.39	**45.33**	0.99	47.51	0.06	0.14	1.95	Black crust
											Side of the beam
											Classification
12	<LOD	0.96	2.50	0.41	**41.35**	1.39	50.39	0.08	0.15	2.39	Black crust
13	<LOD	0.84	4.82	0.33	**42.12**	0.78	48.52	0.06	0.14	2.02	Black crust

(a) **(b)**

Figure 5.9: Beams (a) above the traffic line, and (b) above the bike path

Table 5.4 highlights the effect of grinding at different times in the same spot 13. It can be seen that as the surface was sanded, the sulfur content decreased, and the silica content began to increase due to being closer to the layer where the aggregates were present. Figure 5.10 shows the appearance of the original concrete surface where spot 13 was measured and after the surface was sanded.

Table 5.4: Chemical composition analysis of Sluinerweg Beam 11 with hXRF, spot 13 grinded

	Beam 11										Gradual grinding
Spot	MgO	Al_2O_3	SiO_2	P_2O_5	SO_3	K_2O	CaO	TiO_2	MnO	Fe_2O_3	
13	<LOD	0.84	4.82	0.33	**42.12**	0.78	48.52	0.06	0.14	2.02	Black crust
13*	<LOD	0.79	7.29	0.22	**34.91**	0.93	53.32	0.05	0.13	1.91	Black crust
13**	<LOD	2.91	27.40	0.14	**18.63**	1.70	46.36	0.19	0.08	2.40	Black crust
13***	0.88	3.05	35.91	0.22	**17.29**	1.43	39.06	0.14	0.06	1.94	Black crust
13****	<LOD	3.28	41.39	0.20	**13.29**	1.47	38.17	0.15	0.06	1.94	Black crust

(a) Original surface **(b)** After sand grinding

Figure 5.10: Beam 11 concrete surface before and after grinding

In the case of beam 17, various spots were analyzed throughout the entire beam, as can be observed in Table 5.5. In cases where the weight percentages of SiO_2 were higher than the typical values found in CEM I, it is associated with the presence of aggregates at the concrete surface. For example, when comparing data point 26 with 67.57 wt.% of silica with Figure 5.11e, the presence of the aggregate at the bottom of the beam is evident. In cases of high concentrations of CaO, it is attributed to efflorescence, and finally, elevated values of SO_3 are connected to black crust. Even though in some of the spots there is an increase in some of the oxides, it is still possible to determine the cement type from the other spots analyzed, for instance, 5, 9, 13, etc, where the pure concrete surface is identified.

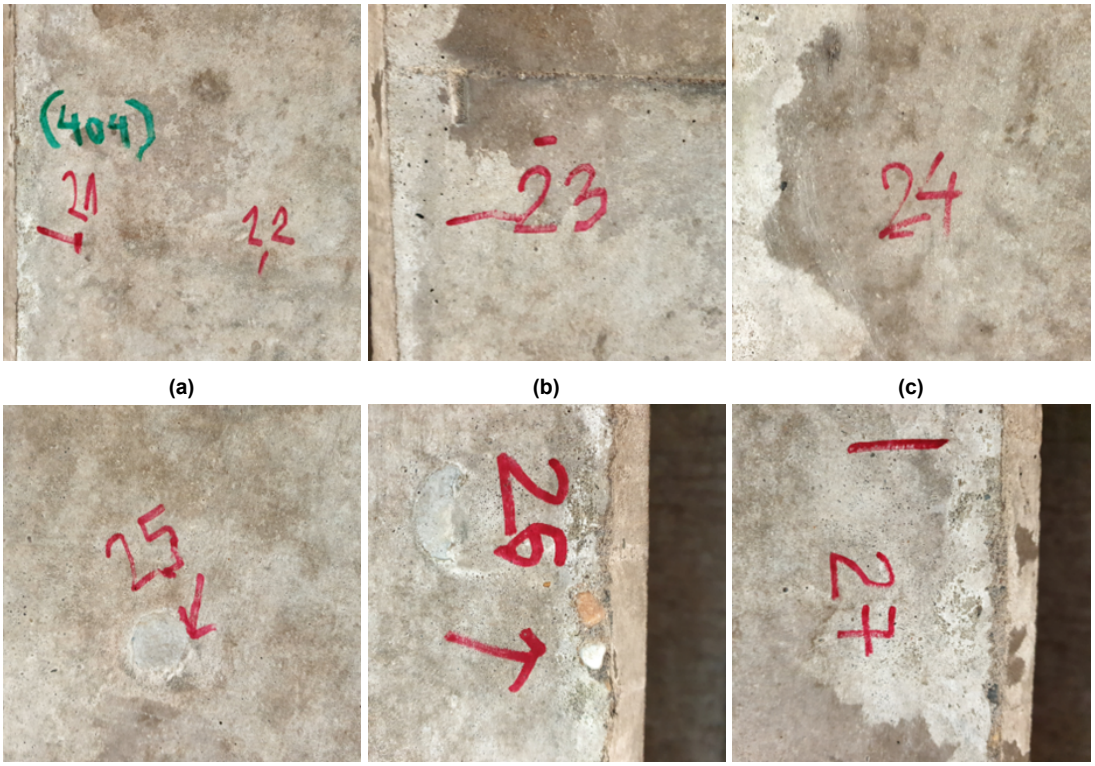

(a) **(b)** **(c)**

(d) **(e)** **(f)**

Figure 5.11: Beam 17 bottom

Table 5.5: Chemical composition analysis of Sluinerweg Beam 17 with hXRF

Beam 17											Bottom of the beam
Spot	MgO	Al_2O_3	SiO_2	P_2O_5	SO_3	K_2O	CaO	TiO_2	MnO	Fe_2O_3	Classification
1	<LOD	5.09	**31.31**	<LOD	1.34	2.79	54.78	0.34	0.06	4.12	Sand on the surface
2	<LOD	4.98	**26.7**	0.37	1.62	2.37	58.24	0.42	0.07	5.11	Sand on the surface
3	1.7	5.14	29.73	0.32	**4.82**	2.67	49.74	0.53	0.1	5.26	Black crust
4	2.23	<LOD	<LOD	0.37	**42.84**	0.87	50.63	<LOD	0.14	2.84	Black crust
5	2.7	4.15	22.54	0.22	1.25	2.3	61.02	0.49	0.09	5.24	Pure concrete surface
6	<LOD	2.57	12.01	0.41	**22.21**	1.9	55.48	0.24	0.13	4.67	Black crust
7	<LOD	2.71	10.84	0.44	**18.42**	2	59.29	0.29	0.14	5.26	Black crust
8	<LOD	0.49	<LOD	0.27	**28.88**	1.2	63.88	0.11	0.13	4.11	Black crust
9	<LOD	3.94	20.39	0.21	1.07	2.46	65.11	0.49	0.09	5.9	Pure concrete surface
10	1.39	5.31	**27.47**	0.12	1.56	2.68	54.82	0.56	0.1	6	Sand on the surface
11	<LOD	4.26	**22.86**	0.24	1.22	2.58	62.48	0.45	0.1	5.51	Sand on the surface
12	<LOD	5.13	**27.08**	0.26	1.37	2.86	57.16	0.45	0.07	5.43	Sand on the surface
13	1.68	4.41	20.75	<LOD	1.37	2.7	62.1	0.48	0.1	6.31	Pure concrete surface
14	2.01	3.34	15.84	0.2	1.15	2.48	**68.92**	0.48	0.1	5.49	Efflorescence (Ca Leaching)
15	<LOD	5.28	**27.61**	0.31	1.72	3.25	55.09	0.53	0.09	5.79	Sand on the surface
16	1.96	4.86	**24.25**	0.2	1.19	3.09	57.58	0.51	0.11	6.25	Sand on the surface
17	<LOD	4.51	21.42	0.29	1.32	2.86	63.17	0.47	0.1	5.57	Pure concrete surface
18	2.26	4.52	**23.39**	<LOD	1.04	2.66	59.82	0.56	0.08	5.63	Sand on the surface
19	<LOD	3.71	19.82	0.25	**12.25**	2.26	55.14	0.36	0.11	5.78	Black crust
20	<LOD	4.61	14.44	0.31	1.45	3.77	**67.83**	0.52	0.09	6.48	Efflorescence (Ca Leaching)
21	1.9	3.63	13.85	0.17	1.45	2.47	**70.71**	0.4	0.1	5.33	Efflorescence (Ca Leaching)
22	<LOD	4.16	17.4	0.29	2.38	2.43	64.26	0.55	0.15	7.75	Pure concrete surface
23	1.96	3.05	17.06	0.25	1.92	1.77	66.73	0.45	0.14	6.68	Pure concrete surface
24	3.64	0.44	<LOD	0.42	**42.55**	0.43	48.97	<LOD	0.13	3.44	Black crust
25	<LOD	0.4	<LOD	0.37	**38.57**	1.04	55.11	0.06	0.15	3.65	Black crust
26	<LOD	4.75	**67.57**	0.26	1.25	2.71	21.11	0.2	0.03	2.13	Sand on the surface
27	<LOD	7.97	**42.21**	0.55	1.72	3.98	36.32	0.64	0.1	6.47	Sand on the surface
											Side of the beam
											Classification
28	<LOD	0.87	5.21	0.41	**41.57**	0.93	48.24	0.09	0.13	2.24	Black crust
29	<LOD	4.25	21.52	0.39	1.45	2.45	64.83	0.42	0.06	4.52	Pure concrete surface
30	1.4	6.34	**30.62**	0.62	1.51	3.35	50.83	0.47	0.06	4.81	Sand on the surface
31	1.28	6.21	**30.24**	0.69	1.51	3.14	51.77	0.46	0.06	4.65	Sand on the surface
32	<LOD	4.26	22.01	0.66	1.52	2.41	63.88	0.41	0.07	4.61	Pure concrete surface
33	<LOD	7.7	**42.01**	0.42	1.63	3.98	38.91	0.48	0.06	4.8	Sand on the surface
34	<LOD	1.43	5.07	0.4	**37.13**	1.42	51.13	0.11	0.14	2.74	Black crust

The raw data and pictures of the other beams that were tested are presented in Appendix D.

In Figure 5.12, core C2S3, representing the core from Column 2, Sample 3, is shown, with an indication of the zone where ESEM-EDS analysis was performed. It is important to mention that, to analyze the chemical composition of concrete, elements associated with expected concrete oxides (MgO, Al_2O_3, SiO_2, P_2O_5, SO_3, K_2O, CaO, TiO_2, MnO, and Fe_2O_2), were selected in the ESEM-EDS software. The results of the element analysis of this core can be found in Table 5.6. The composition indicates to CEM I cement.

In Figure 5.13, Core F1, denoting the core from the Foundation, Sample 1, is shown, with an indication of the zone where ESEM-EDS analysis was performed. In the figure, a black surface and some soil particles can be observed. Due to the unknown composition of that black layer, chemical analysis was carried out for all elements detected by the equipment without specific element selection in the EDS software to observe what is on the surface. The results of the element analysis of this core can be found in Table 5.7. It was reported that the surface contains 52.78 wt.% of CO_2, which might have originated from organic matter that has decomposed over time, releasing carbon dioxide as a byproduct of the decomposition process, or it could be a carbon-based coating. Further analysis and investigation may be necessary to determine the exact nature and origin of the black layer.

It is worth noting that hXRF analysis was not performed in the in-situ assessment of the foundation because some soil was still stuck at the foundation surface, reporting high silica content. This might imply cleaning the surface, for instance, with a brush and water, but no tools were in-situ to dry surfaces. It is advisable to perform hXRF analysis on dry surfaces.

Figure 5.12: Core C2S3

Table 5.6: Chemical composition analysis core C2S3 with EDS

Oxides	Weigth percentage (wt.%)
MgO	0.77
Al_2O_3	3.03
SiO_2	17.38
P_2O_5	0
SO_3	2.65
K_2O	0.11
CaO	73.57
TiO_2	0
MnO	0
Fe_2O_3	2.48
Total	100

In conclusion, for this case study hXRF demonstrates significant potential for rapidly assessing the chemical composition of concrete surfaces. The evaluation of the fourteen concrete structural members involved the identification and definition of measurement areas, and the chemical analysis took approximately 14 hours. In cases where the concrete surface may not be visible or if there is a significant formation of black crust or efflorescence on the concrete surface, surface treatment might have been necessary, which would have extended the time required. In the worst-case scenario, hXRF measurements might not have been feasible. However, this case study has illustrated that hXRF provides valuable information about the chemistry of concrete. Analyzing a few structural members can offer insights into the raw materials used, in addition to identifying the level of contamination or impurities. In this particular case, sulfur was identified in higher concentrations than expected for concrete members cast with CEM I; sulfur acts as an impurity, leading to a significant loss of strength [90]. Consequently, it is essential to be aware of this information to make informed decisions on sorting concrete members before sending them to the recycling plant.

In situations where the results are inconsistent, performing measurements on additional concrete structural members becomes necessary to achieve a more comprehensive characterization of the entire concrete structure.

Figure 5.13: Core F1

Table 5.7: Chemical composition analysis core F1 with EDS

Oxides	Weigth percentage (wt.%)
CO_2	52.78
Na_2O	0.58
MgO	0.68
Al_2O_3	4.53
SiO_2	25.41
P_2O_5	0.12
SO_3	2.23
Cl	0.07
K_2O	0.6
CaO	9.65
TiO_2	0.25
MnO	0.11
Fe_2O_3	2.98
Total	100

5.2. Case study 2: CiTG Faculty, TU Delft

The faculty of Civil Engineering and Geoscience building complex consists of the education building (comprising lecture halls and offices) along Mekelweg road in Delft, the Netherlands, and the Stevin I, II, and III laboratories, which are connected on the first floor via air bridges. The entire complex was completed at the end of 1973.

The construction of the education building and laboratories comprises concrete columns, beams, and a floor system. In general, prefabricated prestressing heads, cast-in-place prestressed cantilever and edge beams, and prefabricated intermediate (longitudinal and transverse) beams were used.

Figure 5.14: Civil Engineering and Geoscience Faculty, TU Delft

Having knowledge that the faculty was constructed using a combination of prefabricated and cast-in-situ elements is valuable information for determining suitable locations for hXRF measurements. It is not known whether the cast-in-situ elements were fabricated using the same type of cement. Utilizing this technique could help verify this information. Consequently, the assessment began with a quick visual inspection to identify the various concrete elements and evaluate the condition of the concrete surfaces. At first glance, the concrete surface appears smooth, with minimal fissures. In some instances, the surfaces featured paintings or drawings.

It was decided to conduct the first set of measurements with the hXRF on a wall in the basement of the faculty (see Figure 5.15). However, before proceeding with the assessment in a systematic manner, including defining the measurement area, marking measurement points, and conducting measurements, preliminary testing was performed. Surprisingly, the device reported a sulfur trioxide (SO_3) content of 33.21 wt.% (as shown in Table 5.8), which is extremely high when compared to the average sulfur oxide content typically found in concrete made with any cement type. For instance, Andrade et al. [79] reported the chemical composition of different cement types, with the highest weight percentage of SO_3 being 3.80 wt.%. Three additional measurements were taken from different points on the wall, each of which reported high sulfur concentrations (see Table 5.8). Therefore, it was decided to analyze other elements to determine if the obtained data would be consistent with the wall's results.

The next test was conducted on a column located outside, adjacent to the Stevin III laboratory (see Figure 5.16). Figure 5.17 displays the surface condition of the column used for the hXRF analysis, along with the measurement points. The surface of the column appeared as if it had been sanded previously. Thus, three measurements were taken: one on the original-smooth surface, and the other two where the outer skin was removed.

Figure 5.15: Wall basement CiTG Faculty, TU Delft

Table 5.8: Chemical composition analysis CiTG wall basement with hXRF

No. Measurements	MgO	Al_2O_3	SiO_2	P_2O_5	SO_3	K_2O	CaO	TiO_2	MnO	Fe_2O_3
1	<LOD	0.42	2.71	0.37	**33.21**	0.14	59.90	0.26	0.41	2.21
2	1.74	1.09	4.10	0.21	**35.84**	0.47	52.91	0.37	0.45	2.82
3	<LOD	1.25	3.60	0.28	**40.65**	0.26	51.50	0.18	0.31	1.63
4	<LOD	2.63	12.50	0.26	**39.36**	0.44	41.76	0.31	0.31	2.13

Figure 5.16: View Stevin III

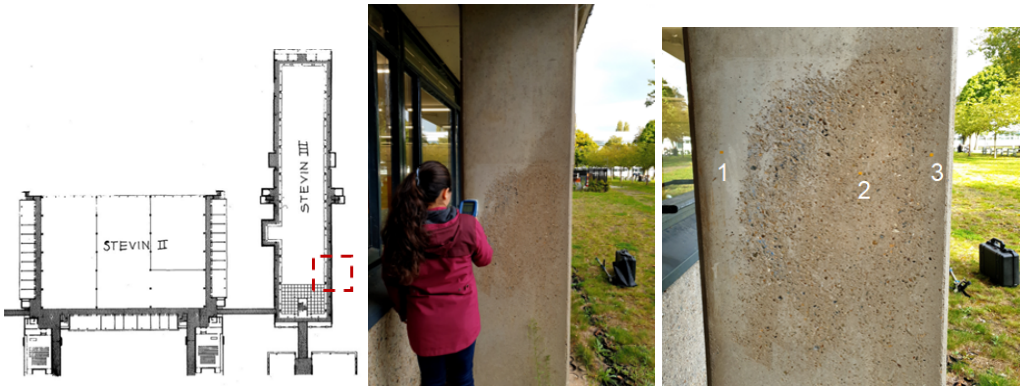

(a) Plan view, Stevin III **(b)** hXRF measurement **(c)** Measurement points

Figure 5.17: Column Stevin III CiTG Faculty, TU Delft

In Table 5.9, the elemental analysis of each spot using hXRF is reported. The analysis conducted at point 1 showed 18.73 wt% of SO_3, which is still higher than the average sulfur oxide content typically found in concrete made with any cement type. In points 2 and 3, SiO_2 concentrations higher than 70% were reported. This is attributed to the aggregates being visible on the grinded surface and, consequently, reflecting the high silica content.

Table 5.9: Chemical composition analysis CiTG column with hXRF

Spot	MgO	Al_2O_3	SiO_2	P_2O_5	SO_3	K_2O	CaO	TiO_2	MnO	Fe_2O_3
1	2.17	11.32	39.62	0.38	**18.73**	0.71	24.87	0.47	0.15	1.57
2	1.50	8.20	**75.67**	0.21	3.63	0.96	7.02	0.28	0.09	2.43
3	1.59	8.40	**76.67**	0.29	1.78	1.39	8.15	0.30	0.09	1.34

Additional tests were conducted on concrete facade surfaces and some columns, and the high concentration of sulfur continued to be detected.

It is assumed that some form of transparent coating or release agent was applied, which, strangely, may contain sulfur. However, no reports could be found in the literature about sulfur-based coatings used in concrete. For this reason, further research will be required to determine the cement type used in the faculty. Perhaps destructive testing (core extraction) might be necessary to perform laboratory chemical analysis.

In this case study, certain limitations of using hXRF were encountered. It proved impossible to detect and identify the characteristic oxides of concrete due to the presence of a finishing layer or some type of coating. To potentially recognize the cement type used, an exhaustive surface treatment must be conducted, or alternatively, laboratory tests.

Although the cement type could not be specified using the handheld X-ray fluorescence (hXRF) method, information was found in archive documents for the CiTG building complex provided by ”Campus Real Estate and Faculty Management (CREFM).” These documents indicate that the concrete structural members, such as foundation beams and ground floor, were cast with Portland cement (see Figure 5.18). Furthermore, in other documents, Portland cement is predominantly addressed in the context of the construction (see Figure 5.19). This study provides an initial insight into the chemical composition of the concrete elements and serves as motivation for future research.

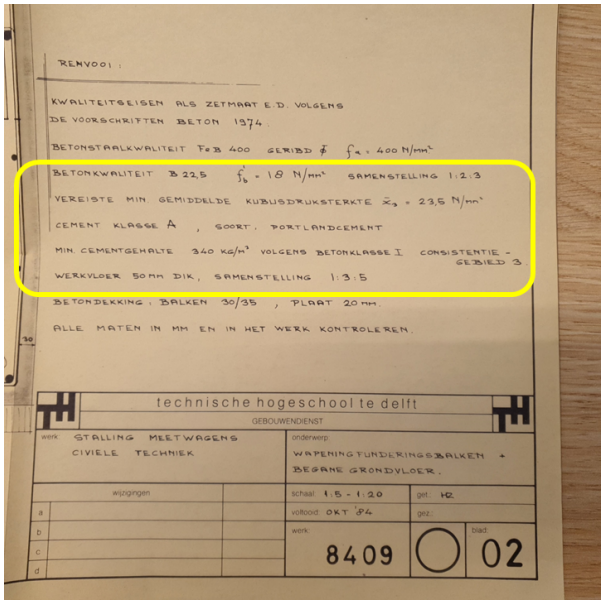

RENVOOI :

KWALITEITSEISEN ALS ZETMAAT E.D. VOLGENS
DE VOORSCHRIFTEN BETON 1974.

BETONSTAALKWALITEIT Fe B 400 GERIBD Ø f_a = 400 N/mm²

BETONKWALITEIT B 22,5 f_b = 18 N/mm² SAMENSTELLING 1:2:3

VEREISTE MIN. GEMIDDELDE KUBUSDRUKSTERKTE $\bar{x}_b$ = 23,5 N/mm²

CEMENT KLASSE A , SOORT: PORTLANDCEMENT

MIN. CEMENTGEHALTE 340 kg/m³ VOLGENS BETONKLASSE I CONSISTENTIE - GEBIED 3

WERKVLOER 50 mm DIK, SAMENSTELLING 1:3:5

BETONDEKKING : BALKEN 30/35 , PLAAT 20 mm.

ALLE MATEN IN MM EN IN HET WERK KONTROLEREN.

technische hogeschool te delft
GEBOUWENDIENST
werk: STALLING MEETWAGENS CIVIELE TECHNIEK
onderwerp: WAPENINGTUNDERINGSBALKEN + BEGANE GRONDVLOER.
wijzigingen
schaal: 1:5 - 1:20 get.: HZ
voltooid: OKT '84 gez.:
werk: 8409 blad: 02

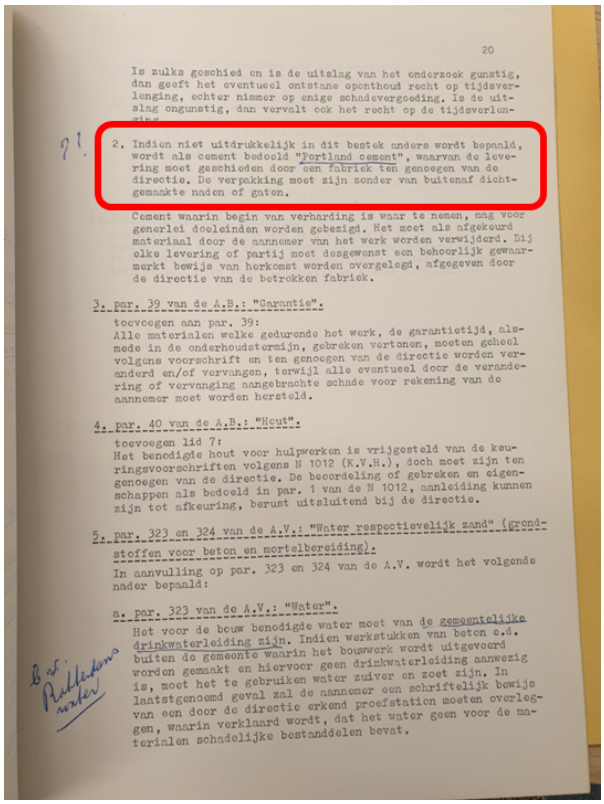

20

Is zulks geschied en is de uitslag van het onderzoek gunstig, dan geeft het eventueel ontstane oponthoud recht op tijdsverlenging, echter nimmer op enige schadevergoeding. Is de uitslag ongunstig, dan vervalt ook het recht op de tijdsverlen-

2. Indien niet uitdrukkelijk in dit bestek anders wordt bepaald, wordt als cement bedoeld "Portland cement", waarvan de levering moet geschieden door een fabriek ten genoegen van de directie. De verpakking moet zijn zonder van buitenaf dichtgemaakte naden of gaten.

Cement waarin begin van verharding is waar te nemen, mag voor generlei doeleinden worden gebezigd. Het moet als afgekeurd materiaal door de aannemer van het werk worden verwijderd. Bij elke levering of partij moet desgewenst een behoorlijk gewaarmerkt bewijs van herkomst worden overgelegd, afgegeven door de directie van de betrokken fabriek.

3. par. 39 van de A.B.: "Garantie".

toevoegen aan par. 39:
Alle materialen welke gedurende het werk, de garantietijd, alsmede in de onderhoudstermijn, gebreken vertonen, moeten geheel volgens voorschrift en ten genoegen van de directie worden verandert en/of vervangen, terwijl alle eventueel door de verandering of vervanging aangebrachte schade voor rekening van de aannemer moet worden hersteld.

4. par. 40 van de A.B.: "Hout".

toevoegen lid 7:
Het benodigde hout voor hulpwerken is vrijgesteld van de keuringsvoorschriften volgens N 1012 (K.V.H.), doch moet zijn ten genoegen van de directie. De beoordeling of gebreken en eigenschappen als bedoeld in par. 1 van de N 1012, aanleiding kunnen zijn tot afkeuring, berust uitsluitend bij de directie.

5. par. 323 en 324 van de A.V.: "Water respectievelijk zand" (grondstoffen voor beton en mortelbereiding).

In aanvulling op par. 323 en 324 van de A.V. wordt het volgende nader bepaald:

a. par. 323 van de A.V.: "Water".

Het voor de bouw benodigde water moet van de gemeentelijke drinkwaterleiding zijn. Indien werkstukken van beton o.d. buiten de gemeente waarin het bouwwerk wordt uitgevoerd worden gemaakt en hiervoor geen drinkwaterleiding aanwezig is, moet het te gebruiken water zuiver en zoet zijn. In laatstgenoemd geval zal de aannemer een schriftelijk bewijs van een door de directie erkend proefstation moeten overleggen, waarin verklaard wordt, dat het water geen voor de materialen schadelijke bestanddelen bevat.

Figure 5.18: Cement type specification foundation beams and ground floor, CiTG (credits to CREFM)

Figure 5.19: Cement type identification general report, CiTG (credits to CREFM)

5.3. Case study 3: SHCC-Concrete beam

The Strain Hardening Cementitious Composite (SHCC)-Concrete beam under study is located in an open garden behind the TU Delft Faculty of Electrical Engineering, Mathematics, and Computer Science. It was cast by the PhD candidate Shan He from the Faculty of Civil Engineering and Geoscience and has dimensions of 40 cm x 33 cm.

Once in place, a visual inspection was conducted to assess its condition and determine where to proceed with the surface chemical assessment using the handheld XRF. The first observation was that some areas of both the front and back surfaces were covered with paint (the front of the beam is shown in Figure 5.20). Additionally, the beam consisted of two distinct sections or layers. However, the left and right faces of the beam appeared suitable for conducting the hXRF measurements. Before commencing formal testing, some preliminary measurements were taken to quickly assess whether the oxide concentrations reported by the portable device were generally consistent with what is expected from the chemical composition of concrete.

Figure 5.20: Hybrid SHCC-Concrete beam

As shown in Figure 5.21, the measurement areas were divided into two: Measured Area I and Measured Area II. In each area, 20 measurement points were taken, with 10 from the top layer and 10 from the bottom layer. To track the measurement points, they were marked with small yellow tape squares, and then photographs of the analyzed areas were captured. This information was utilized to create the heat maps presented in Figure 5.22, Figure 5.23, Figure 5.24, Figure 5.25, and Figure 5.26. The darker color in these heat maps indicates a lower concentration of the specific oxide. Notably, among the depicted graphs, Figure 5.22, corresponding to magnesium weight percentage, reveals a clear distinction between the top (light green and yellow) and bottom layers (dark blue and dark green), as well as the case corresponding to iron weight percentage Figure 5.26, reveals a clear distinction between the top (dark purple and blue) and bottom layers (light green and yellow).

(a) Measured Area I **(b)** Measured Area II

Figure 5.21: Beam measured areas

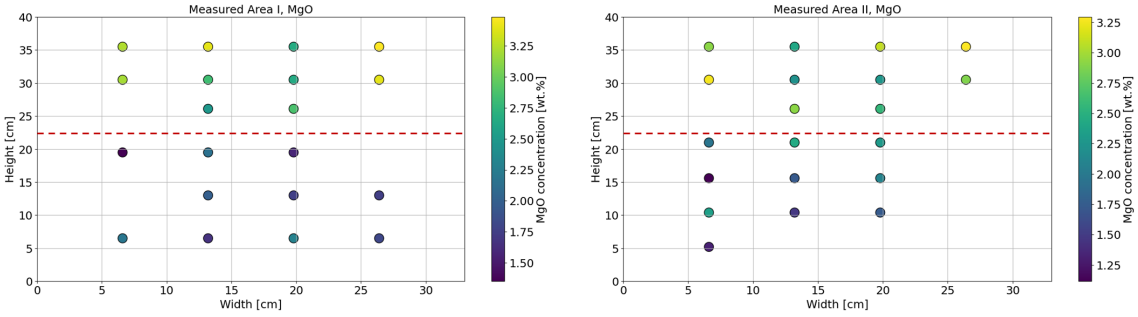

(a) Measured Area I **(b)** Measured Area II

Figure 5.22: Heat map measurement points [MgO]

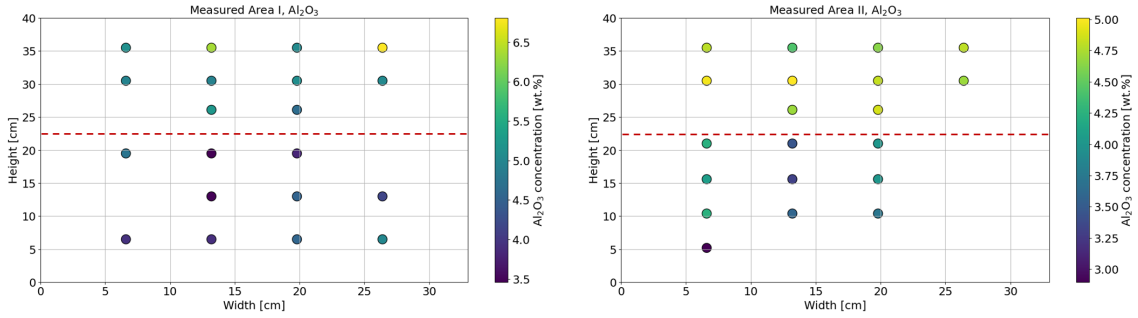

(a) Measured Area I **(b)** Measured Area II

Figure 5.23: Heat map measurement points [Al_2O_3]

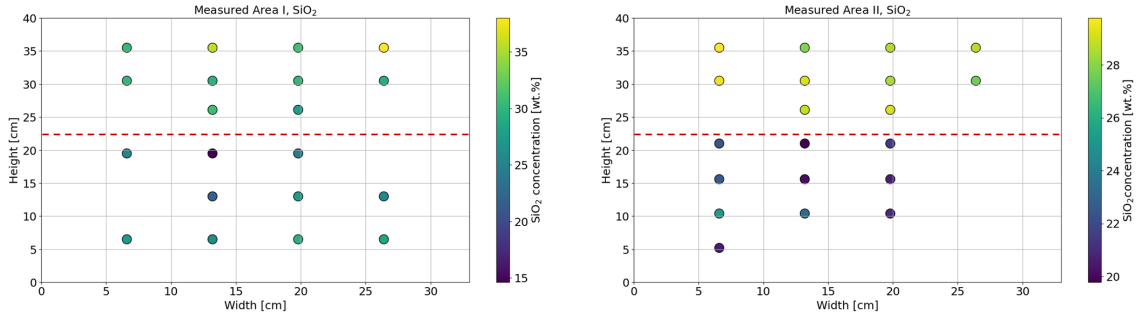

(a) Measured Area I **(b)** Measured Area II

Figure 5.24: Heat map measurement points [SiO_2]

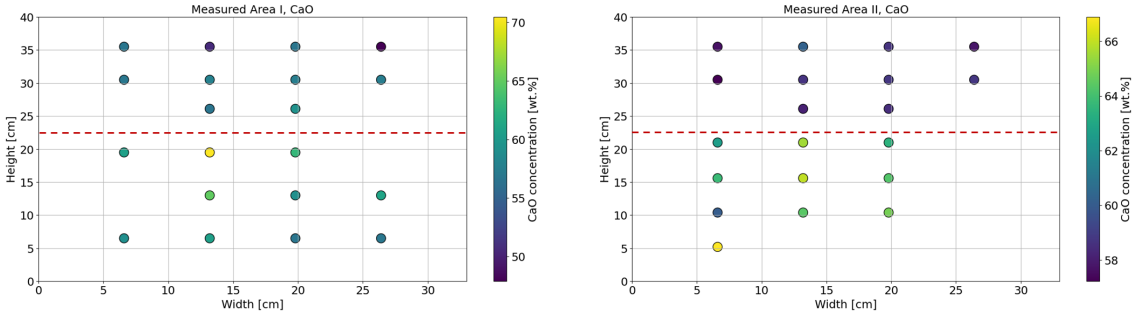

(a) Measured Area I **(b)** Measured Area II

Figure 5.25: Heat map measurement points [CaO]

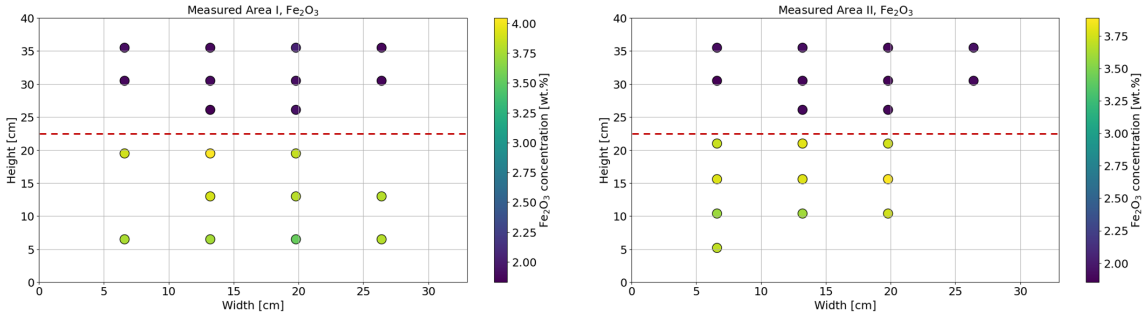

(a) Measured Area I **(b)** Measured Area II

Figure 5.26: Heat map measurement points [Fe_2O_3]

Descriptive statistics, including the average, standard deviation, and coefficient of variation, for the data obtained from the hXRF analysis of the top and bottom layers of the two measured areas, are summarized in Tables Table 5.10 and Table 5.11. A clear distinction can be noticed between the two layers, indicating the use of different cementitious materials in each layer. For instance, the weight percentage of magnesium oxide reported for the top layer in Area I was 3.02 wt%, while it was 1.85 wt% for the bottom layer in Area II. Calcium oxide content was 55.75 wt% for the top layer in Area I and 61.22 wt% for the bottom layer in Area II. Iron oxide was found to be 1.90 wt% in the top layer of Area I, and it increased to 3.81 wt%, almost twice the concentration, in the bottom layer of Area II. Similar tendencies are observed for the oxide results in Area II.

The precision of measurements varies between Area I and Area II. A more precise set of values indicates that more data points are closer to the average. For SiO_2, the standard deviation in the top layers of Area I and Area II is 3.14 wt% and 0.70 wt%, respectively. In the bottom layers of Area I and Area II, the standard deviation for SiO_2 is 4.24 wt% and 1.66 wt%, respectively. Similarly, for CaO, the standard deviation in the top layers of Area I and Area II is 3.57 wt% and 0.80 wt%, respectively, and in the bottom layers of Area I and Area II, the standard deviation for CaO is 4.10 wt% and 1.92 wt%, respectively.

The smaller standard deviations indicate lower absolute variability of the data points relative to the mean. The differences in the concrete matrix (with a higher presence of fine aggregates at the surface) and localized efflorescence in the cement skin could explain the variations in precision.

Table 5.10: Chemical composition analysis Beam Area I with hXRF

		MgO	Al_2O_3	SiO_2	P_2O_5	SO_3	K_2O	CaO	TiO_2	MnO	Fe_2O_3
Top layer Area I	Average (wt.%)	3.02	5.32	31.22	0.21	1.58	0.56	55.72	0.39	0.10	1.90
	Std. Dev (wt.%)	0.36	0.69	3.14	0.05	0.42	0.04	3.57	0.03	0.00	0.06
	CoV (%)	0.12	0.13	0.10	0.26	0.26	0.08	0.06	0.08	0.05	0.03
Bottom layer Area I	Average (wt.%)	1.85	4.16	24.98	0.38	1.98	0.99	61.22	0.53	0.09	3.81
	Std. Dev (wt.%)	0.30	0.53	4.24	0.07	0.28	0.36	4.10	0.03	0.01	0.13
	CoV (%)	0.16	0.13	0.17	0.18	0.14	0.37	0.07	0.05	0.07	0.03

Table 5.11: Chemical composition analysis Beam Area II with hXRF

		MgO	Al_2O_3	SiO_2	P_2O_5	SO_3	K_2O	CaO	TiO_2	MnO	Fe_2O_3
Top layer Area II	Average (wt.%)	2.78	4.77	28.77	0.25	2.03	0.60	58.43	0.37	0.10	1.89
	Std. Dev (wt.%)	0.40	0.17	0.70	0.06	0.38	0.04	0.82	0.01	0.01	0.02
	CoV (%)	0.14	0.04	0.02	0.25	0.19	0.07	0.01	0.02	0.05	0.01
Bottom layer Area II	Average (wt.%)	1.85	3.76	21.67	0.39	2.76	1.07	64.18	0.50	0.09	3.73
	Std. Dev (wt.%)	0.46	0.44	1.66	0.06	0.29	0.31	1.92	0.02	0.01	0.09
	CoV (%)	0.25	0.12	0.08	0.15	0.10	0.29	0.03	0.04	0.10	0.02

By comparing the results obtained from the handheld XRF analysis of the top and bottom layers with the oxide concentrations reported in the experimental results of this thesis and the typical oxide content found in the literature for CEM I and CEM III/B, one may conclude that the cement type used in the top layer was some form of CEM III, while CEM I was used in the bottom layer. Fortunately, the PhD candidate had knowledge of the cementitious materials used in the fabrication of the beam. To confirm the composition, the mix design of the beam was requested from the candidate, as depicted in Table 5.12. The top layer, which corresponds to the strain-hardening cementitious composite (SHCC), was cast using CEM III/B and limestone powder, while CEM I was used in the bottom layer (concrete). The use of limestone powder (530 kg) in a binder of the top layer prevented the identification of pure CEM III/B cement which is a very valuable example. Blends of cement can be identified with hXRF, but not their individual components.

Table 5.12: Mixture compositions of SHCC and concrete [unit in kg/m^3] [91]

Material	SHCC	Concrete
CEM I 52.5 R	-	260
CEM III/B 42.5 N	1060	-
Limestone powder	530	-
Sand (0.125-4 mm)	-	847
Gravel (4-16 mm)	-	1123
PVA fiber	26	-
Water	424	-
Superplasticizer	2	0.26

In summary, commencing the chemical composition assessment with the handheld XRF, subsequent to a visual inspection, proves valuable for identifying potential measurement areas, especially

those with visible cement skin, devoid of any coating or paint, as well as areas with cracks. Moreover, conducting a preliminary measurement with the portable device on the concrete beam under study is a critical step as it provides an initial insight into the oxide concentrations at the concrete surface. This aids in the decision-making process, helping determine the feasibility and convenience of proceeding with the formal analysis.

In this case study, the cement type used in the bottom layer was recognized from the data obtained with the hXRF. However, the recognition of the cement type of the top layer was more challenging because it was not only composed of CEM III/B but also limestone powder. For this particular case, introducing the typical ranges for oxides of concretes cast with different cementitious materials could provide a more accurate answer to the cement type.

6

Guideline for In-situ testing of concrete structures with hXRF

This guideline is established for the in-situ appraisal and classification of concrete structural members prior their demolition through the chemical composition analysis using a Handheld X-ray Fluorescence analyzer. This is based on the learning gained from the literature review (chapter 2), the laboratory experiments (chapter 4), and the case studies (chapter 5). Figure 6.1 shows the guideline developed for in-situ testing of concrete chemical composition assessment.

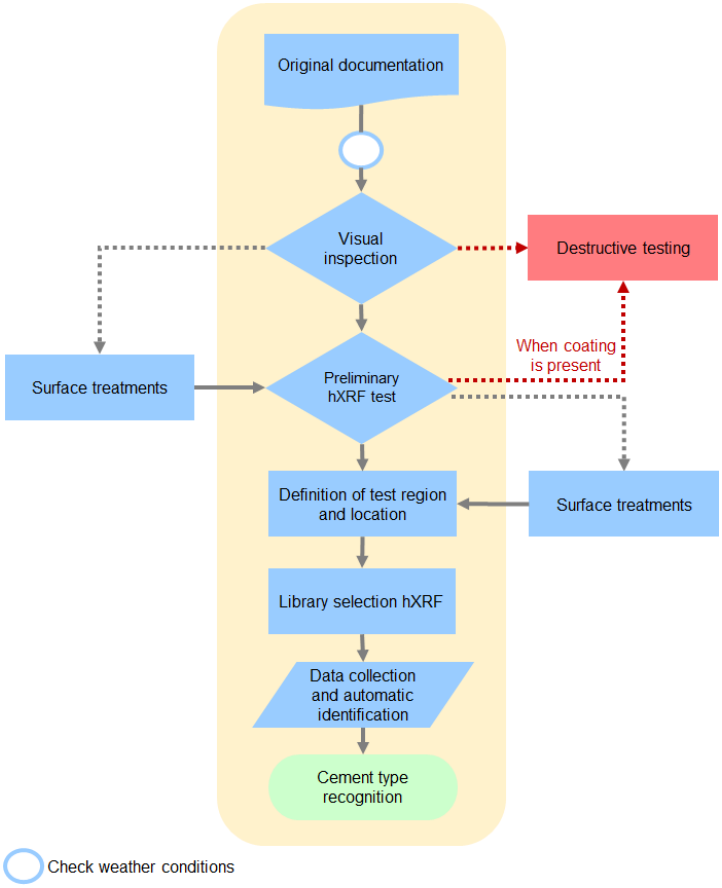

Figure 6.1: Guideline for in-situ testing of concrete chemical composition with cement type driven recognition

The description of each of the steps Figure 6.1 of the proposed guideline is given next:

Original documentation: Before commencing an in-situ assessment, it is essential to collect construction documentation related to the concrete structure, particularly if there is evidence that such documentation exists. This should include information on construction methods, drawings, and design. Obtaining records such as construction drawings and specifications can provide valuable insights into the presence of precast or cast-in-situ elements. This information may be useful for determining suitable test region (TR) for handheld XRF measurements. Additionally, if it is not known whether the cast-in-situ elements were fabricated using the same type of cement; utilizing this technique could help verify this information.

Perhaps, for old structures historical documentation might not be available, therefore, this step can be skipped.

Check weather conditions: Handheld XRF analysis on concrete structural members must be carried out on dried concrete surfaces, as a result, before going to the field the weather should be checked.

Visual inspection: This step involves the examination of the concrete surfaces to identify prospective regions for hXRF analysis. The appearance of concrete surfaces can change due to aging, loading, or interaction with the environment to which they are exposed. Figure 6.2 is provided to illustrate the various examples of concrete surfaces.

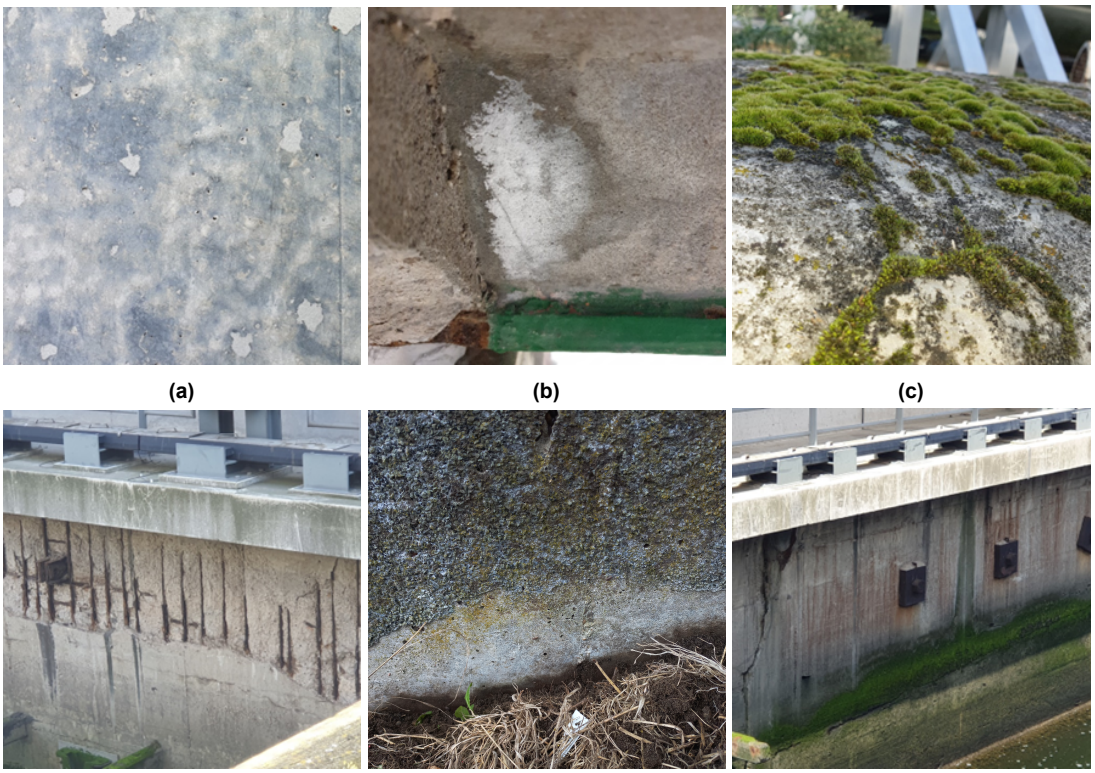

Figure 6.2: Concrete surface texture examples: (a) Concrete coated, (b) Concrete efflorescence, (c) Algae growth, (d) Steel corrosion and concrete cover damage, (e) Concrete coated and visible concrete surface, (f) Crack, dirt and dust

For situations in which all the concrete structural members are fully coated, painted, or entirely covered by any type of biological compound or contain efflorescence, i.e. there is no visible concrete surface, a surface treatment may be needed. Destructive testing may be required only in cases where surface treatment is not feasible or possible, and there is a need to determine the composition of the raw materials (e.g., cement type).

In addition, some concrete surfaces might have cracks or fissures. It is advised to avoid performing hXRF measurements where these imperfections are present, as the secondary X-rays' penetration depth may extend beyond the concrete surface, potentially reporting higher silica concentrations due to the fine and coarse aggregates present in the concrete, making cement-type detection difficult.

If there is a localized presence of algae, fissures, efflorescence, or other types of deterioration, it might be possible to detect concrete surfaces where these are not very pronounced, and element analysis should be possible without any surface treatment.

Preliminary hXRF test: This action is necessary to quickly verify that there is no presence of unexpected oxide concentrations. Three preliminary measurements are sufficient to obtain the first impression of the surface's chemical composition. In cases where unexpected concentrations are reported, it may indicate some kind of contamination, for instance, black crust, or that even though the concrete surface was visible and appeared in good condition, some type of finalizing layer or coating was used, which is not visible to the naked eye but is revealed in the preliminary analysis with hXRF. If this is the case, it should be considered for surface treatment. However, if this is not possible or feasible, destructive testing may be required.

Note: For testing in a safe work environment and to have full access to all concrete structural members, safety measures must be considered. For instance, the rental of equipment such as a cherry picker and scaffolding.

Definition of test region (TR) and locations (TL): Once the suitable concrete surfaces were identified in the visual inspection or the surfaces were treated for the situations where necessary, the limitation of the test region and the test location is the next step.

The test region (TR) represents a defined area chosen for measuring the chemical composition of one or more concrete structural members, as illustrated in Figure 6.3. It is recommended to specify a test region for each structural member category. Multiple test regions can be defined within a concrete component category, this might depend on the available concrete surface area suitable for hXRF measurements. For instance, one can define a test region for analyzing beams, another for the deck, and another for a column, as needed, particularly in the case of a bridge. Additionally, it is important to consider whether the elements were prefabricated or cast in situ if this information is available. It is assumed that the composition of each structural member category remains consistent. Therefore, there is no necessity to analyze every concrete structural member throughout the entire structure.

The test locations (TL) refer to the measurement point or hXRF measurement (see Figure 6.3). From the literature [10] and chapter 4, it was found that 20 measurements is enough to identify the cement type. These measurements can be distributed in one or more TR.

Maintaining a record of the test locations is useful for further data analysis if required, or for inclusion in a final report along with photographic records of where the measurements were taken. The test locations can be marked before proceeding with data collection using a template, as shown in Figure 6.4.

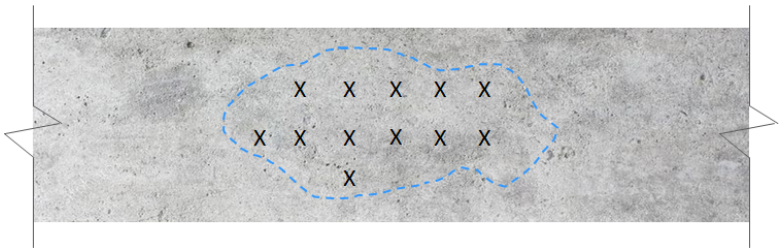

Figure 6.3: Illustration of test region and test location (blue dash line= test region, black "X"= hXRF measurement/test location)

Figure 6.4: Template for marking test locations

Library selection hXRF: This step involves turning on the handheld XRF device, ensuring that the cement mode is selected, setting the measurement time to 30 seconds with a power of 15 kV, and selecting the cement library (as depicted in Figure 6.5). The library selection enables the examination of potential matches with the in-situ measurements being conducted.

Note: for this thesis, the cement and aggregate libraries were not available yet so this was not used, however, it was decided to add this step in this guideline because the libraries are already under development.

Figure 6.5: Cement library selection

Data collection and automatic identification: After performing the visual inspection, deciding on the TR and TL, and selecting the required library, the last step is to proceed with the formal element analysis using the hXRF. In other words, the data collection and automatic identification (Figure 6.6).

Cement type recognition: This is the final step of the guideline, where the cement type has been identified, and the demolishers can be personally informed with a final assessment report. With this information, they will be able to separate the concrete structural members (foundation, columns, beams, walls, supporting beams) into different batches based not only, for instance, on concrete strength, and aggregate type but also on cement type.

In the particular case that one also wants to identify the aggregate type used in the concrete mix, the assessment process is divided into three main stages, as illustrated in Figure 6.7. First, the concrete surface should be sanded, making the aggregates visible. An example of the contrast between a regular concrete surface and a sanded concrete surface is shown in Figure 6.8. Next, the aggregates library must be selected and lastly, the aggregates elemental analysis with the hXRF is carried out.

(a) (b)

Figure 6.6: (a) Data collection, (b) Automatic identification

To summarize, before going to the site of the concrete structure to be analyzed, it is necessary to collect the original documentation of the structure if it exists in order to obtain information on the elements that were prefabricated and cast in-situ, and to check the weather conditions. It is not necessary to make a seasonal distinction, but it is necessary to check that it is not raining on the day of the in-situ analysis. After this, while in-situ, proceed with a visual inspection in order to evaluate the appearance and condition of the concrete surfaces, and identify possible regions for chemical composition analysis with the hXRF. In some cases, surface treatment may be required as mentioned above, and in very specific situations destructive testing may be required. Then, it is recommended to do a preliminary analysis to evaluate that there are no unexpected concentrations of the element oxides, depending on this preliminary analysis it can be decided if it is also necessary to treat the surface. The last steps are the definition of the regions and locations for the hXRF analysis, the data collection, and finally the recognition of the cement type. For the recognition of aggregate type, the concrete surface should be sanded, and then proceed with the hXRF measurements.

The aim of this guideline is to propose a systematic approach for the in-situ assessment of concrete structures before their demolition through chemical composition analysis using hXRF. Thanks to its portability and rapid results, hXRF allows for field assessments. It is important to highlight that this procedure can be followed, for example, in cases where cultural heritage needs to be assessed. Another advantage is that hXRF is a non-destructive technique, making it very convenient for testing structures that are intended for preservation, or for testing the quality of concrete in existing structures from which remaining service life needs to be determined, or in case of structural and technical repair (e.g., use of hXRF to quantify chloride ions in-situ: as study of structural repair [18]).

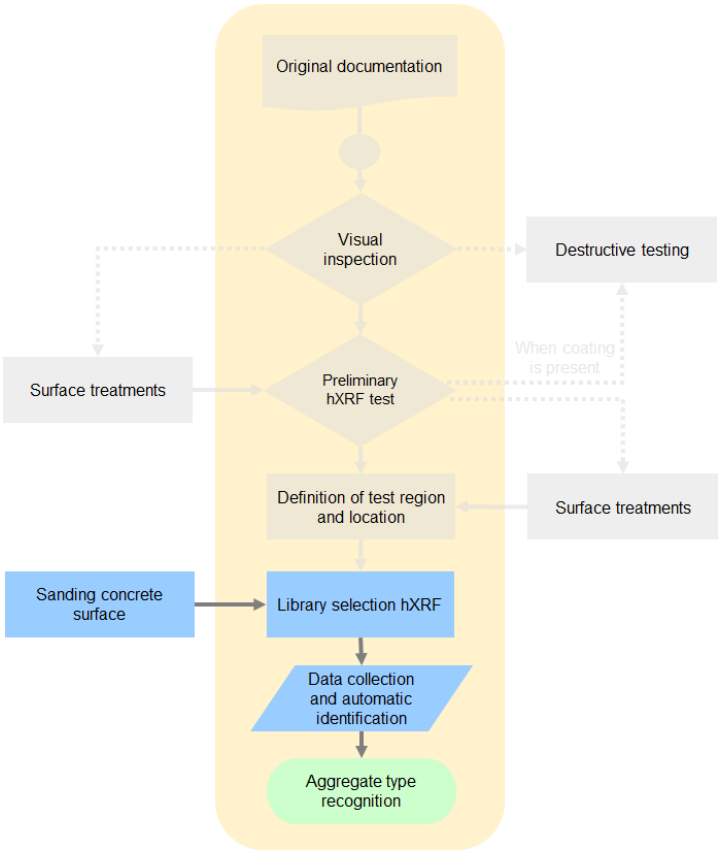

Figure 6.7: Guideline for in-situ testing of concrete chemical composition with aggregate type driven recognition

(a) **(b)**

Figure 6.8: (a) Concrete surface, (b) Sanded concrete surface

7

Conclusions and recommendations

In this study, four test series were conducted to investigate the influence of concrete mix designs with varying water-to-cement ratios, the age of concrete samples, and exposure to different relative humidities and carbonation on the analysis of their surface chemical composition using hXRF. The primary goal was to validate hypotheses and gain insights into additional factors that may impact hXRF measurements. Subsequently, in-situ measurements were conducted across various case studies and guideline for in-situ testing of concrete structures with hXRF was developed. The following conclusions and recommendations can be drawn:

- The hXRF analysis on paste and concrete surfaces is independent of the water-to-cement ratio, curing age, and carbonation.
- Higher relative humidity conditions than 75% cause efflorescence on paste/concrete surface and affect the measurements with hXRF, potentially posing challenges in terms of data reproducibility and cement-type recognition.
- Handheld XRF shows considerable potential as a non-destructive technique for rapidly assessing the chemical composition and quality of concrete. This would be beneficial for guaranteeing the recognition of concrete right at its origin, enhancing the efficiency of demolition, and providing guidance for the quality of recycled concrete.
- It is essential that the cement paste skin on the various concrete elements to be analyzed with hXRF is visible and free from any coatings or paint. The presence of coatings may pose challenges for chemical analysis or imply prior surface treatments.
- When conducting in-situ element analysis with hXRF, it is important to mark or delineate the test locations and maintain a record, such as a photograph and notes of the measurement reference from the device, in case some data points need to be verified or double-check in later stages of the appraisal.
- Detecting the cement type with hXRF in situ can be challenging, considering that concrete structures are typically exposed to various environmental conditions during their service life. However, a more in-depth analysis can focus on concrete's characteristic oxides that are less influenced or unaffected by environmental conditions. The oxides, such as MgO, P_2O_5, TiO_2, MnO, and Fe_2O_3 can serve as characteristic oxides for cement-type identification.
- To avoid the effect of efflorescence at the paste/concrete surface specimens on the hXRF measurements, it is important to fully dry the specimens, and in case not all the specimens are tested on the same day, it is recommended to leave them in places with RH below 70% and cover them with plastic foil.
- For future work, it is recommended to further investigate how to quantify chloride concentration quantitatively. Quantifying the degree of contamination or chloride content could be valuable for quality control testing of concrete.
- Further research should be done for the identification of the optimum number of test locations and test regions for the chemical appraisal of concrete structural members in-situ.

A

Effect of water-to-cement ratio

A.1. Bar plots Test Series 1

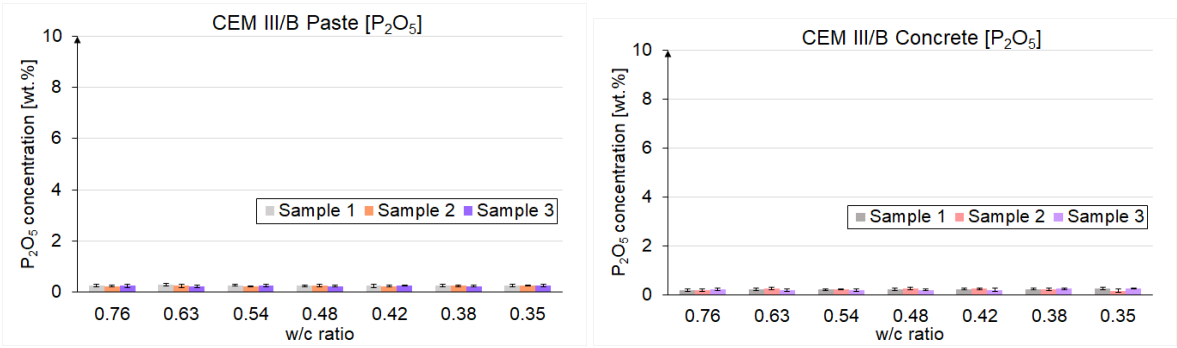

(a) CEM III/B Paste

(b) CEM III/B Concrete

Figure A.1: Chemical composition analysis [P_2O_5] with hXRF on paste and concrete surfaces with different w/c ratios

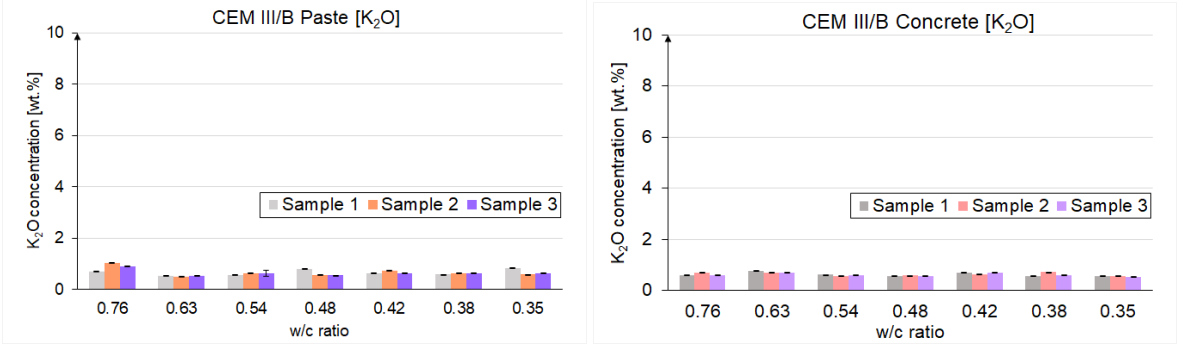

(a) CEM III/ Paste

(b) CEM III/B Concrete

Figure A.2: Chemical composition analysis [K_2O] with hXRF on paste and concrete surfaces with different w/c ratios

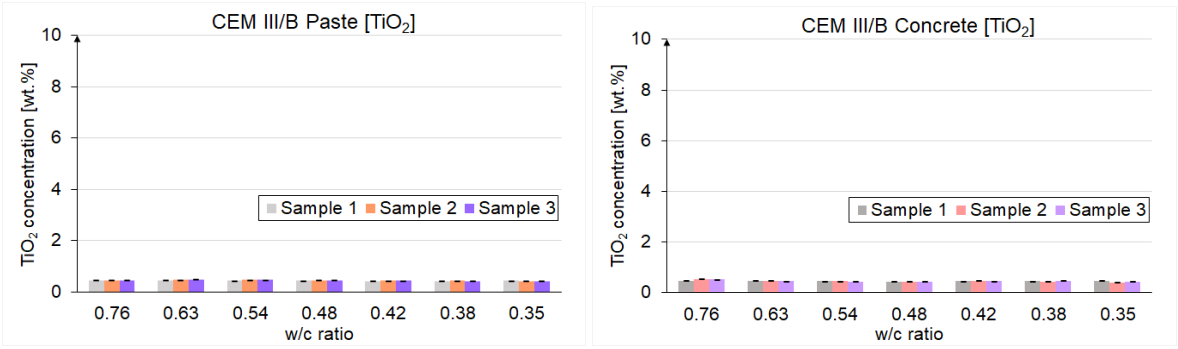

(a) CEM III/B Paste **(b)** CEM III/B Concrete

Figure A.3: Chemical composition analysis [TiO_2] with hXRF on paste and concrete surfaces with different w/c ratios

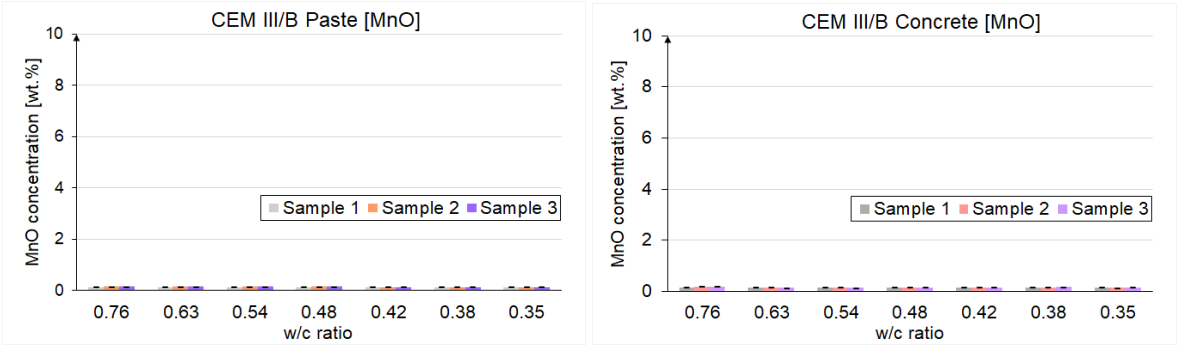

(a) CEM III/B Paste **(b)** CEM III/B Concrete

Figure A.4: Chemical composition analysis [MnO] with hXRF on paste and concrete surfaces with different w/c ratios

A.2. Summary tables Test Series 1

Table A.1: Chemical composition analysis of paste samples M1

Sample	w/c		MgO	Al_2O_3	SiO_2	P_2O_5	SO_3	K_2O	CaO	TiO_2	MnO	Fe_2O_3
		Average (wt.%)	3.79	6.67	32.68	0.27	2.70	0.69	50.21	0.46	0.14	2.38
		Std. Dev (wt.%)	0.40	0.13	0.17	0.05	0.02	0.02	0.30	0.01	0.00	0.02
M1-1	0.76	CoV (%)	10.47	1.88	0.53	18.44	0.73	2.45	0.59	1.32	2.02	1.03
		Minimum (wt.%)	3.26	6.49	32.47	0.19	2.68	0.66	49.72	0.45	0.14	2.34
		Maximum (wt%)	4.33	6.85	32.98	0.33	2.74	0.71	50.62	0.47	0.15	2.43
		Average (wt.%)	3.83	7.05	31.41	0.24	3.77	1.04	49.72	0.47	0.15	2.32
		Std. Dev (wt.%)	0.42	0.13	0.12	0.03	0.03	0.01	0.27	0.01	0.00	0.02
M1-2	0.76	CoV (%)	10.84	1.83	0.39	14.36	0.68	0.74	0.54	1.65	2.00	0.84
		Minimum (wt.%)	3.19	6.85	31.24	0.17	3.74	1.03	49.34	0.46	0.14	2.29
		Maximum (wt%)	4.69	7.31	31.57	0.29	3.81	1.05	50.05	0.48	0.15	2.34
		Average (wt.%)	3.76	7.00	31.95	0.25	3.89	0.90	49.36	0.46	0.15	2.30
		Std. Dev (wt.%)	0.28	0.12	0.11	0.06	0.04	0.01	0.17	0.00	0.00	0.02
M1-3	0.76	CoV (%)	7.46	1.67	0.35	24.10	0.99	1.16	0.35	0.90	2.68	0.69
		Minimum (wt.%)	3.35	6.82	31.80	0.10	3.82	0.89	49.14	0.45	0.14	2.27
		Maximum (wt%)	4.22	7.18	32.15	0.32	3.94	0.92	49.68	0.46	0.15	2.32

Table A.2: Chemical composition analysis of paste samples M2

Sample	w/c		MgO	Al_2O_3	SiO_2	P_2O_5	SO_3	K_2O	CaO	TiO_2	MnO	Fe_2O_3
		Average (wt.%)	3.80	6.51	32.58	0.29	3.47	0.55	49.87	0.44	0.14	2.35
		Std. Dev (wt.%)	0.32	0.12	0.09	0.05	0.03	0.01	0.30	0.01	0.00	0.03
M2-1	0.63	CoV (%)	8.46	1.88	0.26	16.34	0.78	1.94	0.59	2.31	2.80	1.21
		Minimum (wt.%)	3.46	6.33	32.43	0.19	3.43	0.53	49.38	0.42	0.14	2.30
		Maximum (wt%)	4.43	6.74	32.73	0.37	3.53	0.56	50.24	0.46	0.15	2.41
		Average (wt.%)	3.76	6.69	33.05	0.25	3.30	0.50	49.54	0.47	0.15	2.31
		Std. Dev (wt.%)	0.38	0.15	0.11	0.06	0.02	0.01	0.42	0.01	0.00	0.03
M2-2	0.63	CoV (%)	10.05	2.28	0.34	24.26	0.71	2.13	0.85	1.81	3.33	1.40
		Minimum (wt.%)	2.89	6.50	32.89	0.14	3.26	0.48	48.81	0.46	0.14	2.27
		Maximum (wt%)	4.23	7.04	33.25	0.32	3.33	0.51	50.33	0.49	0.16	2.37
		Average (wt.%)	3.81	6.59	32.39	0.23	3.25	0.53	50.21	0.48	0.15	2.38
		Std. Dev (wt.%)	0.30	0.14	0.12	0.04	0.02	0.01	0.23	0.00	0.00	0.02
M2-3	0.63	CoV (%)	7.78	2.15	0.36	16.59	0.72	2.30	0.47	0.99	2.45	0.84
		Minimum (wt.%)	3.33	6.31	32.23	0.17	3.22	0.49	49.96	0.47	0.14	2.35
		Maximum (wt%)	4.27	6.77	32.55	0.28	3.30	0.54	50.70	0.49	0.16	2.41

Table A.3: Chemical composition analysis of paste samples M3

Sample	w/c		MgO	Al_2O_3	SiO_2	P_2O_5	SO_3	K_2O	CaO	TiO_2	MnO	Fe_2O_3
		Average (wt.%)	3.70	6.58	33.21	0.27	3.61	0.56	49.24	0.44	0.14	2.26
		Std. Dev (wt.%)	0.35	0.12	0.14	0.03	0.02	0.02	0.30	0.01	0.00	0.03
M3-1	0.54	CoV (%)	9.51	1.89	0.43	10.68	0.62	3.81	0.62	1.52	2.60	1.20
		Minimum (wt.%)	3.25	6.39	32.97	0.23	3.56	0.52	48.54	0.42	0.13	2.20
		Maximum (wt%)	4.34	6.78	33.39	0.31	3.63	0.58	49.66	0.45	0.14	2.29
		Average (wt.%)	3.56	6.65	31.95	0.24	3.64	0.63	50.37	0.47	0.15	2.34
		Std. Dev (wt.%)	0.50	0.12	0.10	0.02	0.02	0.01	0.42	0.01	0.00	0.02
M3-2	0.54	CoV (%)	13.99	1.86	0.32	8.37	0.42	1.88	0.84	1.62	1.65	1.05
		Minimum (wt.%)	2.65	6.48	31.82	0.19	3.61	0.62	49.92	0.46	0.15	2.29
		Maximum (wt%)	4.12	6.88	32.17	0.25	3.66	0.65	51.16	0.49	0.16	2.37
		Average (wt.%)	3.73	6.70	32.47	0.26	3.50	0.63	49.77	0.47	0.15	2.32
		Std. Dev (wt.%)	0.37	0.09	0.45	0.04	0.10	0.10	0.52	0.01	0.01	0.04
M3-3	0.54	CoV (%)	10.02	1.35	1.40	16.86	2.77	16.16	1.04	1.73	3.72	1.60
		Minimum (wt.%)	3.31	6.57	31.91	0.16	3.36	0.54	48.86	0.46	0.14	2.25
		Maximum (wt%)	4.46	6.87	32.98	0.30	3.60	0.76	50.44	0.49	0.16	2.37

Table A.4: Chemical composition analysis of paste samples M4

Sample	w/c		MgO	Al_2O_3	SiO_2	P_2O_5	SO_3	K_2O	CaO	TiO_2	MnO	Fe_2O_3
		Average (wt.%)	3.78	7.01	32.64	0.25	4.12	0.82	48.47	0.44	0.14	2.17
		Std. Dev (wt.%)	0.38	0.11	0.06	0.04	0.03	0.01	0.31	0.01	0.00	0.02
M4-1	0.48	CoV (%)	10.02	1.60	0.19	17.73	0.79	1.18	0.64	1.30	2.29	1.05
		Minimum (wt.%)	3.33	6.81	32.58	0.17	4.08	0.79	48.05	0.43	0.13	2.15
		Maximum (wt%)	4.44	7.12	32.75	0.34	4.17	0.83	49.00	0.45	0.15	2.22
		Average (wt.%)	3.78	6.68	32.71	0.25	3.70	0.58	49.44	0.46	0.15	2.25
		Std. Dev (wt.%)	0.37	0.13	0.14	0.05	0.03	0.01	0.33	0.00	0.00	0.02
M4-2	0.48	CoV (%)	9.88	1.87	0.43	18.98	0.76	1.86	0.66	1.01	1.82	1.05
		Minimum (wt.%)	2.86	6.49	32.40	0.15	3.64	0.56	49.18	0.46	0.14	2.22
		Maximum (wt%)	4.18	6.85	32.90	0.30	3.73	0.59	50.16	0.47	0.15	2.29
		Average (wt.%)	3.63	6.63	32.43	0.24	3.67	0.55	50.03	0.46	0.15	2.23
		Std. Dev (wt.%)	0.41	0.11	0.12	0.04	0.02	0.01	0.38	0.01	0.00	0.02
M4-3	0.48	CoV (%)	11.36	1.72	0.37	15.16	0.67	1.71	0.76	1.75	2.45	0.94
		Minimum (wt.%)	3.00	6.50	32.23	0.17	3.63	0.54	49.64	0.45	0.14	2.20
		Maximum (wt%)	4.14	6.81	32.58	0.28	3.70	0.56	50.77	0.47	0.15	2.27

Table A.5: Chemical composition analysis of paste samples M5

Sample	w/c		MgO	Al_2O_3	SiO_2	P_2O_5	SO_3	K_2O	CaO	TiO_2	MnO	Fe_2O_3
		Average (wt.%)	3.82	6.65	33.29	0.25	3.83	0.63	48.74	0.43	0.14	2.23
		Std. Dev (wt.%)	0.18	0.10	0.08	0.06	0.02	0.01	0.18	0.00	0.00	0.02
M5-1	0.42	CoV (%)	4.63	1.54	0.24	23.71	0.55	1.83	0.38	1.15	1.50	0.81
		Minimum (wt.%)	3.42	6.53	33.18	0.16	3.81	0.60	48.55	0.42	0.14	2.20
		Maximum (wt%)	4.06	6.87	33.46	0.34	3.88	0.64	49.19	0.44	0.14	2.26
		Average (wt.%)	3.67	6.86	32.49	0.23	4.11	0.72	49.20	0.43	0.14	2.15
		Std. Dev (wt.%)	0.30	0.10	0.10	0.03	0.04	0.01	0.34	0.00	0.00	0.02
M5-2	0.42	CoV (%)	8.21	1.45	0.32	15.21	0.89	1.78	0.68	0.89	2.69	1.04
		Minimum (wt.%)	3.23	6.69	32.34	0.19	4.06	0.70	48.77	0.43	0.14	2.13
		Maximum (wt%)	4.13	7.04	32.65	0.29	4.17	0.74	49.76	0.44	0.15	2.19
		Average (wt.%)	3.77	6.76	33.08	0.25	4.15	0.63	48.62	0.44	0.14	2.16
		Std. Dev (wt.%)	0.24	0.09	0.09	0.01	0.03	0.01	0.14	0.01	0.00	0.01
M5-3	0.42	CoV (%)	6.36	1.29	0.27	5.99	0.73	1.76	0.28	1.92	1.37	0.53
		Minimum (wt.%)	3.39	6.65	32.96	0.22	4.11	0.61	48.36	0.43	0.14	2.14
		Maximum (wt%)	4.29	6.92	33.25	0.26	4.20	0.64	48.80	0.46	0.15	2.18

Table A.6: Chemical composition analysis of paste samples M6

Sample	w/c		MgO	Al_2O_3	SiO_2	P_2O_5	SO_3	K_2O	CaO	TiO_2	MnO	Fe_2O_3
		Average (wt.%)	3.76	6.89	34.25	0.26	3.49	0.59	48.06	0.42	0.13	2.17
		Std. Dev (wt.%)	0.33	0.12	0.14	0.04	0.04	0.01	0.22	0.01	0.00	0.03
M6-1	0.38	CoV (%)	8.76	1.72	0.42	16.11	1.20	1.71	0.46	2.16	3.69	1.51
		Minimum (wt.%)	3.24	6.60	34.08	0.17	3.45	0.57	47.61	0.41	0.13	2.13
		Maximum (wt%)	4.23	7.04	34.51	0.30	3.59	0.60	48.35	0.43	0.14	2.23
		Average (wt.%)	3.69	6.83	32.90	0.24	4.32	0.63	48.68	0.44	0.14	2.15
		Std. Dev (wt.%)	0.43	0.10	0.08	0.02	0.03	0.01	0.37	0.01	0.00	0.02
M6-2	0.38	CoV (%)	11.62	1.52	0.25	10.09	0.61	1.85	0.76	1.34	1.99	0.83
		Minimum (wt.%)	2.82	6.59	32.80	0.20	4.28	0.61	48.27	0.43	0.14	2.12
		Maximum (wt%)	4.14	6.97	33.03	0.28	4.35	0.64	49.33	0.45	0.15	2.18
		Average (wt.%)	3.94	7.05	33.78	0.24	4.28	0.63	47.39	0.43	0.14	2.12
		Std. Dev (wt.%)	0.28	0.10	0.11	0.02	0.03	0.01	0.26	0.01	0.00	0.02
M6-3	0.38	CoV (%)	7.12	1.40	0.32	10.22	0.76	1.46	0.54	1.78	2.09	0.89
		Minimum (wt.%)	3.67	6.85	33.61	0.21	4.25	0.62	46.88	0.42	0.14	2.10
		Maximum (wt%)	4.55	7.19	33.95	0.28	4.34	0.65	47.67	0.44	0.14	2.16

Table A.7: Chemical composition analysis of paste samples M7

Sample	w/c		MgO	Al_2O_3	SiO_2	P_2O_5	SO_3	K_2O	CaO	TiO_2	MnO	Fe_2O_3
		Average (wt.%)	4.10	6.91	33.36	0.26	3.15	0.83	48.56	0.44	0.14	2.25
		Std. Dev (wt.%)	0.29	0.08	0.09	0.06	0.02	0.01	0.32	0.00	0.00	0.02
M7-1	0.35	CoV (%)	7.02	1.18	0.26	21.47	0.58	1.44	0.67	0.97	1.38	0.85
		Minimum (wt.%)	3.66	6.74	33.25	0.11	3.11	0.80	48.04	0.44	0.14	2.22
		Maximum (wt%)	4.60	7.01	33.53	0.32	3.18	0.84	49.14	0.45	0.14	2.27
		Average (wt.%)	3.91	6.76	33.34	0.27	4.17	0.59	48.23	0.43	0.14	2.15
		Std. Dev (wt.%)	0.42	0.13	0.11	0.03	0.04	0.01	0.32	0.01	0.00	0.02
M7-2	0.35	CoV (%)	10.68	1.88	0.32	9.75	0.91	0.99	0.66	1.26	2.04	0.89
		Minimum (wt.%)	3.22	6.54	33.14	0.23	4.12	0.58	47.73	0.42	0.14	2.13
		Maximum (wt%)	4.54	6.95	33.52	0.32	4.23	0.60	48.73	0.44	0.15	2.19
		Average (wt.%)	3.67	6.89	33.27	0.27	4.40	0.63	48.18	0.43	0.14	2.13
		Std. Dev (wt.%)	0.29	0.12	0.05	0.05	0.01	0.01	0.30	0.00	0.00	0.02
M7-3	0.35	CoV (%)	7.94	1.79	0.15	17.16	0.19	2.32	0.62	1.08	2.03	0.74
		Minimum (wt.%)	3.35	6.71	33.18	0.19	4.39	0.61	47.62	0.42	0.14	2.11
		Maximum (wt%)	4.20	7.09	33.34	0.34	4.42	0.65	48.66	0.43	0.14	2.15

Table A.8: Chemical composition analysis of concrete samples M1

Sample	w/c		MgO	Al_2O_3	SiO_2	P_2O_5	SO_3	K_2O	CaO	TiO_2	MnO	Fe_2O_3
		Average (wt.%)	3.28	6.92	31.85	0.18	2.80	0.58	50.96	0.49	0.15	2.83
		Std. Dev (wt.%)	0.44	0.10	0.12	0.06	0.03	0.01	0.32	0.01	0.00	0.03
M1-SI-1	0.76	CoV (%)	13.47	1.44	0.38	35.41	1.07	2.18	0.63	1.50	3.04	1.13
		Minimum (wt.%)	2.47	6.76	31.68	0.11	2.76	0.56	50.46	0.47	0.14	2.79
		Maximum (wt%)	3.85	7.12	32.04	0.27	2.85	0.59	51.26	0.49	0.16	2.88
		Average (wt.%)	3.01	7.37	31.77	0.19	2.70	0.70	50.49	0.54	0.17	3.05
		Std. Dev (wt.%)	0.39	0.07	0.11	0.04	0.04	0.01	0.34	0.01	0.01	0.03
M1-SI-2	0.76	CoV (%)	12.81	0.98	0.34	23.52	1.30	1.40	0.67	1.32	2.90	1.06
		Minimum (wt.%)	2.28	7.23	31.62	0.11	2.63	0.69	49.99	0.53	0.16	2.97
		Maximum (wt%)	3.68	7.47	31.92	0.23	2.75	0.71	51.06	0.56	0.18	3.08
		Average (wt.%)	3.28	7.35	32.73	0.22	2.79	0.59	49.34	0.53	0.17	3.00
		Std. Dev (wt.%)	0.36	0.15	0.14	0.05	0.04	0.01	0.28	0.00	0.00	0.03
M1-SI-3	0.76	CoV (%)	10.85	2.01	0.41	24.59	1.30	1.02	0.57	0.93	1.91	0.90
		Minimum (wt.%)	2.66	7.17	32.50	0.12	2.69	0.58	48.85	0.52	0.17	2.96
		Maximum (wt%)	3.92	7.58	32.94	0.30	2.82	0.60	49.76	0.54	0.18	3.06

Table A.9: Chemical composition analysis of concrete samples M2

Sample	w/c		MgO	Al_2O_3	SiO_2	P_2O_5	SO_3	K_2O	CaO	TiO_2	MnO	Fe_2O_3
		Average (wt.%)	3.64	6.68	36.71	0.23	3.15	0.75	45.50	0.49	0.15	2.72
		Std. Dev (wt.%)	0.42	0.13	0.16	0.05	0.04	0.01	0.27	0.01	0.01	0.03
M2-SI-1	0.63	CoV (%)	11.48	1.88	0.42	19.50	1.13	1.49	0.59	1.39	3.63	1.16
		Minimum (wt.%)	3.20	6.54	36.39	0.15	3.09	0.73	45.12	0.48	0.14	2.66
		Maximum (wt%)	4.25	6.88	37.00	0.28	3.21	0.76	45.83	0.50	0.16	2.77
		Average (wt.%)	3.64	6.40	39.04	0.26	3.54	0.70	43.36	0.46	0.14	2.45
		Std. Dev (wt.%)	0.24	0.14	0.11	0.05	0.02	0.01	0.25	0.01	0.01	0.03
M2-SI-2	0.63	CoV (%)	6.70	2.15	0.27	19.90	0.61	1.22	0.58	2.20	4.40	1.40
		Minimum (wt.%)	3.27	6.22	38.92	0.18	3.51	0.69	42.94	0.45	0.13	2.40
		Maximum (wt%)	4.08	6.65	39.25	0.36	3.58	0.71	43.94	0.48	0.15	2.49
		Average (wt.%)	3.33	6.51	40.11	0.19	3.24	0.70	42.99	0.46	0.13	2.36
		Std. Dev (wt.%)	0.39	0.13	0.10	0.04	0.04	0.01	0.36	0.01	0.00	0.02
M2-SI-3	0.63	CoV (%)	11.80	2.03	0.26	21.72	1.17	1.49	0.83	1.97	2.05	0.90
		Minimum (wt.%)	2.61	6.29	39.96	0.12	3.18	0.69	42.67	0.45	0.13	2.32
		Maximum (wt%)	3.88	6.71	40.29	0.24	3.33	0.72	43.59	0.47	0.13	2.38

Table A.10: Chemical composition analysis of concrete samples M3

Sample	w/c		MgO	Al_2O_3	SiO_2	P_2O_5	SO_3	K_2O	CaO	TiO_2	MnO	Fe_2O_3
		Average (wt.%)	3.42	6.43	36.25	0.21	3.56	0.61	46.46	0.46	0.14	2.49
		Std. Dev (wt.%)	0.44	0.08	0.15	0.04	0.03	0.01	0.30	0.01	0.00	0.03
M3-SI-1	0.54	CoV (%)	12.75	1.27	0.41	17.81	0.89	1.01	0.64	1.32	2.92	1.06
		Minimum (wt.%)	2.79	6.28	36.05	0.15	3.49	0.60	46.00	0.45	0.14	2.45
		Maximum (wt%)	4.28	6.54	36.53	0.26	3.60	0.62	46.93	0.47	0.15	2.52
		Average (wt.%)	2.60	5.77	40.24	0.22	3.05	0.56	44.52	0.46	0.14	2.44
		Std. Dev (wt.%)	0.30	0.10	0.11	0.03	0.03	0.01	0.22	0.00	0.00	0.02
M3-SI-2	0.54	CoV (%)	11.47	1.80	0.27	14.22	0.83	1.29	0.50	0.83	2.70	0.96
		Minimum (wt.%)	2.04	5.61	40.06	0.19	3.02	0.55	44.15	0.45	0.13	2.41
		Maximum (wt%)	3.15	5.92	40.38	0.30	3.11	0.57	44.88	0.46	0.15	2.47
		Average (wt.%)	3.00	6.59	40.14	0.18	3.20	0.58	43.47	0.45	0.13	2.28
		Std. Dev (wt.%)	0.28	0.13	0.10	0.05	0.03	0.01	0.23	0.01	0.00	0.02
M3-SI-3	0.54	CoV (%)	9.35	1.95	0.24	28.45	0.96	1.97	0.54	1.67	2.01	1.03
		Minimum (wt.%)	2.67	6.39	40.01	0.11	3.15	0.56	43.03	0.44	0.13	2.24
		Maximum (wt%)	3.48	6.80	40.28	0.25	3.24	0.60	43.72	0.46	0.14	2.31

Table A.11: Chemical composition analysis of concrete samples M4

Sample	w/c		MgO	Al_2O_3	SiO_2	P_2O_5	SO_3	K_2O	CaO	TiO_2	MnO	Fe_2O_3
		Average (wt.%)	3.25	6.06	37.43	0.21	3.86	0.57	45.72	0.45	0.14	2.37
		Std. Dev (wt.%)	0.34	0.07	0.07	0.06	0.03	0.01	0.31	0.01	0.00	0.03
M4-SI-1	0.48	CoV (%)	10.62	1.07	0.20	26.89	0.68	1.75	0.68	1.55	1.81	1.19
		Minimum (wt.%)	2.76	5.96	37.30	0.15	3.82	0.55	45.32	0.44	0.14	2.32
		Maximum (wt%)	3.82	6.17	37.57	0.30	3.92	0.58	46.11	0.46	0.15	2.42
		Average (wt.%)	3.82	6.56	37.33	0.25	3.33	0.57	45.16	0.45	0.15	2.38
		Std. Dev (wt.%)	0.32	0.07	0.11	0.05	0.03	0.00	0.25	0.01	0.01	0.04
M4-SI-2	0.48	CoV (%)	8.36	1.12	0.29	18.24	0.94	0.86	0.55	1.72	3.47	1.56
		Minimum (wt.%)	3.30	6.41	37.15	0.17	3.28	0.57	44.78	0.44	0.14	2.32
		Maximum (wt%)	4.50	6.65	37.47	0.31	3.37	0.58	45.47	0.46	0.16	2.45
		Average (wt.%)	3.19	6.29	37.00	0.20	3.95	0.55	45.76	0.45	0.14	2.47
		Std. Dev (wt.%)	0.36	0.12	0.15	0.05	0.04	0.01	0.21	0.01	0.01	0.03
M4-SI-3	0.48	CoV (%)	11.30	1.98	0.39	22.78	0.98	2.04	0.47	1.69	3.64	1.09
		Minimum (wt.%)	2.56	6.12	36.82	0.15	3.87	0.54	45.48	0.45	0.13	2.43
		Maximum (wt%)	3.67	6.47	37.26	0.30	4.00	0.57	46.15	0.47	0.15	2.51

Table A.12: Chemical composition analysis of concrete samples M5

Sample	w/c		MgO	Al_2O_3	SiO_2	P_2O_5	SO_3	K_2O	CaO	TiO_2	MnO	Fe_2O_3
		Average (wt.%)	3.35	6.46	34.98	0.23	3.71	0.69	47.56	0.46	0.15	2.44
		Std. Dev (wt.%)	0.21	0.09	0.12	0.03	0.03	0.01	0.20	0.00	0.00	0.02
M5-SI-1	0.42	CoV (%)	6.39	1.41	0.33	13.14	0.67	1.48	0.43	1.08	2.34	1.02
		Minimum (wt.%)	3.11	6.34	34.80	0.20	3.65	0.67	47.26	0.46	0.14	2.40
		Maximum (wt%)	3.69	6.62	35.17	0.28	3.74	0.70	47.82	0.47	0.15	2.47
		Average (wt.%)	3.53	6.34	34.41	0.25	3.66	0.63	48.16	0.47	0.15	2.44
		Std. Dev (wt.%)	0.27	0.11	0.08	0.04	0.05	0.01	0.24	0.01	0.01	0.03
M5-SI-2	0.42	CoV (%)	7.52	1.80	0.24	16.08	1.24	1.72	0.50	1.16	3.68	1.09
		Minimum (wt.%)	3.13	6.17	34.30	0.22	3.60	0.62	47.88	0.47	0.14	2.41
		Maximum (wt%)	3.83	6.45	34.51	0.34	3.73	0.65	48.60	0.49	0.16	2.49
		Average (wt.%)	3.69	6.70	35.46	0.20	3.18	0.69	47.16	0.46	0.14	2.32
		Std. Dev (wt.%)	0.22	0.11	0.09	0.06	0.03	0.01	0.25	0.01	0.00	0.02
M5-SI-3	0.42	CoV (%)	6.08	1.72	0.24	31.09	1.00	1.68	0.54	1.10	2.34	0.95
		Minimum (wt.%)	3.28	6.53	35.33	0.12	3.14	0.67	46.80	0.45	0.14	2.28
		Maximum (wt%)	3.97	6.90	35.61	0.29	3.26	0.71	47.46	0.47	0.15	2.35

Table A.13: Chemical composition analysis of concrete samples M6

Sample	w/c		MgO	Al_2O_3	SiO_2	P_2O_5	SO_3	K_2O	CaO	TiO_2	MnO	Fe_2O_3
		Average (wt.%)	3.24	5.89	34.61	0.23	3.81	0.56	48.61	0.46	0.15	2.48
		Std. Dev (wt.%)	0.32	0.09	0.14	0.03	0.05	0.01	0.27	0.01	0.00	0.02
M6-SI-1	0.38	CoV (%)	9.92	1.60	0.41	12.97	1.20	1.99	0.56	1.18	2.42	0.84
		Minimum (wt.%)	2.85	5.69	34.39	0.18	3.72	0.53	48.13	0.45	0.14	2.46
		Maximum (wt%)	3.85	5.99	34.83	0.28	3.86	0.57	48.99	0.46	0.15	2.52
		Average (wt.%)	3.67	7.10	35.01	0.23	3.66	0.71	46.80	0.44	0.14	2.24
		Std. Dev (wt.%)	0.36	0.09	0.11	0.04	0.02	0.01	0.30	0.01	0.00	0.03
M6-SI-2	0.38	CoV (%)	9.68	1.29	0.32	18.81	0.65	1.19	0.64	1.31	2.86	1.24
		Minimum (wt.%)	3.15	7.01	34.88	0.14	3.62	0.69	46.30	0.44	0.13	2.19
		Maximum (wt%)	4.02	7.30	35.22	0.27	3.69	0.72	47.17	0.45	0.14	2.27
		Average (wt.%)	3.18	5.77	30.79	0.25	4.35	0.60	51.87	0.47	0.16	2.57
		Std. Dev (wt.%)	0.33	0.13	0.10	0.04	0.03	0.01	0.21	0.01	0.00	0.02
M6-SI-3	0.38	CoV (%)	10.22	2.30	0.32	14.34	0.80	1.75	0.40	1.30	1.52	0.73
		Minimum (wt.%)	2.76	5.60	30.65	0.19	4.29	0.58	51.54	0.46	0.16	2.54
		Maximum (wt%)	3.66	5.96	30.88	0.29	4.40	0.62	52.26	0.48	0.16	2.59

Table A.14: Chemical composition analysis of concrete samples M7

Sample	w/c		MgO	Al_2O_3	SiO_2	P_2O_5	SO_3	K_2O	CaO	TiO_2	MnO	Fe_2O_3
		Average (wt.%)	3.66	6.43	34.64	0.25	3.50	0.55	48.00	0.47	0.15	2.37
		Std. Dev (wt.%)	0.23	0.10	0.09	0.06	0.03	0.01	0.28	0.01	0.00	0.03
M7-SI-1	0.35	CoV (%)	6.18	1.60	0.25	23.59	0.76	1.26	0.59	1.22	3.23	1.06
		Minimum (wt.%)	3.27	6.25	34.51	0.14	3.45	0.54	47.65	0.46	0.14	2.34
		Maximum (wt%)	4.00	6.62	34.78	0.33	3.53	0.57	48.39	0.47	0.16	2.41
		Average (wt.%)	3.66	6.57	38.34	0.17	3.65	0.55	44.45	0.41	0.12	2.08
		Std. Dev (wt.%)	0.26	0.12	0.09	0.05	0.03	0.01	0.22	0.00	0.00	0.02
M7-SI-2	0.35	CoV (%)	7.02	1.81	0.24	31.62	0.71	1.84	0.50	1.04	2.13	0.79
		Minimum (wt.%)	3.22	6.38	38.19	0.12	3.62	0.54	44.09	0.40	0.12	2.05
		Maximum (wt%)	4.10	6.73	38.44	0.28	3.69	0.57	44.81	0.41	0.13	2.11
		Average (wt.%)	3.48	6.24	35.62	0.26	3.54	0.52	47.51	0.44	0.14	2.27
		Std. Dev (wt.%)	0.33	0.07	0.15	0.03	0.03	0.01	0.26	0.01	0.00	0.02
M7-SI-3	0.35	CoV (%)	9.40	1.10	0.42	12.33	0.72	1.14	0.55	1.58	2.44	0.79
		Minimum (wt.%)	2.84	6.11	35.43	0.21	3.50	0.51	47.15	0.43	0.13	2.23
		Maximum (wt%)	3.81	6.33	35.85	0.30	3.58	0.53	47.99	0.45	0.14	2.29

B

Effect of relative humidity

B.1. Bar plots Test Series 3

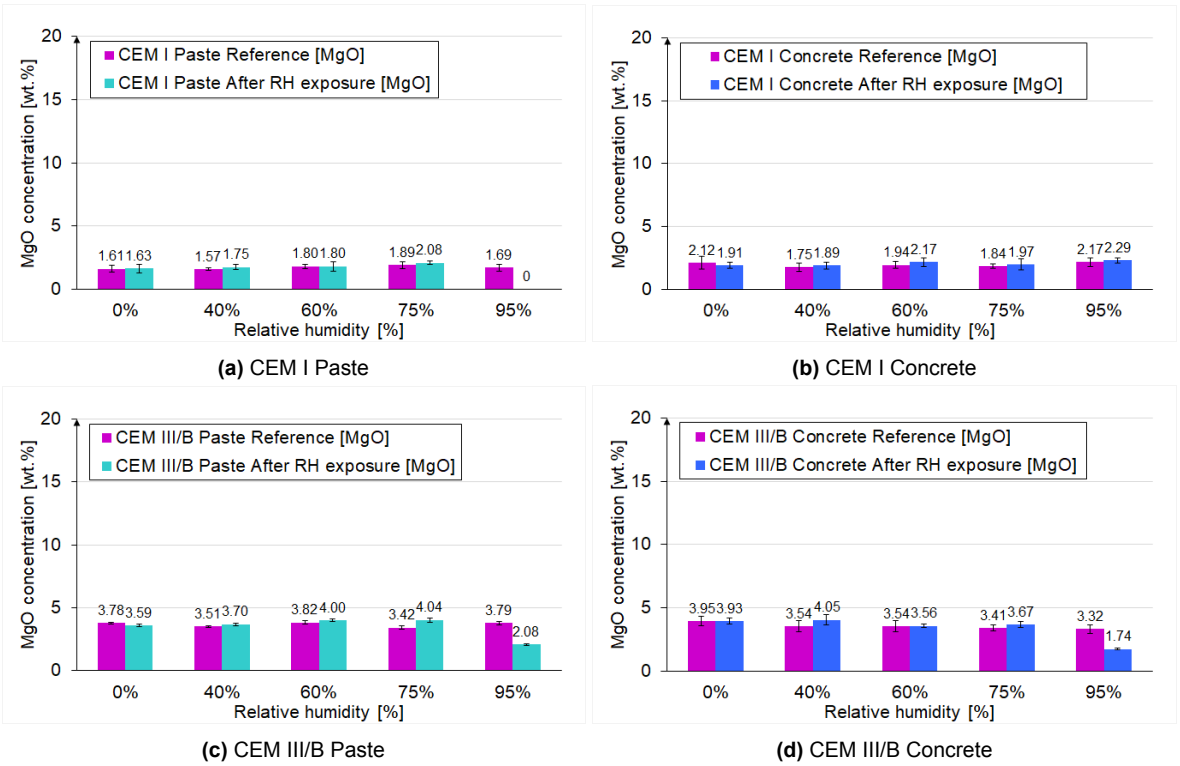

(a) CEM I Paste

(b) CEM I Concrete

(c) CEM III/B Paste

(d) CEM III/B Concrete

Figure B.1: Chemical composition analysis [MgO] with hXRF on pastes and concrete surfaces exposed at different relative humidities

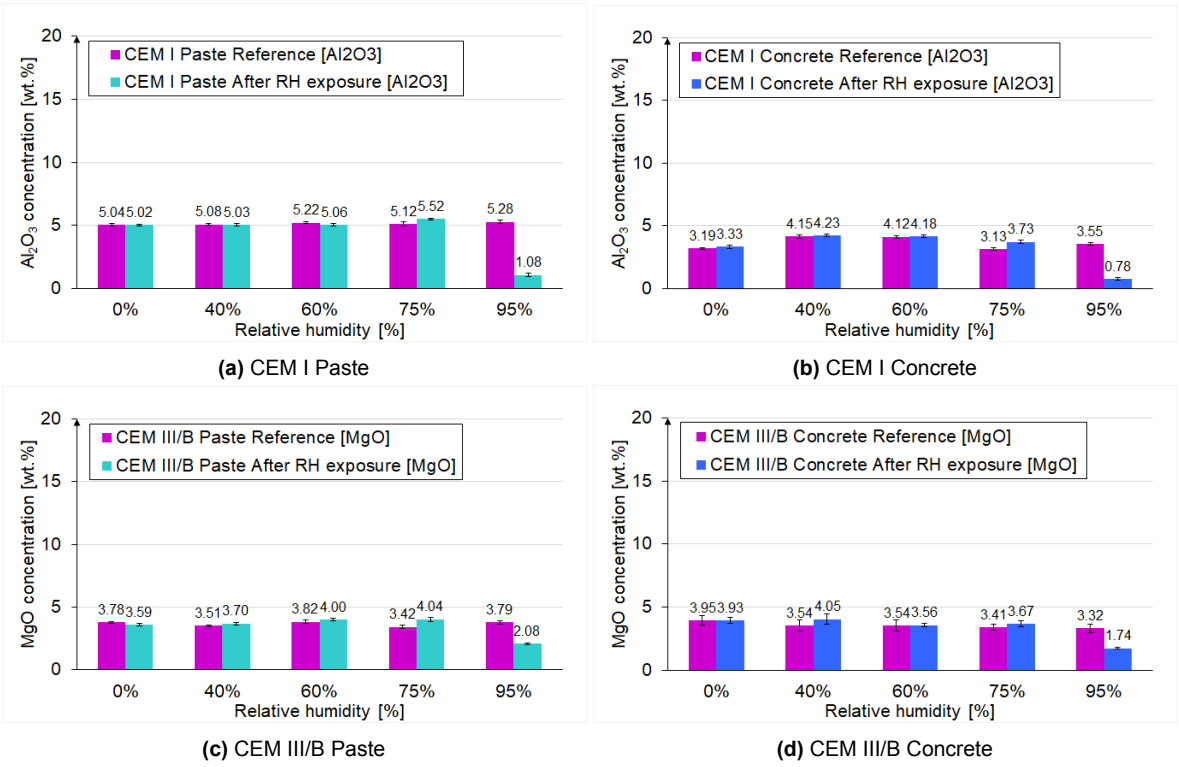

(a) CEM I Paste **(b)** CEM I Concrete

(c) CEM III/B Paste **(d)** CEM III/B Concrete

Figure B.2: Chemical composition analysis [Al_2O_3] with hXRF on pastes and concrete surfaces exposed at different relative humidities

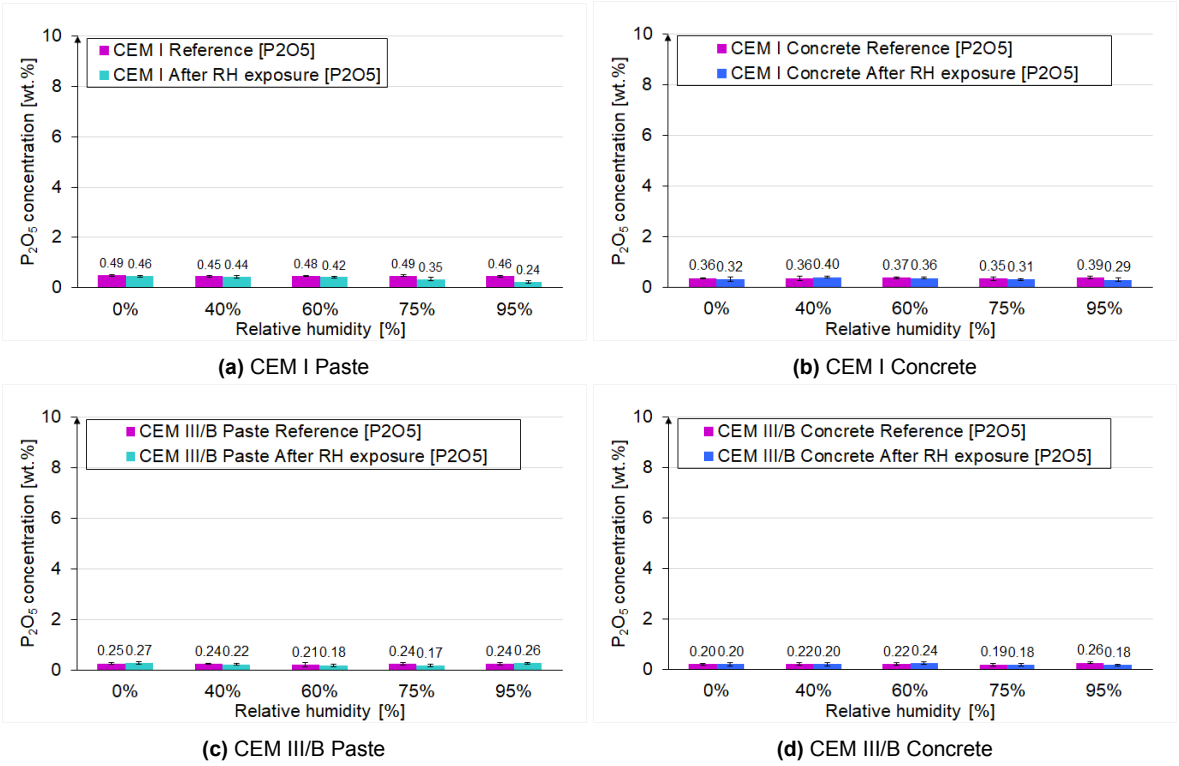

(a) CEM I Paste **(b)** CEM I Concrete

(c) CEM III/B Paste **(d)** CEM III/B Concrete

Figure B.3: Chemical composition analysis [P_2O_5] with hXRF on pastes and concrete surfaces exposed at different relative humidities

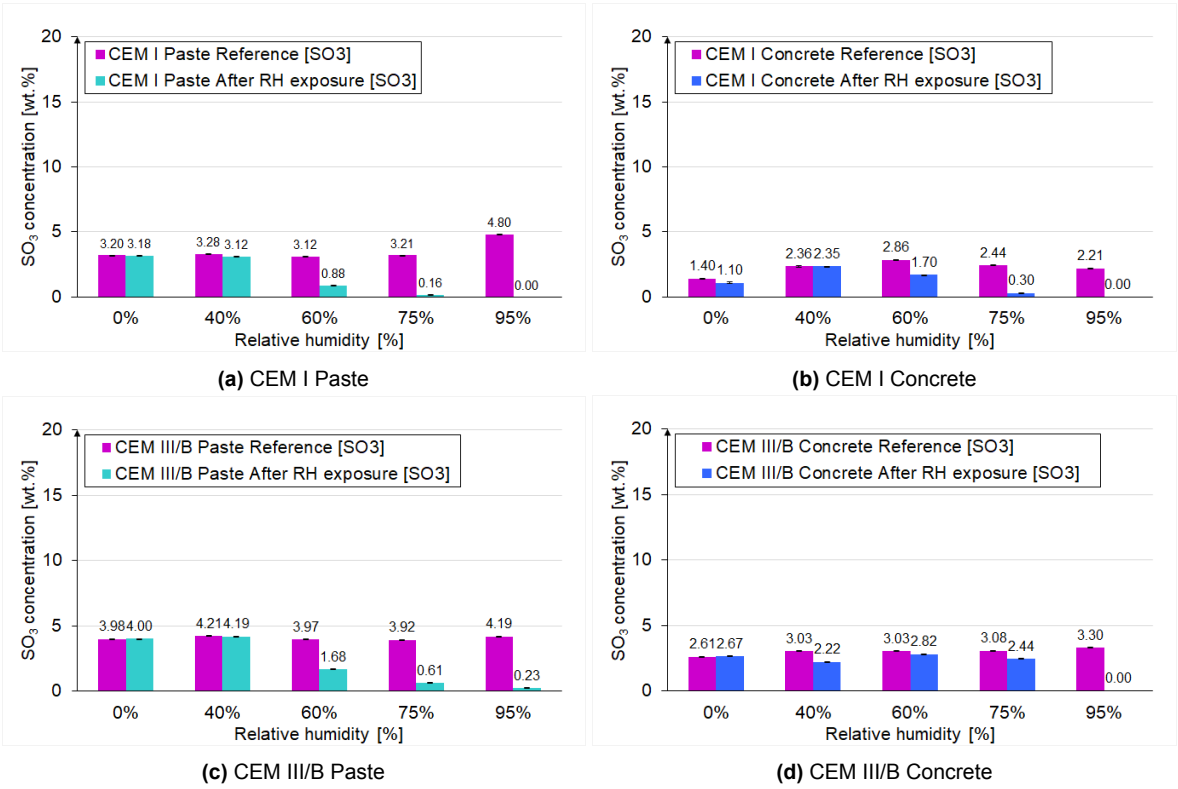

(a) CEM I Paste **(b)** CEM I Concrete

(c) CEM III/B Paste **(d)** CEM III/B Concrete

Figure B.4: Chemical composition analysis [SO_3] with hXRF on pastes and concrete surfaces exposed at different relative humidities

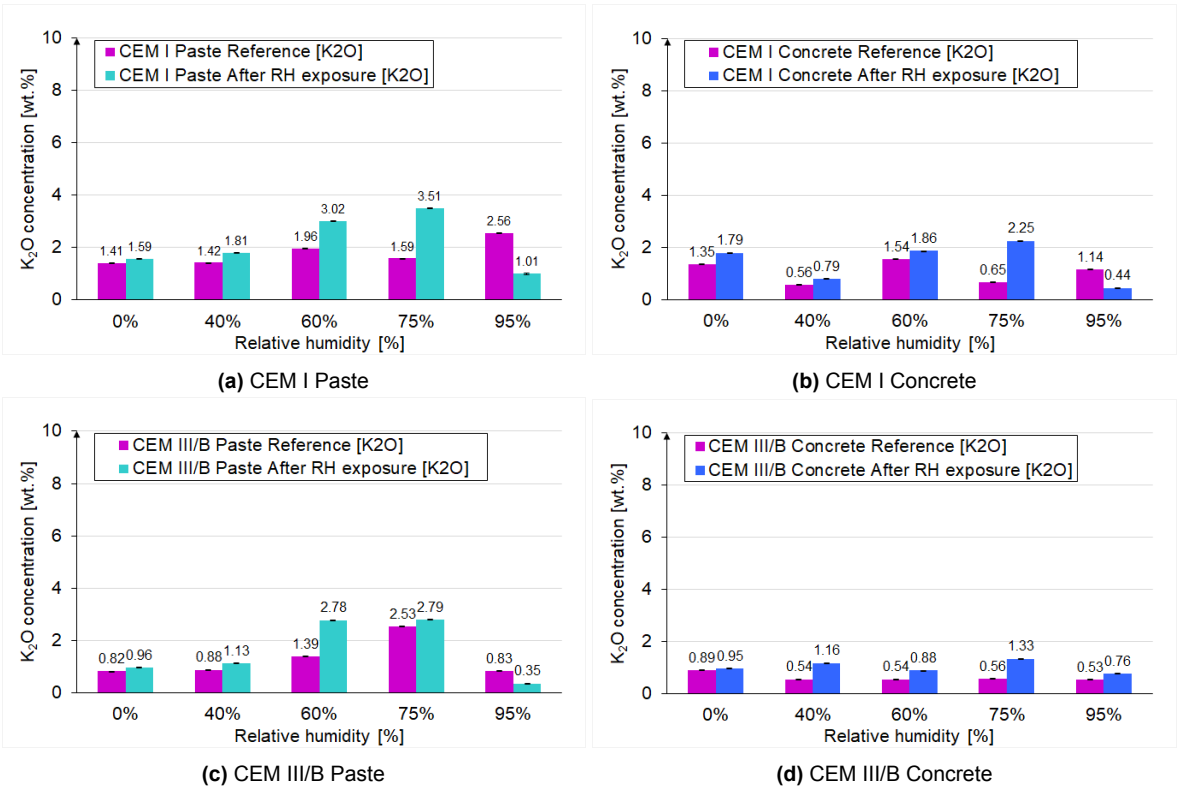

(a) CEM I Paste **(b)** CEM I Concrete

(c) CEM III/B Paste **(d)** CEM III/B Concrete

Figure B.5: Chemical composition analysis [K_2O] with hXRF on pastes and concrete surfaces exposed at different relative humidities

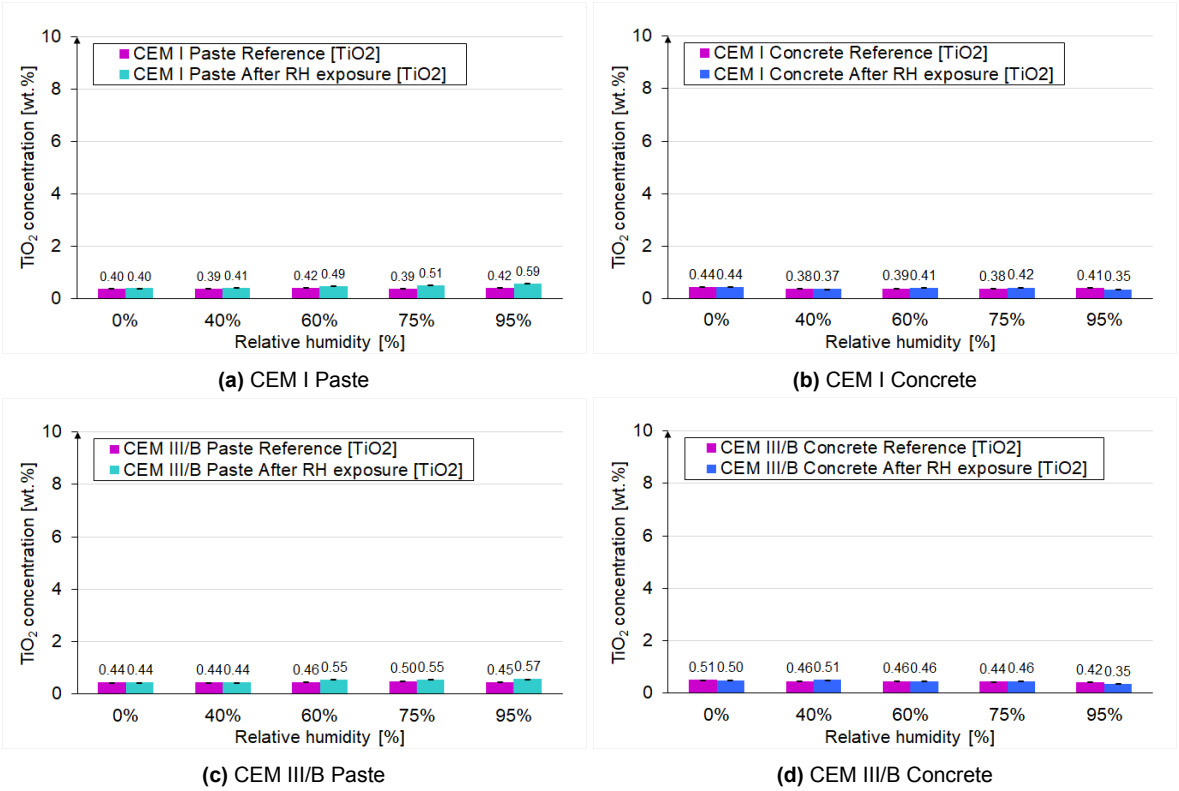

(a) CEM I Paste **(b)** CEM I Concrete

(c) CEM III/B Paste **(d)** CEM III/B Concrete

Figure B.6: Chemical composition analysis [TiO_2] with hXRF on pastes and concrete surfaces exposed at different relative humidities

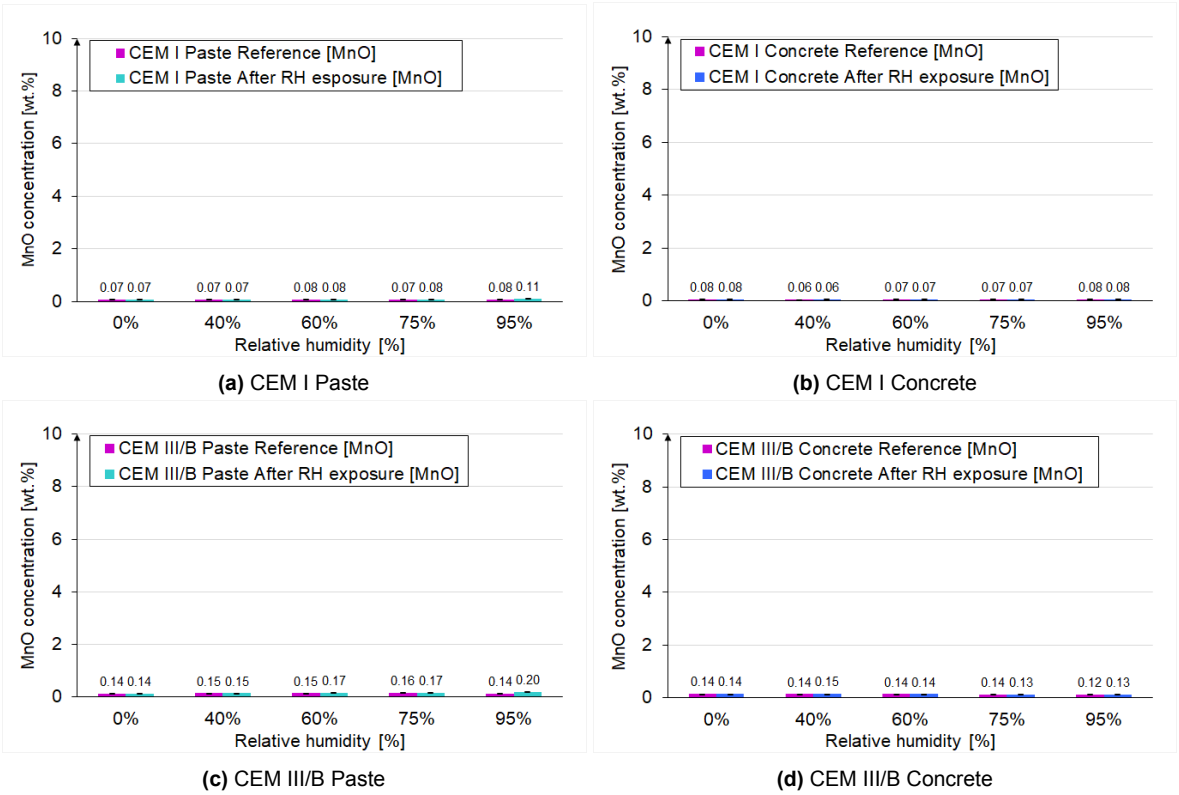

(a) CEM I Paste **(b)** CEM I Concrete

(c) CEM III/B Paste **(d)** CEM III/B Concrete

Figure B.7: Chemical composition analysis [MnO] with hXRF on pastes and concrete surfaces exposed at different relative humidities

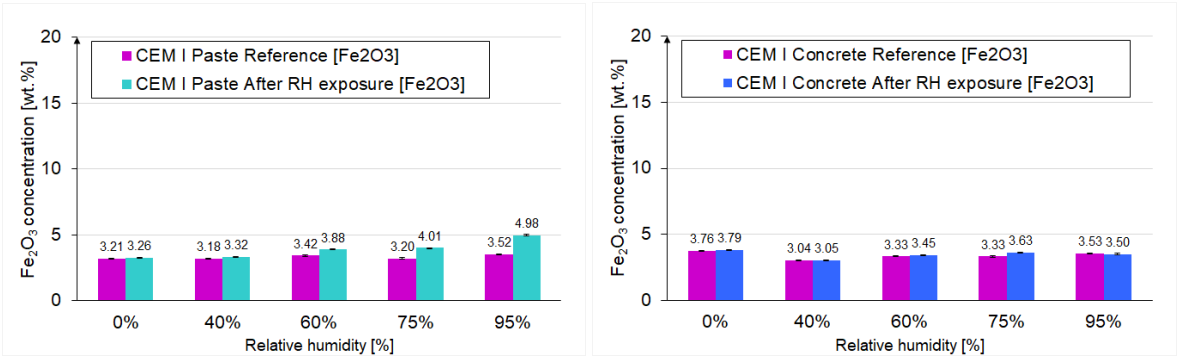

(a) CEM I Paste

(b) CEM I Concrete

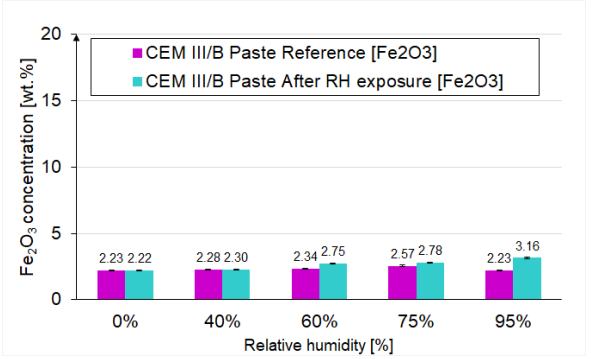

(c) CEM III/B Paste

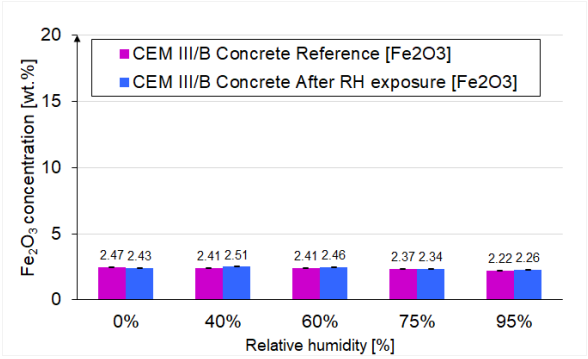

(d) CEM III/B Concrete

Figure B.8: Chemical composition analysis [Fe_2O_2] with hXRF on pastes and concrete surfaces exposed at different relative humidities

C

Effect of carbonation

C.1. Summary tables Teste Series 4

Table C.1: Chemical composition analysis of paste samples before carbonation (CEM I)

Sample	w/c		MgO	Al_2O_3	SiO_2	P_2O_5	SO_3	K_2O	CaO	TiO_2	MnO	Fe_2O_3
		Average (wt.%)	1.73	5.30	20.79	0.45	3.39	2.00	62.89	0.42	0.08	3.40
		Std. Dev (wt.%)	0.25	0.11	0.06	0.04	0.04	0.02	0.71	0.01	0.00	0.05
CEM I-M3-1	0.54	CoV (%)	14.23	2.08	0.29	9.17	1.08	0.84	1.13	2.21	5.05	1.51
		Minimum (wt.%)	1.39	5.10	20.68	0.37	3.33	1.98	62.04	0.41	0.07	3.35
		Maximum (wt%)	2.02	5.43	20.87	0.51	3.44	2.03	63.99	0.44	0.08	3.49
		Average (wt.%)	1.72	5.33	20.73	0.49	3.38	2.01	62.95	0.41	0.07	3.35
		Std. Dev (wt.%)	0.20	0.11	0.11	0.04	0.03	0.02	0.61	0.01	0.01	0.05
CEM I-M3-2	0.54	CoV (%)	11.59	2.13	0.52	7.43	0.88	0.82	0.96	1.88	7.17	1.42
		Minimum (wt.%)	1.51	5.06	20.61	0.43	3.32	1.99	62.40	0.40	0.06	3.29
		Maximum (wt%)	2.04	5.50	20.93	0.55	3.41	2.04	63.89	0.42	0.08	3.44
		Average (wt.%)	1.64	5.46	20.29	0.48	3.45	2.24	62.70	0.42	0.08	3.39
		Std. Dev (wt.%)	0.20	0.11	0.12	0.03	0.04	0.02	0.35	0.01	0.01	0.05
CEM I-M3-3	0.54	CoV (%)	12.16	2.03	0.57	5.67	1.08	1.06	0.56	1.58	7.81	1.40
		Minimum (wt.%)	1.35	5.30	20.17	0.45	3.39	2.19	62.33	0.41	0.07	3.33
		Maximum (wt%)	1.99	5.68	20.48	0.52	3.51	2.27	63.58	0.43	0.08	3.48

Table C.2: Chemical composition analysis of paste samples after carbonation (CEM I)

Sample	w/c		MgO	Al_2O_3	SiO_2	P_2O_5	SO_3	K_2O	CaO	TiO_2	MnO	Fe_2O_3
		Average (wt.%)	-	-	-	-	-	-	-	-	-	-
		Std. Dev (wt.%)	-	-	-	-	-	-	-	-	-	-
CEM I-M3-1	0.54	CoV (%)	-	-	-	-	-	-	-	-	-	-
		Minimum (wt.%)	-	-	-	-	-	-	-	-	-	-
		Maximum (wt%)	-	-	-	-	-	-	-	-	-	-
		Average (wt.%)	-	-	-	-	-	-	-	-	-	-
		Std. Dev (wt.%)	-	-	-	-	-	-	-	-	-	-
CEM I-M3-2	0.54	CoV (%)	-	-	-	-	-	-	-	-	-	-
		Minimum (wt.%)	-	-	-	-	-	-	-	-	-	-
		Maximum (wt%)	-	-	-	-	-	-	-	-	-	-
		Average (wt.%)	2.11	5.05	19.86	0.38	2.12	2.12	64.32	0.44	0.08	3.52
		Std. Dev (wt.%)	0.42	0.06	0.09	0.09	0.04	0.01	0.33	0.01	0.00	0.03
CEM I-M3-3	0.54	CoV (%)	20.01	1.19	0.45	22.94	1.89	0.56	0.51	1.56	4.74	0.90
		Minimum (wt.%)	1.33	4.96	19.71	0.24	2.06	2.09	63.65	0.43	0.07	3.46
		Maximum (wt%)	2.76	5.15	19.99	0.47	2.17	2.14	64.79	0.45	0.08	3.56

Table C.3: Chemical composition analysis of concrete samples before carbonation (CEM I)

Sample	w/c		MgO	Al_2O_3	SiO_2	P_2O_5	SO_3	K_2O	CaO	TiO_2	MnO	Fe_2O_3
		Average (wt.%)	2.34	3.88	29.88	0.39	1.65	0.86	57.17	0.42	0.07	3.35
		Std. Dev (wt.%)	0.42	0.10	0.10	0.07	0.03	0.01	0.37	0.01	0.00	0.04
CEM I-M3-C2-SII-1	0.54	CoV (%)	17.94	2.52	0.35	18.15	2.11	0.74	0.65	1.99	5.40	1.27
		Minimum (wt.%)	1.60	3.78	29.73	0.21	1.55	0.84	56.70	0.40	0.06	3.29
		Maximum (wt%)	2.76	4.06	30.07	0.45	1.68	0.86	57.71	0.43	0.07	3.42
		Average (wt.%)	1.90	4.10	29.34	0.43	1.79	0.70	57.89	0.43	0.07	3.36
		Std. Dev (wt.%)	0.46	0.13	0.21	0.05	0.05	0.06	0.23	0.01	0.00	0.04
CEM I-M3-C2-SII-2	0.54	CoV (%)	24.26	3.10	0.72	12.24	2.68	9.13	0.40	1.74	4.40	1.21
		Minimum (wt.%)	1.23	3.85	29.12	0.30	1.66	0.67	57.52	0.42	0.07	3.31
		Maximum (wt%)	2.80	4.24	29.86	0.50	1.82	0.88	58.14	0.44	0.08	3.45
		Average (wt.%)	2.43	3.75	23.69	0.39	1.57	0.90	62.96	0.46	0.08	3.78
		Std. Dev (wt.%)	0.61	0.09	0.13	0.07	0.03	0.01	0.49	0.01	0.00	0.04
CEM I-M3-C2-SII-3	0.54	CoV (%)	25.11	2.43	0.56	18.43	1.72	1.19	0.78	1.29	4.00	0.97
		Minimum (wt.%)	1.43	3.60	23.43	0.24	1.52	0.87	62.46	0.45	0.07	3.74
		Maximum (wt%)	3.17	3.86	23.86	0.50	1.60	0.91	63.74	0.47	0.08	3.84

Table C.4: Chemical composition analysis of concrete samples after carbonation (CEM I)

Sample	w/c		MgO	Al_2O_3	SiO_2	P_2O_5	SO_3	K_2O	CaO	TiO_2	MnO	Fe_2O_3
		Average (wt.%)	-	-	-	-	-	-	-	-	-	-
		Std. Dev (wt.%)	-	-	-	-	-	-	-	-	-	-
CEM I-M3-C2-SII-1	0.54	CoV (%)	-	-	-	-	-	-	-	-	-	-
		Minimum (wt.%)	-	-	-	-	-	-	-	-	-	-
		Maximum (wt%)	-	-	-	-	-	-	-	-	-	-
		Average (wt.%)	-	-	-	-	-	-	-	-	-	-
		Std. Dev (wt.%)	-	-	-	-	-	-	-	-	-	-
CEM I-M3-C2-SII-2	0.54	CoV (%)	-	-	-	-	-	-	-	-	-	-
		Minimum (wt.%)	-	-	-	-	-	-	-	-	-	-
		Maximum (wt%)	-	-	-	-	-	-	-	-	-	-
		Average (wt.%)	2.45	3.77	23.99	0.39	1.47	0.75	62.91	0.46	0.08	3.73
		Std. Dev (wt.%)	0.41	0.11	0.13	0.06	0.02	0.01	0.41	0.01	0.00	0.05
CEM I-M3-C2-SII-3	0.54	CoV (%)	16.53	2.94	0.54	14.30	1.59	0.77	0.65	1.49	4.60	1.38
		Minimum (wt.%)	1.76	3.62	23.78	0.29	1.43	0.75	62.46	0.45	0.08	3.67
		Maximum (wt%)	2.96	4.04	24.20	0.45	1.49	0.77	63.65	0.47	0.09	3.82

Table C.5: Chemical composition analysis of paste samples before carbonation (CEM III/B)

Sample	w/c		MgO	Al_2O_3	SiO_2	P_2O_5	SO_3	K_2O	CaO	TiO_2	MnO	Fe_2O_3
		Average (wt.%)	3.89	7.20	29.24	0.24	3.78	1.57	51.07	0.47	0.15	2.38
		Std. Dev (wt.%)	0.23	0.12	0.10	0.03	0.02	0.01	0.23	0.01	0.00	0.02
CEM III/B-M3-1	0.54	CoV (%)	6.02	1.70	0.34	13.22	0.57	0.52	0.45	1.96	2.67	0.89
		Minimum (wt.%)	3.48	7.03	29.03	0.19	3.75	1.56	50.82	0.45	0.15	2.35
		Maximum (wt%)	4.18	7.37	29.38	0.29	3.82	1.59	51.42	0.48	0.16	2.42
		Average (wt.%)	3.53	7.33	28.56	0.25	3.68	1.74	51.90	0.48	0.15	2.41
		Std. Dev (wt.%)	0.31	0.11	0.12	0.04	0.03	0.01	0.23	0.01	0.00	0.02
CEM III/B-M3-2	0.54	CoV (%)	8.71	1.57	0.43	18.28	0.93	0.52	0.44	1.17	3.04	0.86
		Minimum (wt.%)	3.16	7.10	28.41	0.19	3.63	1.72	51.50	0.47	0.15	2.38
		Maximum (wt%)	4.05	7.51	28.74	0.31	3.73	1.75	52.22	0.49	0.16	2.44
		Average (wt.%)	3.88	7.44	29.20	0.27	3.75	1.73	50.72	0.48	0.15	2.38
		Std. Dev (wt.%)	0.31	0.10	0.09	0.03	0.03	0.01	0.25	0.01	0.01	0.03
CEM III/B-M3-3	0.54	CoV (%)	8.03	1.36	0.30	12.22	0.80	0.54	0.50	1.15	3.46	1.27
		Minimum (wt.%)	3.39	7.26	29.08	0.21	3.71	1.71	50.34	0.47	0.15	2.35
		Maximum (wt%)	4.51	7.63	29.34	0.34	3.80	1.74	51.29	0.48	0.16	2.45

Table C.6: Chemical composition analysis of paste samples after carbonation (CEM III/B)

Sample	w/c		MgO	Al_2O_3	SiO_2	P_2O_5	SO_3	K_2O	CaO	TiO_2	MnO	Fe_2O_3
		Average (wt.%)	-	-	-	-	-	-	-	-	-	-
		Std. Dev (wt.%)	-	-	-	-	-	-	-	-	-	-
CEM III/B-M3-1	0.54	CoV (%)	-	-	-	-	-	-	-	-	-	-
		Minimum (wt.%)	-	-	-	-	-	-	-	-	-	-
		Maximum (wt%)	-	-	-	-	-	-	-	-	-	-
		Average (wt.%)	-	-	-	-	-	-	-	-	-	-
		Std. Dev (wt.%)	-	-	-	-	-	-	-	-	-	-
CEM III/B-M3-2	0.54	CoV (%)	-	-	-	-	-	-	-	-	-	-
		Minimum (wt.%)	-	-	-	-	-	-	-	-	-	-
		Maximum (wt%)	-	-	-	-	-	-	-	-	-	-
		Average (wt.%)	3.54	6.30	30.38	0.25	4.14	0.72	51.54	0.48	0.16	2.49
		Std. Dev (wt.%)	0.22	0.09	0.04	0.03	0.02	0.01	0.22	0.01	0.01	0.03
CEM III/B-M3-3	0.54	CoV (%)	6.08	1.42	0.15	12.89	0.43	0.76	0.44	1.53	3.56	1.06
		Minimum (wt.%)	3.24	6.20	30.32	0.19	4.10	0.72	51.20	0.46	0.16	2.45
		Maximum (wt%)	3.92	6.46	30.45	0.28	4.17	0.73	51.85	0.49	0.18	2.55

Table C.7: Chemical composition analysis of concrete samples before carbonation (CEM III/B)

Sample	w/c		MgO	Al_2O_3	SiO_2	P_2O_5	SO_3	K_2O	CaO	TiO_2	MnO	Fe_2O_3
		Average (wt.%)	4.11	7.23	37.34	0.25	3.53	0.77	43.89	0.45	0.13	2.33
		Std. Dev (wt.%)	0.42	0.08	0.11	0.06	0.03	0.01	0.31	0.01	0.00	0.03
CEM III/B-M3-C2-SI-1	0.54	CoV (%)	10.10	1.10	0.30	24.64	0.84	0.95	0.70	1.22	2.93	1.29
		Minimum (wt.%)	3.40	7.13	37.20	0.14	3.48	0.75	43.40	0.44	0.13	2.27
		Maximum (wt%)	4.74	7.33	37.50	0.31	3.57	0.78	44.38	0.46	0.14	2.37
		Average (wt.%)	4.09	7.07	36.99	0.21	3.28	0.81	44.48	0.47	0.14	2.45
		Std. Dev (wt.%)	0.32	0.11	0.11	0.06	0.03	0.01	0.19	0.01	0.00	0.04
CEM III/B-M3-C2-SI-2	0.54	CoV (%)	7.70	1.58	0.30	28.24	0.82	1.14	0.43	1.44	3.42	1.47
		Minimum (wt.%)	3.53	6.88	36.74	0.11	3.24	0.80	44.22	0.46	0.14	2.41
		Maximum (wt%)	4.51	7.22	37.15	0.30	3.33	0.83	44.76	0.48	0.15	2.52
		Average (wt.%)	4.18	6.93	35.22	0.21	3.12	0.84	46.37	0.48	0.15	2.52
		Std. Dev (wt.%)	0.26	0.07	0.07	0.06	0.03	0.01	0.14	0.01	0.00	0.02
CEM III/B-M3-C2-SI-3	0.54	CoV (%)	6.10	0.99	0.19	28.83	1.01	1.56	0.31	1.45	2.45	0.65
		Minimum (wt.%)	3.81	6.84	35.13	0.10	3.06	0.82	46.20	0.47	0.15	2.51
		Maximum (wt%)	4.64	7.05	35.33	0.32	3.16	0.86	46.64	0.49	0.16	2.57

Table C.8: Chemical composition analysis of concrete samples after carbonation (CEM III/B)

Sample	w/c		MgO	Al_2O_3	SiO_2	P_2O_5	SO_3	K_2O	CaO	TiO_2	MnO	Fe_2O_3
		Average (wt.%)	-	-	-	-	-	-	-	-	-	-
		Std. Dev (wt.%)	-	-	-	-	-	-	-	-	-	-
CEM III/B-M3-C2-SI-1	0.54	CoV (%)	-	-	-	-	-	-	-	-	-	-
		Minimum (wt.%)	-	-	-	-	-	-	-	-	-	-
		Maximum (wt%)	-	-	-	-	-	-	-	-	-	-
		Average (wt.%)	-	-	-	-	-	-	-	-	-	-
		Std. Dev (wt.%)	-	-	-	-	-	-	-	-	-	-
CEM III/B-M3-C2-SI-2	0.54	CoV (%)	-	-	-	-	-	-	-	-	-	-
		Minimum (wt.%)	-	-	-	-	-	-	-	-	-	-
		Maximum (wt%)	-	-	-	-	-	-	-	-	-	-
		Average (wt.%)	4.04	6.89	35.40	0.23	3.11	0.75	46.42	0.48	0.15	2.53
		Std. Dev (wt.%)	0.31	0.12	0.14	0.06	0.03	0.01	0.24	0.01	0.01	0.03
CEM III/B-M3-C2-SI-3	0.54	CoV (%)	7.62	1.76	0.40	25.93	1.02	0.70	0.52	1.11	4.19	1.14
		Minimum (wt.%)	3.68	6.77	35.21	0.17	3.06	0.74	45.91	0.47	0.14	2.49
		Maximum (wt%)	4.61	7.20	35.61	0.34	3.17	0.76	46.73	0.49	0.17	2.59

D

Practical case studies

D.1. Cores description

Core description

Date of coring:	September 18, 2023
Structure part:	Foundation
Core type:	Cylinder
Sample name:	F1
General details	
Cross section:	64.4 mm
Diameter:	86.3 mm

Figure D.1: Core F1

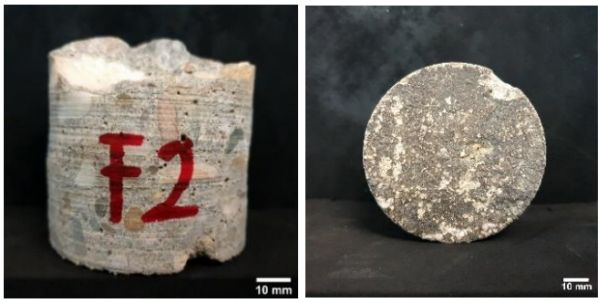

Core description

Date of coring:	September 18, 2023
Structure part:	Foundation
Core type:	Cylinder
Sample name:	F2
General details	
Cross section:	64.4 mm
Diameter:	68.0 mm

Figure D.2: Core F2

Core description

Date of coring:	September 18, 2023
Structure part:	Foundation
Core type:	Cylinder
Sample name:	F3
General details	
Cross section:	64.4 mm
Diameter:	86.3 mm

Figure D.3: Core F3

Core description

Date of coring:	September 18, 2023
Structure part:	Column
Core type:	Cylinder
Sample name:	C1S1
General details	
Cross section:	44.5 mm
Diameter:	38.7 mm

Figure D.4: Core C1S1

Core description

Date of coring:	September 18, 2023
Structure part:	Column
Core type:	Cylinder
Sample name:	C1S2
General details	
Cross section:	44.5 mm
Diameter:	40.5 mm

Figure D.5: Core C1S2

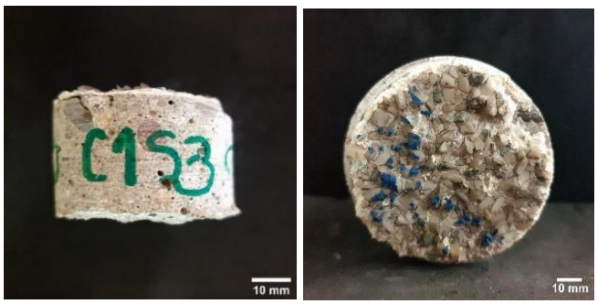

Core description

Date of coring:	September 18, 2023
Structure part:	Column
Core type:	Cylinder
Sample name:	C1S3
General details	
Cross section:	44.5 mm
Diameter:	31.6 mm

Figure D.6: Core C1S3

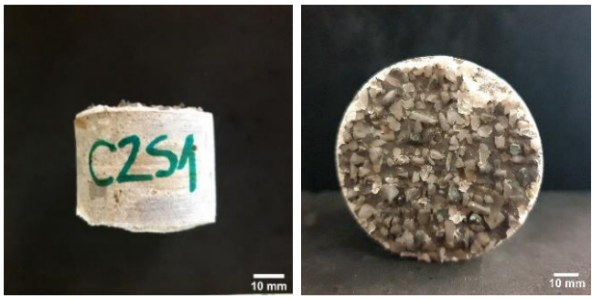

Core description

Date of coring:	September 18, 2023
Structure part:	Column
Core type:	Cylinder
Sample name:	C2S1
General details	
Cross section:	44.5 mm
Diameter:	35.3 mm

Figure D.7: Core C2S1

Core description

Date of coring:	September 18, 2023
Structure part:	Column
Core type:	Cylinder
Sample name:	C2S2
General details	
Cross section:	44.5 mm
Diameter:	41.0 mm

Figure D.8: Core C2S2

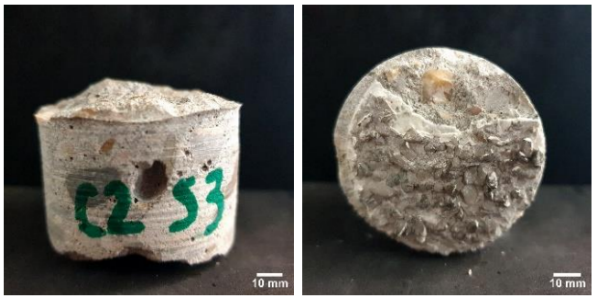

Core description

Date of coring:	September 18, 2023
Structure part:	Column
Core type:	Cylinder
Sample name:	C2S3
General details	
Cross section:	44.5 mm
Diameter:	38.5 mm

Figure D.9: Core C2S3

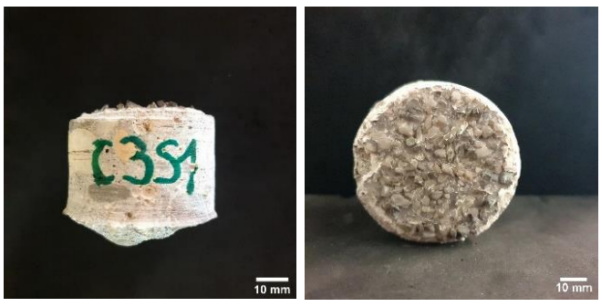

Core description

Date of coring:	September 18, 2023
Structure part:	Column
Core type:	Cylinder
Sample name:	C3S1
General details	
Cross section:	44.5 mm
Diameter:	39.4 mm

Figure D.10: Core C3S1

Core description

Date of coring:	September 18, 2023
Structure part:	Column
Core type:	Cylinder
Sample name:	C3S2
General details	
Cross section:	44.5 mm
Diameter:	34.4 mm

Figure D.11: Core C3S2

Core description

Date of coring:	September 18, 2023
Structure part:	Column
Core type:	Cylinder
Sample name:	C3S3
General details	
Cross section:	44.5 mm
Diameter:	44.3 mm

Figure D.12: Core C3S3

D.2. Sluinerweg beams 2, 9, 10, 12, 13, 14, 15, 16, 22 and 23 pictures and raw data

Figure D.13: Beam 2

Table D.1: Chemical composition analysis of Sluinerweg Beam 2 with hXRF

	Beam 2										Bottom of the beam
Spot	MgO	Al_2O_3	SiO_2	P_2O_5	SO_3	K_2O	CaO	TiO_2	MnO	Fe_2O_3	Classification
1	<LOD	4.08	21.55	0.39	2.00	2.27	64.04	0.44	0.08	4.92	Pure concrete surface
2	<LOD	1.27	4.98	0.27	5.27	1.40	**82.65**	0.22	0.08	3.34	Efflorescence (Ca Leaching)
3	<LOD	0.34	1.01	0.35	**35.37**	0.61	59.68	<LOD	0.15	2.01	Black crust
4	<LOD	7.23	**39.88**	0.31	1.38	3.90	40.47	0.60	0.09	5.99	Sand on the surface
5	<LOD	<LOD	2.89	0.41	**33.50**	0.60	59.78	0.04	0.14	1.91	Black crust
6	<LOD	3.53	22.74	<LOD	0.71	1.75	66.82	0.35	0.05	3.69	Pure concrete surface
7	<LOD	0.39	1.19	0.32	**35.98**	0.88	58.65	0.03	0.15	2.03	Black crust
8	<LOD	3.66	15.37	0.25	1.10	2.52	**72.35**	0.38	0.07	4.05	Efflorescence (Ca Leaching)
9	<LOD	<LOD	<LOD	0.29	**53.06**	0.27	44.48	<LOD	0.13	1.31	Black crust
10	<LOD	0.91	7.79	0.31	**40.77**	0.49	48.34	<LOD	0.12	1.01	Black crust
11	<LOD	<LOD	<LOD	0.57	**48.84**	0.10	48.60	<LOD	0.12	1.16	Black crust

Figure D.14: Beam 9

Table D.2: Chemical composition analysis of Sluinerweg Beam 9 with hXRF

	Beam 9										Bottom of the beam
Spot	MgO	Al_2O_3	SiO_2	P_2O_5	SO_3	K_2O	CaO	TiO_2	MnO	Fe_2O_3	Classification
1	1.27	5.69	**40.08**	0.29	1.35	2.86	43.29	0.41	0.07	4.67	Sand on the surface
2	1.31	5.99	**45.82**	0.30	1.39	3.02	37.47	0.42	0.06	4.24	Sand on the surface
3	0.98	6.09	**69.88**	0.22	1.30	3.02	14.72	0.39	0.07	3.33	Sand on the surface
4	<LOD	1.39	5.05	0.16	0.76	1.11	**87.63**	0.22	0.06	3.18	Efflorescence (Ca Leaching)
5	1.14	5.40	29.93	<LOD	0.80	2.46	**56.48**	0.32	0.05	3.35	Removal of the efflorescence

Figure D.15: Beam 10

Table D.3: Chemical composition analysis of Sluinerweg Beam 10 with hXRF

	Beam 10										Bottom of the beam
Spot	MgO	Al_2O_3	SiO_2	P_2O_5	SO_3	K_2O	CaO	TiO_2	MnO	Fe_2O_3	Classification
1	<LOD	4.53	**25.68**	0.35	1.72	2.48	58.84	0.55	0.13	5.17	Sand on the surface
2	<LOD	0.68	0.46	0.50	**23.95**	0.88	69.64	0.11	0.14	3.21	Black crust
3	1.45	4.64	22.97	0.35	**5.58**	2.28	57.57	0.44	0.11	4.61	Black crust
4	<LOD	4.73	**28.59**	0.18	3.08	2.15	55.61	0.45	0.09	4.99	Sand on the surface
5	0.85	6.27	**46.41**	0.34	1.83	2.61	37.39	0.42	0.05	3.83	Sand on the surface
6	<LOD	3.73	22.92	0.39	**15.28**	1.94	50.90	0.30	0.12	4.14	Black crust
7	1.45	4.56	**33.50**	0.13	1.82	2.19	52.10	0.34	0.06	3.86	Sand on the surface
8	1.33	6.22	**55.57**	0.25	1.02	2.51	28.69	0.38	0.07	3.97	Sand on the surface
9	<LOD	6.50	**33.83**	0.18	1.21	2.82	50.92	0.40	0.06	4.09	Sand on the surface
10	<LOD	2.07	8.37	0.42	1.34	1.47	**81.36**	0.29	0.08	4.11	Efflorescence (Ca Leaching)
11	1.38	3.21	17.40	0.42	1.06	1.93	**69.94**	0.36	0.06	4.25	Efflorescence (Ca Leaching)
12	<LOD	3.99	21.26	0.23	0.87	2.62	66.20	0.36	0.06	4.20	Pure concrete surface
13	<LOD	0.54	2.62	0.30	**42.17**	0.89	50.89	0.03	0.14	2.01	Black crust

Figure D.16: Beam 12

Table D.4: Chemical composition analysis of Sluinerweg Beam 12 with hXRF

	Beam 12										Bottom of the beam
Spot	MgO	Al_2O_3	SiO_2	P_2O_5	SO_3	K_2O	CaO	TiO_2	MnO	Fe_2O_3	Classification
1	2.24	2.73	19.53	0.29	4.89	1.27	63.84	0.47	0.10	4.64	Pure concrete surface
2	<LOD	4.18	24.53	0.48	**8.35**	1.83	54.58	0.46	0.14	5.02	Black crust
3	<LOD	3.57	20.60	0.41	5.44	2.15	62.41	0.38	0.09	4.63	Pure concrete surface
4	<LOD	3.85	18.44	0.36	2.12	2.04	**67.37**	0.44	0.10	4.92	Efflorescence (Ca Leaching)
5	1.48	4.51	23.51	0.26	1.88	2.71	60.45	0.48	0.09	4.62	Pure concrete surface
6	<LOD	4.94	**34.98**	0.38	5.27	2.09	47.09	0.42	0.11	4.61	Sand on the surface
7	1.80	1.17	6.75	0.29	0.92	0.82	**85.08**	0.22	0.06	2.89	Efflorescence (Ca Leaching)
8	<LOD	1.43	8.32	0.43	**37.66**	1.36	46.60	0.12	0.14	3.38	Black crust
9	<LOD	0.89	3.82	0.33	**35.75**	1.04	55.11	0.08	0.14	2.37	Black crust
10	<LOD	0.93	4.28	0.34	**41.24**	1.13	49.29	0.09	0.14	2.17	Black crust
11	1.07	7.38	**35.36**	0.60	1.56	3.86	44.23	0.54	0.09	5.31	Sand on the surface
12	<LOD	7.14	**40.25**	0.37	2.11	3.05	41.87	0.50	0.08	4.64	Sand on the surface

Figure D.17: Beam 13

Table D.5: Chemical composition analysis of Sluinerweg Beam 13 with hXRF

	Beam 13										Bottom of the beam
Spot	MgO	Al_2O_3	SiO_2	P_2O_5	SO_3	K_2O	CaO	TiO_2	MnO	Fe_2O_3	Classification
1	1.81	6.31	**35.92**	0.33	3.11	3.44	41.98	0.59	0.12	6.40	Sand on the surface
2	2.78	3.42	17.25	0.35	**11.99**	2.09	56.80	0.35	0.10	4.87	Black crust
3	<LOD	3.77	18.61	0.35	1.71	2.02	66.04	0.53	0.15	6.41	Pure concrete surface
4	<LOD	5.22	**28.80**	0.19	3.31	2.81	52.00	0.49	0.12	6.87	Sand on the surface
5	<LOD	4.19	23.48	0.31	**4.48**	2.10	57.77	0.44	0.15	6.80	Black crust
6	2.03	3.67	18.48	0.33	3.89	2.08	63.64	0.42	0.13	5.34	Pure concrete surface
7	<LOD	5.30	22.83	0.38	2.18	2.87	61.02	0.45	0.08	4.69	Pure concrete surface
8	<LOD	3.65	21.54	0.21	4.16	2.04	63.04	0.39	0.09	4.74	Pure concrete surface
9	<LOD	0.72	3.80	0.41	**40.44**	1.07	50.83	0.07	0.14	2.15	Black crust
10	<LOD	0.95	3.29	0.43	**43.82**	1.21	47.50	0.06	0.15	2.21	Black crust

Figure D.18: Beam 14

Table D.6: Chemical composition analysis of Sluinerweg Beam 14 with hXRF

	Beam 14										Bottom of the beam
Spot	MgO	Al_2O_3	SiO_2	P_2O_5	SO_3	K_2O	CaO	TiO_2	MnO	Fe_2O_3	Classification
1	<LOD	5.14	**30.67**	0.14	1.16	2.07	55.39	0.44	0.08	4.86	Sand on the surface
2	<LOD	2.23	12.54	0.26	1.62	1.03	**77.95**	0.30	0.08	3.69	Efflorescence (Ca Leaching)
3	<LOD	5.38	**26.47**	0.27	1.46	2.57	58.76	0.42	0.09	4.49	Sand on the surface
4	<LOD	1.89	10.17	0.30	0.87	1.01	**81.38**	0.30	0.09	3.68	Efflorescence (Ca Leaching)
5	<LOD	0.40	4.09	0.40	**46.60**	0.90	44.77	0.05	0.14	2.21	Black crust
6	<LOD	3.99	21.24	0.24	2.14	1.76	65.88	0.36	0.08	4.14	Pure concrete surface
7	<LOD	4.12	20.02	0.28	1.67	2.21	65.21	0.46	0.13	5.63	Pure concrete surface
8	<LOD	2.04	11.75	<LOD	0.81	1.72	**76.24**	0.50	0.12	6.30	Efflorescence (Ca Leaching)
9	<LOD	<LOD	<LOD	0.39	**45.11**	0.65	50.20	<LOD	0.14	2.79	Black crust
10	<LOD	<LOD	<LOD	0.26	**52.82**	0.05	44.89	<LOD	0.11	1.15	Black crust

Figure D.19: Beam 15

Table D.7: Chemical composition analysis of Sluinerweg Beam 15 with hXRF

	Beam 15										Bottom of the beam
Spot	MgO	Al_2O_3	SiO_2	P_2O_5	SO_3	K_2O	CaO	TiO_2	MnO	Fe_2O_3	Classification
1	1.78	3.72	17.28	0.24	2.37	2.08	**67.64**	0.37	0.10	4.42	Efflorescence (Ca Leaching)
2	2.35	3.73	18.33	0.25	1.59	2.04	66.63	0.39	0.10	4.58	Pure concrete surface
3	<LOD	5.80	**36.26**	0.14	1.73	2.74	47.67	0.46	0.08	5.04	Sand on the surface
4	1.66	3.85	22.05	<LOD	1.53	2.00	63.27	0.39	0.09	5.08	Pure concrete surface
5	<LOD	4.84	**28.78**	<LOD	1.34	3.00	55.22	0.50	0.10	5.81	Sand on the surface
6	<LOD	3.71	18.04	0.42	1.70	2.22	**67.41**	0.48	0.13	5.56	Efflorescence (Ca Leaching)
7	1.73	4.24	20.07	0.26	2.02	2.41	63.57	0.46	0.10	5.15	Pure concrete surface
8	<LOD	3.64	18.42	<LOD	2.45	2.04	**67.15**	0.43	0.11	5.47	Efflorescence (Ca Leaching)
9	<LOD	0.68	3.62	0.39	**49.36**	0.83	42.73	0.03	0.13	1.84	Black crust
10	<LOD	0.88	4.70	0.39	**38.68**	1.31	50.63	0.13	0.14	2.76	Black crust
11	1.37	6.49	**40.15**	0.51	2.22	2.51	41.60	0.46	0.07	4.63	Sand on the surface
12	<LOD	6.16	**35.01**	0.43	1.65	2.96	48.20	0.48	0.07	5.04	Sand on the surface

Figure D.20: Beam 16

Table D.8: Chemical composition analysis of Sluinerweg Beam 16 with hXRF

	Beam 16										Bottom of the beam
Spot	MgO	Al_2O_3	SiO_2	P_2O_5	SO_3	K_2O	CaO	TiO_2	MnO	Fe_2O_3	Classification
1	1.06	5.67	**36.51**	0.44	1.60	2.53	45.88	0.45	0.11	5.77	Sand on the surface
2	<LOD	5.34	**32.89**	0.36	2.35	2.47	50.75	0.42	0.09	5.24	Sand on the surface
3	1.67	4.11	24.02	0.14	1.70	2.02	61.26	0.40	0.08	4.61	Pure concrete surface
4	<LOD	3.62	19.42	0.31	1.91	2.41	66.19	0.43	0.09	5.23	Pure concrete surface
5	<LOD	3.49	15.24	0.24	1.82	2.43	**70.73**	0.43	0.09	5.21	Efflorescence (Ca Leaching)
6	1.91	4.35	20.92	0.25	3.37	2.53	61.64	0.39	0.07	4.59	Pure concrete surface
7	<LOD	1.45	7.44	0.27	1.28	1.23	**83.02**	0.35	0.08	4.46	Efflorescence (Ca Leaching)
8	<LOD	4.60	**28.36**	0.22	1.56	2.65	57.01	0.42	0.08	4.92	Sand on the surface
9	<LOD	4.01	20.80	0.23	1.29	2.45	64.86	0.47	0.10	5.47	Pure concrete surface
10	<LOD	4.71	**47.69**	0.40	2.65	2.24	37.24	0.36	0.07	4.54	Sand on the surface
11	<LOD	4.40	**26.95**	0.35	1.89	2.19	57.73	0.49	0.10	5.41	Sand on the surface
12	<LOD	4.27	**30.00**	0.25	1.54	2.13	55.97	0.38	0.07	5.17	Sand on the surface
13	<LOD	5.39	**28.38**	0.44	1.27	3.09	56.43	0.42	0.06	4.49	Sand on the surface
14	1.32	4.67	21.48	0.24	1.34	2.71	63.14	0.44	0.07	4.58	Pure concrete surface
15	<LOD	1.17	5.41	0.21	1.06	0.73	**87.54**	0.21	0.06	3.02	Efflorescence (Ca Leaching)
16	1.25	6.15	**30.49**	0.52	1.34	3.26	51.73	0.44	0.06	4.76	Sand on the surface
17	1.70	<LOD	3.31	0.32	**49.06**	0.45	43.76	<LOD	0.11	1.28	Black crust
18	<LOD	<LOD	<LOD	0.34	**51.98**	0.14	45.49	<LOD	0.10	1.19	Black crust
19	<LOD	<LOD	<LOD	0.36	**50.49**	0.45	45.78	<LOD	0.12	1.98	Black crust

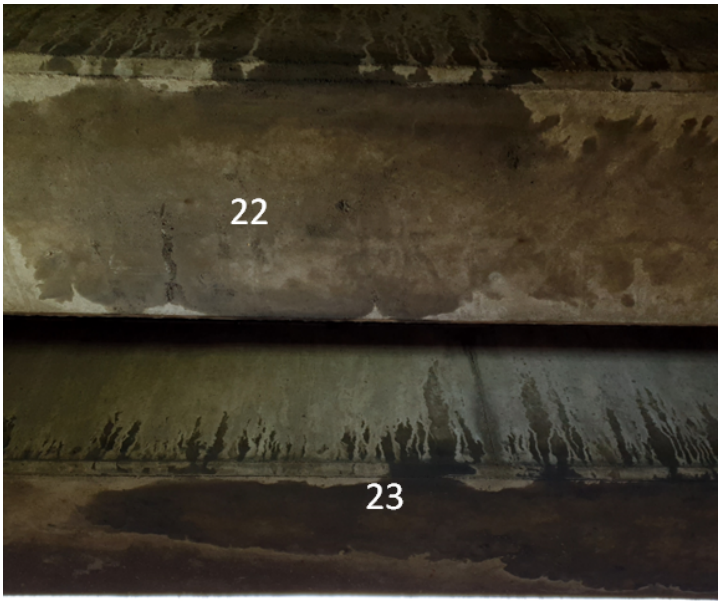

Figure D.21: Beam 22 and 23

Table D.9: Chemical composition analysis of Sluinerweg Beams 22 and 23 with hXRF

	Beams 22 and 23										Bottom of the beam
Spot	MgO	Al_2O_3	SiO_2	P_2O_5	SO_3	K_2O	CaO	TiO_2	MnO	Fe_2O_3	Classification
1	<LOD	<LOD	1.47	0.42	**49.24**	0.38	44.51	<LOD	0.13	2.84	Black crust
2	<LOD	4.89	**27.90**	0.46	2.16	2.28	56.02	0.47	0.09	5.45	Sand on the surface
3	<LOD	0.49	6.93	0.38	**44.51**	0.61	43.60	<LOD	0.11	2.70	Black crust
4	<LOD	<LOD	<LOD	0.42	**47.55**	0.37	47.44	<LOD	0.13	2.99	Black crust
5	<LOD	1.86	10.08	0.33	**31.73**	1.13	51.08	0.09	0.11	3.15	Black crust
6	<LOD	<LOD	<LOD	0.31	**40.05**	0.05	56.21	<LOD	0.09	1.58	Black crust
7	<LOD	<LOD	<LOD	0.27	**53.53**	0.05	43.47	<LOD	0.12	1.83	Black crust
8	<LOD	<LOD	4.47	0.36	**49.53**	0.54	42.10	<LOD	0.12	2.14	Black crust
9	<LOD	<LOD	3.51	0.39	**47.25**	0.45	44.68	<LOD	0.13	2.85	Black crust
10	<LOD	<LOD	1.30	0.38	**49.05**	0.50	45.65	<LOD	0.14	2.25	Black crust

References

[1] C. Zhang, M. Hu, F. D. Maio, B. Sprecher, X. Yang, and A. Tukker, "An overview of the waste hierarchy framework for analyzing the circularity in construction and demolition waste management in europe," *Science of The Total Environment*, pp. 1–13, 2021. DOI: https://doi.org/10.1016/j.scitotenv.2021.149892. [Online]. Available: https://www.sciencedirect.com/science/article/pii/S0048969721049676.

[2] C. Zhang, M. Hu, X. Yang, B. Miranda-Xicotencatl, B. Sprecher, F. D. Maio, X. Zhong, and A. Tukker, "Upgrading construction and demolition waste management from downcycling to recycling in the netherlands," *Cleaner Production*, pp. 1–12, 2020. DOI: https://doi.org/10.1016/j.jclepro.2020.121718. [Online]. Available: https://www.sciencedirect.com/science/article/pii/S0959652620317650.

[3] A. D. Maria, J. Eyckmans, and K. V. Acker, "Downcycling versus recycling of construction and demolition waste: Combining LCA and LCC to support sustainable policy making," *Waste Management*, vol. 75, pp. 3–21, 2018. DOI: 10.1016/j.wasman.2018.01.028. [Online]. Available: https://doi.org/10.1016%2Fj.wasman.2018.01.028.

[4] M. Nedeljković, N. Tošić, E. Schlangen, and S. Fennis, "Pre-demolition concrete waste stream identification," pp. 1–25, 2021. DOI: https://doi.org/10.5937/GRMK2301001N. [Online]. Available: https://repository.tudelft.nl/islandora/object/uuid%3A89d9bee9-b433-451e-94d5-3ab96677ac55.

[5] B. M. Xicotencatl, "Scenarios for concrete-rubble recycling in the netherlands," pp. 1–80, 2017. [Online]. Available: https://repository.tudelft.nl/islandora/object/uuid%3A1eb96393-0d86-476b-b563-5a4035104b66.

[6] E. C. J. R. Centre., *Use of recycled aggregates in concrete: opportunities for upscaling in Europe.* Publications Office, 2023. DOI: 10.2760/144802. [Online]. Available: https://data.europa.eu/doi/10.2760/144802.

[7] D. circulaire bouweconomie, "Kwaliteitsbeoordeling en -borging bij hergebruik uit bestaande bouw," pp. 1–56, 2023.

[8] T. Omar, M. L. Nehdi, and T. Zayed, "Performance of ndt techniques in appraising condition of reinforced concrete bridge decks," *Journal of Performance of Constructed Facilities*, pp. 1–16, 2017. DOI: https://doi.org/10.1061/(ASCE)CF.1943-5509.0001098. [Online]. Available: https://ascelibrary.org/doi/10.1061/%28ASCE%29CF.1943-5509.0001098.

[9] Y. Boussahoua, S. Kenai, Z. M. Sbartai, D. Breysse, and K. Ali-Benyahia, "Influence of the number of cores on concrete strength assessment by nondestructive tests in old existing structures," *Asian Journal of Civil Engineering volume*, pp. 1–15, 2023. DOI: https://doi.org/10.1007/s42107-023-00599-0. [Online]. Available: https://link.springer.com/article/10.1007/s42107-023-00599-0.

[10] J. Aoustin. "Identification of the cement type at the concrete surface with ordinary portland cement and supplementary cementitious materials with a handheld x-ray fluorescence analyser." (2023), [Online]. Available: http://resolver.tudelft.nl/uuid:6e394791-799e-436d-aabb-c01cef597b80.

[11] J. H. Bungey and M. G. Grantham, *Testing of concrete in Structures*. Taylor and Francis, 2006.

[12] P. Moioli and C. Seccaroni, "Analysis of art objects using a portable x-ray fluorescence spectrometer," *X-Ray Spectrometry*, vol. 29, no. 1, pp. 48–52, 2000. DOI: 10.1002/(sici)1097-4539(200001/02)29:1<48::aid-xrs404>3.0.co;2-h. [Online]. Available: https://doi.org/10.1002%2F%28sici%291097-4539%28200001%2F02%2929%3A1%3C48%3A%3Aid-xrs404%3E3.0.co%3B2-h.

[13] A. Steiner, R. Conrey, and J. Wolff, "PXRF calibrations for volcanic rocks and the application of in-field analysis to the geosciences," *Chemical Geology*, vol. 453, pp. 35–54, 2017. DOI: 10.1016/j.chemgeo.2017.01.023. [Online]. Available: https://doi.org/10.1016%2Fj.chemgeo.2017.01.023.

[14] M. Nicholas and P. Manti, "Testing the applicability of handheld portable xrf to the characterisation of archaeological copper alloys," 2014. [Online]. Available: https://www.researchgate.net/publication/266564964_Testing_the_applicability_of_handheld_portable_XRF_to_the_characterisation_of_archaeological_copper_alloys.

[15] M. Nedeljković, N. Tošić, P. Holthuizen, F. F. de Mendonça Filho, O. Çopuroğlu, E. Schlangen, and S. Fennis, "Non-destructive screening methodology based on handheld XRF for the classification of concrete: Cement type-driven separation," *Materials and Structures*, vol. 56, no. 3, 2023. DOI: 10.1617/s11527-023-02147-3. [Online]. Available: https://doi.org/10.1617%2Fs11527-023-02147-3.

[16] P. C. Taylor, E. Yurdakul, and H. Ceylan, "The application of x-ray fluorescence to assess proportions of fresh concrete," 2012. [Online]. Available: https://dr.lib.iastate.edu/server/api/core/bitstreams/ef09a247-1e45-42a6-bd1e-19afe490b02c/content.

[17] S. Chinchón-Payá, J. E. T. Martín, A. S. Toledo, and J. S. Montero, "Quantification of chlorides and sulphates on concrete surfaces using portable x-ray fluorescence. optimization of the measurement method using monte carlo simulation," *Materials*, vol. 14, no. 24, p. 7892, 2021. DOI: 10.3390/ma14247892. [Online]. Available: https://doi.org/10.3390%2Fma14247892.

[18] S. Chinchón-Payá, J. E. T. Martín, N. R. Ramos, and J. S. Montero, "Use of a handheld x-ray fluorescence analyser to quantify chloride ions in situ: A case study of structural repair," *Materials*, vol. 14, no. 3, p. 571, 2021. DOI: 10.3390/ma14030571. [Online]. Available: https://doi.org/10.3390%2Fma14030571.

[19] *The skin of concrete composition and properties - Materials and Structures — link.springer.com*, https://link.springer.com/article/10.1007/BF02479083, [Accessed 18-10-2023].

[20] S. Czarnecki and Ł. Sadowski, "Morphological properties of the cement skin: Understanding the effect of contact with formwork," *Case Studies in Construction Materials*, vol. 16, e01007, 2022. DOI: 10.1016/j.cscm.2022.e01007. [Online]. Available: https://doi.org/10.1016%2Fj.cscm.2022.e01007.

[21] H. Krour, R. Trauchessec, A. Lecomte, C. Diliberto, L. Barnes-Davin, B. Bolze, and A. Delhay, "Incorporation rate of recycled aggregates in cement raw meals," *Construction and Building Materials*, vol. 248, p. 118 217, 2020. DOI: 10.1016/j.conbuildmat.2020.118217. [Online]. Available: https://doi.org/10.1016%2Fj.conbuildmat.2020.118217.

[22] E. Kwon, J. Ahn, B. Cho, and D. Park, "A study on development of recycled cement made from waste cementitious powder," *Construction and Building Materials*, vol. 83, pp. 174–180, 2015. DOI: 10.1016/j.conbuildmat.2015.02.086. [Online]. Available: https://doi.org/10.1016%2Fj.conbuildmat.2015.02.086.

[23] Y. Villagrán-Zaccardi, E. Sosa, L. Carrizo, and C. Zega, "Use of recycled fines from waste concrete as an admixture in new concrete," in *The Structural Integrity of Recycled Aggregate Concrete Produced with Fillers and Pozzolans*, Elsevier, 2022, pp. 39–65. DOI: 10.1016/b978-0-12-824105-9.00020-2. [Online]. Available: https://doi.org/10.1016%2Fb978-0-12-824105-9.00020-2.

[24] F. Pacheco-Torgal, *Advances in Construction and Demolition Waste Recycling: Management, Processing and Environmental Assessment*. Woodhead Publishing, 2020.

[25] I. Europe. "Collection and recycling of construction and demolition waste: Key learnings." Online; accessed 17-05-2023. (2022), [Online]. Available: https://www.interregeurope.eu/find-policy-solutions/webinar/collection-and-recycling-of-construction-and-demolition-waste-key-learnings#:~:text=About%20450%20%E2%80%93%20500%20million%20tonnes,as%20well%20as%20road%20maintenance..

[26] P. V. Saez and M. Osmani, “A diagnosis of construction and demolition waste generation and recovery practice in the european union,” *Cleaner Production*, pp. 1–11, 2019. DOI: https://doi.org/10.1016/j.jclepro.2019.118400. [Online]. Available: https://www.sciencedirect.com/science/article/pii/S0959652619332706.

[27] J. L. G. Martos, D. Styles, H. Schoenberger, and B. Zeschmar-Lahl, “Construction and demolition waste best management practice in europe,” *Resources, Conservation and Recycling*, pp. 1–13, 2018. DOI: https://doi.org/10.1016/j.resconrec.2018.04.016. [Online]. Available: https://www.sciencedirect.com/science/article/pii/S0921344918301538.

[28] J. Pacheco and J. de Brito, “Recycled aggregates produced from construction and demolition waste for structural concrete: Constituents, properties and production,” *Materials*, pp. 1–18, 2021. DOI: https://doi.org/10.3390/ma14195748. [Online]. Available: https://www.mdpi.com/1996-1944/14/19/5748.

[29] R. Magazine. “Zenrobotics’ recycling robots to sort out chinese construction waste.” Online; accessed 18-08-2023. (2016), [Online]. Available: https://www.recycling-magazine.com/2016/12/20/zenrobotics-recycling-robots-to-sort-out-chinese-construction-waste/.

[30] R. Žurauskienė and M. Valentukevi, “Experimental research on quality parameters of recycled concrete,” *Materials*, pp. 1–14, 2020. DOI: https://doi.org/10.3390/ma13112538. [Online]. Available: https://www.mdpi.com/1996-1944/13/11/2538.

[31] W. M. Shaban, J. Yang, H. Su, K. H. Mo, L. Li, and J. Xie, “Quality improvement techniques for recycled concrete aggregate: A review,” *Advanced Concrete Technology*, pp. 1–17, 2019. DOI: https://doi.org/10.3151/jact.17.151. [Online]. Available: https://www.jstage.jst.go.jp/article/jact/17/4/17_151/_article.

[32] V. W. Tam, M. Soomro, and A. C. J. Evangelista, “Quality improvement of recycled concrete aggregate by removal of residual mortar: A comprehensive review of approaches adopted,” *Construction and Building Materials*, pp. 1–22, 2021. DOI: https://doi.org/10.1016/j.conbuildmat.2021.123066. [Online]. Available: https://www.sciencedirect.com/science/article/pii/S0950061821008266?via%3Dihub.

[33] A. T. Gebremariam, F. D. Maio, A. Vahidi, and P. Rem, “Innovative technologies for recycling end-of-life concrete waste in the built environment,” *Resources, Conservation and Recycling*, vol. 163, p. 104 911, 2020. DOI: 10.1016/j.resconrec.2020.104911. [Online]. Available: https://doi.org/10.1016%2Fj.resconrec.2020.104911.

[34] S. Pantini and L. Rigamonti, “Is selective demolition always a sustainable choice?” *Waste Management*, pp. 1–8, 2019. DOI: https://doi.org/10.1016/j.wasman.2019.12.033. [Online]. Available: https://www.sciencedirect.com/science/article/pii/S0956053X19307871?via%3Dihub.

[35] F. Pacheco-Torgal, V. Tam, J. Labrincha, Y. Ding, and J. de Brito, *Handbook of Recycled Concrete and Demolition Waste*. Woodhead Publishing, 2013.

[36] I. Khaliq and M. Khan, “Effect of parent concrete on the performance of recycled aggregate concrete,” *Sustainability*, pp. 1–9, 2021. DOI: https://doi.org/10.3390/su12229399. [Online]. Available: https://www.mdpi.com/2071-1050/12/22/9399.

[37] A. Kumar and G. J. Singh, “Recycled concrete aggregate classification based on quality parameters and performance,” *Iranian Journal of Science and Technology, Transactions of Civil Engineering*, pp. 1–22, 2023. DOI: https://doi.org/10.1007/s40996-023-01139-1. [Online]. Available: https://link.springer.com/article/10.1007/s40996-023-01139-1.

[38] M. Nedeljković, J. Visser, B. Šavija, S. Valcke, and E. Schlangen, “Use of fine recycled concrete aggregates in concrete: A critical review,” *Journal of Building Engineering*, vol. 38, p. 102 196, 2021. DOI: 10.1016/j.jobe.2021.102196. [Online]. Available: https://doi.org/10.1016%2Fj.jobe.2021.102196.

[39] M. Nedeljković, J. Visser, B. Savija, S. Valcke, and E. Schlangen, “Use of fine recycled concrete aggregates in concrete: A critical review,” *Journal of Building Engineering*, pp. 1–27, 2021. DOI: https://doi.org/10.1016/j.jobe.2021.102196. [Online]. Available: https://www.sciencedirect.com/science/article/pii/S2352710221000528?via%3Dihub.

[40] K. Schabowicz, “Non-destructive testing of materials in civil engineering,” *Materials*, pp. 1–13, 2019. DOI: 10.3390/ma12193237. [Online]. Available: https://www.ncbi.nlm.nih.gov/pmc/articles/PMC6804297/.

[41] G. Wilsch, F. Weritz, D. Schaurich, and H. Wiggenhauser, “Determination of chloride content in concrete structures with laser-induced breakdown spectroscopy,” *Construction and Building Materials*, pp. 1–7, 2005. DOI: https://doi.org/10.1016/j.conbuildmat.2005.06.001. [Online]. Available: https://www.sciencedirect.com/science/article/pii/S0950061805001467.

[42] D. Breysse, J.-P. Balayssac, S. Biondi, D. Corbett, A. Goncalves, M. Grantham, V. A. M. Luprano, A. Masi, A. V. Monteiro, and Z. M. Sbartai, “Recommendation of rilem tc249-isc on non-destructive in situ strength assessment of concrete,” *Materials and Structures*, pp. 1–21, 2019. DOI: https://doi.org/10.1617/s11527-019-1369-2. [Online]. Available: https://link.springer.com/article/10.1617/s11527-019-1369-2.

[43] *Non-Destructive In Situ Strength Assessment of Concrete*. Springer, 2021.

[44] Y. C. Kog, “Testing plan for estimating in situ concrete strength,” *Practice Periodical on Structural Design and Construction*, pp. 1–10, 2019. DOI: https://doi.org/10.1061/(ASCE)SC.1943-5576.0000410. [Online]. Available: https://ascelibrary.org/doi/10.1061/%28ASCE%29SC.1943-5576.0000410.

[45] “Nen-en 12504-1 testing concrete in structures - part 1: Cored specimens - taking, examining, and testing in compression.” (2019).

[46] N. Taefi, M. Khalaji, and S. Tavassoli, “Determination of elemental composition of cement powder by spark induced breakdown spectroscopy,” *Cement and Concrete Research*, vol. 40, no. 7, pp. 1114–1119, 2010. DOI: 10.1016/j.cemconres.2010.03.003. [Online]. Available: https://doi.org/10.1016%2Fj.cemconres.2010.03.003.

[47] F. Kleiner, M. Decker, C. Rößler, H. Hilbig, and H.-M. Ludwig, “Combined LA-ICP-MS and SEM-EDX analyses for spatially resolved major, minor and trace element detection in cement clinker phases,” *Cement and Concrete Research*, vol. 159, p. 106 875, 2022. DOI: 10.1016/j.cemconres.2022.106875. [Online]. Available: https://doi.org/10.1016%2Fj.cemconres.2022.106875.

[48] M. Bonta, A. Eitzenberger, S. Burtscher, and A. Limbeck, “Quantification of chloride in concrete samples using LA-ICP-MS,” *Cement and Concrete Research*, vol. 86, pp. 78–84, 2016. DOI: 10.1016/j.cemconres.2016.05.002. [Online]. Available: https://doi.org/10.1016%2Fj.cemconres.2016.05.002.

[49] B. Huber, H. Hilbig, M. M. Mago, J. E. Drewes, and E. Müller, “Comparative analysis of biogenic and chemical sulfuric acid attack on hardened cement paste using laser ablation-ICP-MS,” *Cement and Concrete Research*, vol. 87, pp. 14–21, 2016. DOI: 10.1016/j.cemconres.2016.05.003. [Online]. Available: https://doi.org/10.1016%2Fj.cemconres.2016.05.003.

[50] T. Völker, S. Millar, C. Strangfeld, and G. Wilsch, “Identification of type of cement through laser-induced breakdown spectroscopy,” *Construction and Building Materials*, vol. 258, p. 120 345, 2020. DOI: 10.1016/j.conbuildmat.2020.120345. [Online]. Available: https://doi.org/10.1016%2Fj.conbuildmat.2020.120345.

[51] G. S. Senesi, R. S. Harmon, and R. R. Hark, “Field-portable and handheld laser-induced breakdown spectroscopy: Historical review, current status and future prospects,” *Spectrochimica Acta Part B: Atomic Spectroscopy*, vol. 175, p. 106 013, 2021. DOI: 10.1016/j.sab.2020.106013. [Online]. Available: https://doi.org/10.1016%2Fj.sab.2020.106013.

[52] “Handheld libs analyzers | vulcan+ range.” Online; accessed 22-09-2023. (), [Online]. Available: https://hha.hitachi-hightech.com/en/product-range/products/handheld-xrf-libs-analyzers/handheld-libs-analyzers.

[53] “Libs technology for non-scientists.” Online; accessed 22-09-2023. (), [Online]. Available: https://assets.thermofisher.com/TFS-Assets/CAD/Scientific-Resources/libs-technology-nonscientists-ebook.pdf?icid=CAD_blog_metals_2021Aug#:~:text=The%20LIBS%20technique%20utilizes%20a,ablated%20and%20enters%20the%20plasma..

[54] "Handheld xrf analyzers." Online; accessed 22-09-2023. (), [Online]. Available: https://www.geotechenv.com/handheld_xrf_analyzers.html.

[55] "Technology focus: X-ray fluorescence (xrf) in mining." Online; accessed 22-09-2023. (), [Online]. Available: https://www.thermofisher.com/blog/mining/technology-focus-x-ray-fluorescence-xrf-in-mining/.

[56] V. Laperche and B. Lemière, "Possible pitfalls in the analysis of minerals and loose materials by portable xrf, and how to overcome them," *Minerals*, p. 25, 2020. DOI: 10.3390/min1101. [Online]. Available: https://www.mdpi.com/2075-163X/11/1/33.

[57] J. Pringle, A. Jeffery, A. Ruffell, I. Stimpson, D. Pirrie, E. Bergslien, C. Madden, I. Oliver, K. Wisniewski, J. Cassella, N. Lamont, S. Gormley, and J. Partridge, "The use of portable XRF as a forensic geoscience non-destructive trace evidence tool for environmental and criminal investigations," *Forensic Science International*, vol. 332, p. 111 175, 2022. DOI: 10.1016/j.forsciint.2022.111175. [Online]. Available: https://doi.org/10.1016%2Fj.forsciint.2022.111175.

[58] X. Zhang, A. J. Specht, E. Wells, M. G. Weisskopf, J. Weuve, and L. H. Nie, "Evaluation of a portable XRF device for in vivo quantification of lead in bone among a US population," *Science of The Total Environment*, vol. 753, p. 142 351, 2021. DOI: 10.1016/j.scitotenv.2020.142351. [Online]. Available: https://doi.org/10.1016%2Fj.scitotenv.2020.142351.

[59] G. E. Hall, G. F. Bonham-Carter, and A. Buchar, "Evaluation of portable x-ray fluorescence (pXRF) in exploration and mining: Phase 1, control reference materials," *Geochemistry: Exploration, Environment, Analysis*, vol. 14, no. 2, pp. 99–123, 2014. DOI: 10.1144/geochem2013-241. [Online]. Available: https://doi.org/10.1144%2Fgeochem2013-241.

[60] E. Calparsoro, M. Maguregui, H. Morillas, G. Arana, and J. Iñañez, "Non-destructive screening methodology based on ED-XRF for the classification of medieval and post-medieval archaeological ceramics," *Ceramics International*, vol. 45, no. 8, pp. 10 672–10 683, 2019. DOI: 10.1016/j.ceramint.2019.02.138. [Online]. Available: https://doi.org/10.1016%2Fj.ceramint.2019.02.138.

[61] A. M. Hunt and R. J. Speakman, "Portable XRF analysis of archaeological sediments and ceramics," *Journal of Archaeological Science*, vol. 53, pp. 626–638, 2015. DOI: 10.1016/j.jas.2014.11.031. [Online]. Available: https://doi.org/10.1016%2Fj.jas.2014.11.031.

[62] T. Radu and D. Diamond, "Comparison of soil pollution concentrations determined using AAS and portable XRF techniques," *Journal of Hazardous Materials*, vol. 171, no. 1-3, pp. 1168–1171, 2009. DOI: 10.1016/j.jhazmat.2009.06.062. [Online]. Available: https://doi.org/10.1016%2Fj.jhazmat.2009.06.062.

[63] R. N. Brent, H. Wines, J. Luther, N. Irving, J. Collins, and B. L. Drake, "Validation of handheld x-ray fluorescence for in situ measurement of mercury in soils," *Journal of Environmental Chemical Engineering*, vol. 5, no. 1, pp. 768–776, 2017. DOI: 10.1016/j.jece.2016.12.056. [Online]. Available: https://doi.org/10.1016%2Fj.jece.2016.12.056.

[64] A. Gianoncelli, J. Castaing, L. Ortega, E. Dooryhée, J. Salomon, P. Walter, J.-L. Hodeau, and P. Bordet, "A portable instrument for iin situ/i determination of the chemical and phase compositions of cultural heritage objects," *X-Ray Spectrometry*, vol. 37, no. 4, pp. 418–423, 2008. DOI: 10.1002/xrs.1025. [Online]. Available: https://doi.org/10.1002%2Fxrs.1025.

[65] C. García-Florentino, M. Maguregui, H. Morillas, I. Marcaida, and J. M. Madariaga, "A fast in situ non-invasive approach to classify mortars from a construction of high historical value," *Microchemical Journal*, vol. 133, pp. 104–113, 2017. DOI: 10.1016/j.microc.2017.03.020. [Online]. Available: https://doi.org/10.1016%2Fj.microc.2017.03.020.

[66] F. M. Filho, H. Morillas, H. Derluyn, M. Maguregui, and D. Grégoire, "In-situ versus laboratory characterization of historical site in marine environment using x-ray fluorescence and raman spectroscopy," *Microchemical Journal*, vol. 147, pp. 905–913, 2019. DOI: 10.1016/j.microc.2019.02.014. [Online]. Available: https://doi.org/10.1016%2Fj.microc.2019.02.014.

[67] A. Dey, "Chemical characterization of recycled concrete aggregates using a handheld x-ray fluorescence device," 2020. [Online]. Available: https://www.proquest.com/openview/85c0df8f37bc667d8a01322350b42569/1?pq-origsite=gscholar&cbl=18750&diss=y5.

[68] J. Pacheco Farias, "Corrosion of steel in cracked concrete," Ph.D. dissertation, 2015. DOI: 10.4233/UUID:BC726EAD-0999-4FE4-BAD1-5C26C0E50405. [Online]. Available: http://resolver.tudelft.nl/uuid:bc726ead-0999-4fe4-bad1-5c26c0e50405.

[69] R. Yagi and K. Tsuji, "Confocal micro-XRF analysis of light elements with rh x-ray tube and its application for painted steel sheet," *X-Ray Spectrometry*, vol. 44, no. 3, pp. 186–189, 2015. DOI: 10.1002/xrs.2599. [Online]. Available: https://doi.org/10.1002%2Fxrs.2599.

[70] A. Sánchez, J. Tuñón, M. Montejo, P. Amate, B. Ceprián, A. Rousaki, M. Costa, D. Saelens, S. Lycke, and P. Vandenabeele, "First insights into the archaeometric analysis of the los amores mosaic in cástulo (linares, spain): The judgement of paris," *Heritage Science*, vol. 9, no. 1, 2021. DOI: 10.1186/s40494-021-00483-7. [Online]. Available: https://doi.org/10.1186%2Fs40494-021-00483-7.

[71] "Klimaatimpact van betongebruik in de nederlandse bouw." Online; accessed 21-10-2023. (2020), [Online]. Available: https://www.betonakkoord.nl/wp-content/uploads/sites/43/166796/ce_delft_190417_klimaatimpact_betongebruik_in_nederlandse_bouw_def.pdf.

[72] Bruker. "S1 titan handheld xrf analyzer for elemental analysis." Online; accessed 17-10-2023. (2023), [Online]. Available: https://www.bruker.com/en/products-and-solutions/elemental-analyzers/handheld-xrf-spectrometers/S1-TITAN.html.

[73] "Bruker s1 titan 800 handheld xrf analyzer (s1titan800)." Online; accessed 17-10-2023. (2023), [Online]. Available: https://www.bergeng.com/mm5/downloads/bruker/Bruker%20S1%20TITAN%20Handheld%20XRF%20Analyzer%20Brochure.pdf.

[74] "Wavelength dispersive x-ray fluorescence (wdxrf)." Online; accessed 17-10-2023. (2023), [Online]. Available: https://www.malvernpanalytical.com/en/products/technology/xray-analysis/x-ray-fluorescence/wavelength-dispersive-x-ray-flourescence.

[75] L. Greenspan, "Humidity fixed points of binary saturated aqueous solutions," *Journal of Research of the National Bureau of Standards Section A: Physics and Chemistry*, vol. 81A, no. 1, p. 89, 1977. DOI: 10.6028/jres.081a.011. [Online]. Available: https://doi.org/10.6028%2Fjres.081a.011.

[76] M. Bediako and E. O. Amankwah, "Analysis of chemical composition of portland cement in ghana: A key to understand the behavior of cement," *Advances in Materials Science and Engineering*, vol. 2015, pp. 1–5, 2015. DOI: 10.1155/2015/349401. [Online]. Available: https://doi.org/10.1155%2F2015%2F349401.

[77] Z. Osmanovic, N. Haračić, and J. Zelić, "Properties of blastfurnace cements (CEM III/a, b, c) based on portland cement clinker, blastfurnace slag and cement kiln dusts," *Cement and Concrete Composites*, vol. 91, pp. 189–197, 2018. DOI: 10.1016/j.cemconcomp.2018.05.006. [Online]. Available: https://doi.org/10.1016%2Fj.cemconcomp.2018.05.006.

[78] N. Winter, *Understanding Cement. An introduction to cement production, cement hydration and deleterious processes in concrete*. 2012.

[79] C. Andrade and M. Sanjuán, "Updating carbon storage capacity of spanish cements," *Sustainability*, vol. 10, no. 12, p. 4806, 2018. DOI: 10.3390/su10124806. [Online]. Available: https://doi.org/10.3390%2Fsu10124806.

[80] Q. T. Phung, L. Frederickx, T. N. Nguyen, and V. T. Nguyen, "Resistance of ordinary and low-carbon cements to carbonation: Microstructural and mineralogical alteration," *Cement and Concrete Composites*, vol. 143, p. 105 260, 2023. DOI: 10.1016/j.cemconcomp.2023.105260. [Online]. Available: https://doi.org/10.1016%2Fj.cemconcomp.2023.105260.

[81] J. Bai, "Durability of sustainable concrete materials," in *Sustainability of Construction Materials*. Elsevier, 2009, pp. 239–253. DOI: 10.1533/9781845695842.239. [Online]. Available: http://dx.doi.org/10.1533/9781845695842.239.

[82] T. Nijland and J. Larbi, "Microscopic examination of deteriorated concrete," in *Non-Destructive Evaluation of Reinforced Concrete Structures*. Elsevier, 2010, pp. 137–179. DOI: 10.1533/9781845699536.2.137. [Online]. Available: http://dx.doi.org/10.1533/9781845699536.2.137.

[83] P. López-Arce, L. Gómez-Villalba, S. Martínez-Ramírez, M. Á. de Buergo, and R. Fort, "Influence of relative humidity on the carbonation of calcium hydroxide nanoparticles and the formation of calcium carbonate polymorphs," *Powder Technology*, vol. 205, no. 1-3, pp. 263–269, 2011. DOI: 10.1016/j.powtec.2010.09.026. [Online]. Available: https://doi.org/10.1016%2Fj.powtec.2010.09.026.

[84] L. Lavagna and R. Nisticò, "An insight into the chemistry of cement—a review," *Applied Sciences*, vol. 13, no. 1, p. 203, 2022. DOI: 10.3390/app13010203. [Online]. Available: https://doi.org/10.3390%2Fapp13010203.

[85] M. Nedeljković, "Carbonation mechanism of alkali-activated fly ash and slag materials," Ph.D. dissertation, 2019. DOI: 10.4233/UUID:97B9EABE-159E-43E1-8B35-EDC61B1AA682. [Online]. Available: http://resolver.tudelft.nl/uuid:97b9eabe-159e-43e1-8b35-edc61b1aa682.

[86] M. Elsalamawy, A. R. Mohamed, and E. M. Kamal, "The role of relative humidity and cement type on carbonation resistance of concrete," *Alexandria Engineering Journal*, vol. 58, no. 4, pp. 1257–1264, Dec. 2019, ISSN: 1110-0168. DOI: 10.1016/j.aej.2019.10.008. [Online]. Available: http://dx.doi.org/10.1016/j.aej.2019.10.008.

[87] R. E. Bevins, N. J. Pearce, D. Pirrie, R. A. Ixer, S. Hillier, P. Turner, and M. Power, "Assessing the authenticity of a sample taken from the altar stone at stonehenge in 1844 using portable XRF and automated SEM-EDS," *Journal of Archaeological Science: Reports*, vol. 49, p. 103 973, 2023. DOI: 10.1016/j.jasrep.2023.103973. [Online]. Available: https://doi.org/10.1016%2Fj.jasrep.2023.103973.

[88] D. Mitsos, V. Kantarelou, E. Palamara, A. Karydas, N. Zacharias, and E. Gerasopoulos, "Characterization of black crust on archaeological marble from the library of hadrian in athens and inferences about contributing pollution sources," *Journal of Cultural Heritage*, vol. 53, pp. 236–243, Jan. 2022, ISSN: 1296-2074. DOI: 10.1016/j.culher.2021.12.003. [Online]. Available: http://dx.doi.org/10.1016/j.culher.2021.12.003.

[89] F. Wang, Y. Fu, D. Li, Y. Huang, and S. Wei, "Study on the mechanism of the black crust formation on the ancient marble sculptures and the effect of pollution in beijing area," *Heliyon*, vol. 8, no. 9, e10442, Sep. 2022, ISSN: 2405-8440. DOI: 10.1016/j.heliyon.2022.e10442. [Online]. Available: http://dx.doi.org/10.1016/j.heliyon.2022.e10442.

[90] C. Thomas, A. Cimentada, J. Polanco, J. Setién, D. Méndez, and J. Rico, "Influence of recycled aggregates containing sulphur on properties of recycled aggregate mortar and concrete," *Composites Part B: Engineering*, vol. 45, no. 1, pp. 474–485, Feb. 2013, ISSN: 1359-8368. DOI: 10.1016/j.compositesb.2012.05.019. [Online]. Available: http://dx.doi.org/10.1016/j.compositesb.2012.05.019.

[91] S. He, S. Mustafa, Z. Chang, M. Liang, E. Schlangen, and M. Luković, "Ultra-thin strain hardening cementitious composite (shcc) layer in reinforced concrete cover zone for crack width control," *Engineering Structures*, vol. 292, p. 116 584, 2023, ISSN: 0141-0296. DOI: 10.1016/j.engstruct.2023.116584. [Online]. Available: http://dx.doi.org/10.1016/j.engstruct.2023.116584.